Andreas Larsson

Die-attach for high-temperature electronics

A PhD dissertation in
Applied Micro- and Nanosystems

Faculty of Technology, Natural Sciences and Maritime Studies
University of South-Eastern Norway
Horten, 2019

Doctoral dissertations at the University of South-Eastern Norway no. 47
ISSN: 2535-5244(print)
ISSN: 2535-5252 (online)

ISBN: 978-82-7860-392-5 (print)
ISBN: 978-82-7860-393-2 (online)

Print: University of South-Eastern Norway

To my loving and patient family.

Preface

This thesis is submitted in partial fulfillment of the requirements for the degree of Philosophiae Doctor (Ph.D.) from the Department of Microsystems, at the University of South-Eastern Norway (USN). This doctoral work has mainly been conducted at the Department of Microsystems (IMS), Faculty of Technology, Natural Sciences and Maritime Sciences, at the University of South-Eastern Norway (USN) in Borre, Norway. Experiments have also been carried out at the University of Oslo (UiO) in Oslo, Norway, XYZTec in Panningen, Netherlands, and at the European synchrotron radiation facility (ESRF) in Grenoble, France. The work was performed in collaboration with TECHNI AS (Borre, Norway) and TEGma AS (Drammen, Norway). The work has been under the supervision of Professor Knut E. Aasmundtveit at USN, Chief Technology Officer Dr. Torleif A. Tollefsen at TEGma AS, and Senior Scientist Dr. Ole Martin Løvvik at SINTEF Industry.

This project was funded by TECHNI AS, TEGma AS and the Research Council of Norway (Project No.: 244915).

Acknowledgments

I would like to thank my supervisors for their support, advice, and directions throughout the project. Prioritizing challenges and opportunities, and selecting tasks are not easy. Thank you for guiding me through this paramount of choices and many paths to follow.

I would also like to thank Ph.D. candidate Christian Thoresen for countless and fruitful discussions on daily challenges and other topics. They have helped me see clearly and forced me to think beyond my present knowledge. Our “coffee breaks” have been most joyful. Without them, I would not have come this far.

I would like to take the opportunity to thank all laboratory personal assisting me at various locations. To the team at USN; Ole-Henrik Gusland, Dr. Thai Anh Tuan Nguyen, Zekija Ramic, Thomas Martinsen, Dr. Muhammad Tayyib, and Ragnar Dahl Johansen, you made it all possible.

Further, I would like to express my gratitude to my fellow students at USN who included me into groups and for all our interesting chats. Dr. Birgitte Kasin Hønsvall deserves a special mention. You have been a role model to me and someone I could go to for support or a relaxing chat.

I would like to thank my colleagues at TECHNI for inspiring me to pursue this project. I want to acknowledge Christian Petersen in particular. Thank you for our many discussions on possibilities and opportunities. And, for all the challenges you’ve given me to see the project and the generated results from a different perspective, put it into other contexts and expanding my horizon in general.

I would like to give a special thanks to Jan Martin Bendiksen for our countless discussions on a great variety of topics related, and not related to the project. They have helped me understand current problems and issues, and they have challenged me to broaden my general knowledge within a wide variety of disciplines such as physics, chemistry, biology, fabrication, mechanics, electronics, nuclear physics, and woodworking, to mention a few. I am looking forward to many more!

To all my friends and family that have been there for me. Thank you!

Finally, I would like to express my deepest gratitude to my closest family for your endless support and patience. You are my haven where I can relax and disconnect from work and where I recharge. Mariann, you are awesome just the way you are!

Lier, March 2019

Andreas Larsson

Abstract

Applications in harsh environments push the boundaries for electronic systems. High temperatures put great stress on electronic components. The die-attach is an enabling component that makes the system work. It needs to reliably and predictably attach electronic components to circuit boards. It must function mechanically, thermally and electrically for the system to work properly. Two applications that offer great challenges are thermoelectric devices and power electronics. Thermoelectric generators require a temperature difference to able to convert heat energy into electrical energy. High-temperature heat sources offer abundant heat that may be harvested. Power electronics dissipate lots of heat during operation. These losses make them particularly hot and unforgiving when applied in high-temperature environments.

This work set out to investigate two different die-attach technologies for high-temperature applications: Liquid solid diffusion (LSD) bonding and solid-liquid interdiffusion (SLID) bonding.

LSD was at an idea stage when this project started. The hypothesis was that it could be possible to form off-eutectic joints that comprised a microstructure that could have structural load capacity in a partially liquid state. This thesis has shown that such joints may be formed using the binary Au–Ge system. A melting point depressant material, *i.e.*, eutectic Au–Ge preforms, were sandwiched between Au substrates to form joints, forming a Au | $Au_{72}Ge_{28}$ | Au structure. The preforms were melted, and solid-liquid interdiffusion between the adjoined materials change the composition into a Au rich off-eutectic composition. Cooling solidifies the joint into a hypoeutectic (Au-rich) compound

with an overall Au | Au–Ge | Au structure. Investigations on the microstructure reveled that a network of columnar like solid single-phase structures of Au forms a connection between joined components. These Au structures were surrounded by a hypereutectic (Ge-rich) compound. These Au structures have a significantly higher melting point (up to 1064 °C) than the eutectic preform that was used to fabricate them, which melts at 361 °C. The fabricated joints had a significant structural capacity ranging from approximately 140 MPa at room temperature to about 40 MPa in a partially liquid state at 410 °C.

SLID bonding is done by melting a melting point depressant material between two substrates that are to be joined. Solid and liquid interdiffusion between the adjoined materials transform these into an intermetallic compound (IMC). The joint solidifies isothermally. The Ni–Sn system was used to fabricate SLID joints. Joints were successfully formed using a layered Ni | Sn | Ni structure that was transformed into a Ni | Ni–Sn IMC | Ni structure. The fabricated joints were flawed with voids caused by idiomorphic (needle-like) Ni_3Sn_4 structures growing at the Ni surface into the Sn melt during fabrication. Acting as spacers, they restrict volumetric contraction of the joint materials. The contraction is forced by phase transformation from Sn(l) and Ni(s) into Ni–Sn IMCs by as much as up to 17 vol.%. This cause the voids to form. Despite this, the shear strength was very high, up to 230 MPa was measured. These findings were confirmed by contemporary researchers.

Keywords: Die-attach, joining, bonding, off-eutectic, Au–Ge, solid-liquid interdiffusion (SLID), transient liquid phase (TLP), Ni–Sn, high-temperature, thermoelectrics

List of papers omitted due to publishers'restrictions

Article 1

A. Larsson and K. E. Aasmundtveit (2019). On the microstructure of off-eutectic Au–Ge joints — A high-temperature joint. *J. Metall. Mater. Trans. A*, *Submitted*

Article 2

A. Larsson, T. A. Tollefsen, and K. E. Aasmundtveit (2019). Shear strength of off-eutectic Au–Ge joints at high temperature, *Microelectron. Reliab.,* **99**, pp. 31-43, DOI: 10.1016/j.microrel.2019.05.002

Article 3

A. Larsson and C. B. Thoresen (2019). Off-Eutectic Au–Ge Die-Attach — Microstructure, Mechanical Strength, and Electrical Resistivity, *IEEE Trans. Compon., Packag., Manuf. Technol.*, DOI: 10.1109/TCPMT.2019.2926528

Article 4

A. Larsson, T. A. Tollefsen, O. M. Løvvik, and K. E. Aasmundtveit (2019). A Review of Eutectic Au–Ge Solder Joints. *Metall. Mater. Trans. A,* ***50A***, pp. 4632-41, DOI: 10.1007/s11661-019-05356-0

Article 5

A. Larsson, T. A. Tollefsen, O. M. Løvvik, and K. E. Aasmundtveit (2017). Liquid Solid Diffusion (LSD) bonding: A novel joining technology, *in. Proc. Eur. Micro-electron. Packag. Conf. (EMPC)*, Warsaw, Poland, pp. 1-3, DOI: 10.23919/EMPC.2017.8346886

Article 6

A. Larsson, T. A. Tollefsen, O. M. Løvvik, and K. E. Aasmundtveit (2017). Thermoelectric Module for High Temperature Application, *in Proc. Intersoc. Conf. Therm. Thermo-mech. Phenom. Electron. Sys. (ITHERM)*, Orlando, USA, pp. 719-25, DOI: 10.1109/ITHERM.2017.7992557

Article 7

A. Larsson, T. A. Tollefsen, and K. E. Aasmundtveit (2016). Ni–Sn solid liquid interdiffusion (SLID) bonding – Process, bond characteristics and strength, *in Proc. Electron. Sys.-Integr. Technol. Conf. (ESTC)*, Grenoble, France, pp. 1-6, DOI: 10.1109/ESTC.2016.7764673

Article 8

A. Larsson, T. A. Tollefsen, O. M. Løvvik, and K. E. Aasmundtveit (2015). Ni–Sn Solid-Liquid Interdiffusion (SLID) Bonding for Thermo-Electric Elements in Extreme Environments – FEA of the joint stress, *in Proc. Eur. Micro-electron. Packag. Conf. (EMPC)*, Friedrichshafen, Germany, pp. 1-6, ISBN: 978-0-9568-0862-2

In addition, I have contributed to the following publications:

Article I

A. Larsson, C. B. Thoresen, and T. Aamli (2019). Partially Liquid Interconnects with The Au–Ge System – Mechanical Strength and Electrical Resistivity, *in Proc. Pan Pac. Microelectron. Symp. (PANPAC)*, *In print*

Article II

K. E. Aasmundtveit, T. T. Luu, H. V. Nguyen, A. Larsson, T. A. Tollefsen (2019). Solid-Liquid InterDiffusion (SLID) bonding, for thermally challenging applications, *in Proc. IEEE Electron. Compon. Technol. Conf. (ECTC)*, Las Vegas, USA, *Accepted*

Book chapter I

K. E. Aasmundtveit, T. T. Luu, H. V. Nguyen, A. Larsson, T. A. Tollefsen (2018) Intermetallic Bonding for High-Temperature Microelectronics and Microsystems: Solid-Liquid Interdiffusion Bonding, *in Intermetallic Compounds - Formation and Applications*, London, United Kingdom: IntechOpen, Ch. 3, 43-72, DOI: 10.5772/intechopen.75139

Patent I

A. Larsson and T. A. Tollefsen (2016). Method for forming a joint in a binary system and joint thereof, Eur. Pat. Office, Appl. No.: EP16163263

Patent II

A. Larsson and T. A. Tollefsen (2016). Thermoelectric half-cell and method of production, Norw. Ind. Prop. Office, Pat. No.: NO341705

Patent III

T. A. Tollefsen, M. Engvoll, O. M. Løvvik, and A. Larsson (2014). Method for pre-processing semiconducting thermoelectric materials for metallization, interconnection and bonding, Eur. Pat. Office, Pat. No.: EP3218941

Patent IV

T. A. Tollefsen and A. Larsson (2017). A device for generating electric power for installation to an exhaust conduit, Norw. Ind. Prop. Office, Pat. No.: 342455

Presentation I

A. Larsson, T. A. Tollefsen, O. M. Løvvik, K. E. Aasmundtveit (2016). Liquid Solid Diffusion (LSD) Bonding: Joint Structure and Bonding Method, *at Mater. Sci. Technol. (MS&T),* Salt Lake City, USA

Presentation II

A. Larsson, (2016). Ni-Sn solid liquid interdiffusion bonding, *at 7th annu. Workshop Norwegian Ph.D. Network Nanotechnol. Microsys.,* Trondheim, Norway

Presentation III

A. Larsson (2018). Electronic joints for harsh environments, *at USN – Research dissemination competition.,* Borre, Norway, Finalist

Presentation IV

A. Larsson (2016). Electronic packaging for harsh environments, *Invited talk at Næringslivsdagen 2016 - Uten grenser,* Oslo, Norway,

Poster I

A. Larsson, T. A. Tollefsen, O. M. Løvvik, and K. E. Aasmundtveit (2017). Liquid Solid Diffusion (LSD) bonding, *in Proc. Intersoc. Conf. Therm. Thermo-mech. Phenom. Electron. Sys. (ITHERM)*, Orlando, USA, 3rd place winner

Artwork I

A. Larsson (2017). Continuous and coherent, *at Intersoc. Conf. Therm. Thermo-mech. Phenom. Electron. Sys. (ITHERM) Art-in-Sci.*, Orlando, USA, Conf. feature artwork.

I have also held several public and closed forum presentations and presented work related to this thesis in various forums.

Table of contents

1 pennyweight by weight of soda burnt cream of tartar as much as you think right, 1 pennyweight by weight of borax: compound these with water, and coat the brass with it; afterwards sprinkle over it roasted tin powder; afterwards heat it in a furnace beneath the coals, as in the case of [soldering] gold, until it is well joined.

— NOMEN NESCIO, *ca.* 12th century A.D.[1]

[1] Cyril Stanley Smith and John G. Hawthorne, Mappae Clavicula: A little key to the world of medieval techniques, Transactions of the American Philosophical Society, **64**(4), 1974

1 Introduction

Electronic systems comprise discrete or integrated components attached to circuit boards to form systems. These systems are often intricate and may preform various functions. Electronic systems are used to survey physical conditions (sensors), operate equipment (actuators) or used for signal conversion (transducers). Common electronic components used in electronic devices include resistors, capacitors, inductors, diodes, transistors, integrated circuits (IC), and micro-electro-mechanical systems (MEMS). Interconnects are used to attach and electrically connect the components to the circuit board and to each other to form functional systems. The interconnects may be in the form of a die-attach, flip-chip, tape-automated bonding (TAB), or wire bonds depending on the application.

1.1 High-temperature electronics

There is a drive to implement electronic systems in high-temperature environments[1–8]. Many physical processes are accelerated at high temperature. Such processes include; diffusion, creep, fatigue, chemical decomposition (polymer chain breakdown and oxidation) into new molecules which may cause electronics to fail catastrophically, often prematurely. In addition, other failure mechanisms may be triggered at high temperature, such as avalanche breakdown in semiconductive components, depolarization of piezoelectric components, and abrupt changes in material properties, *e.g.* passing the glass transition point in polymeric materials, structural changes in crystalline materials, and phase transitions, which may lead to failures or unwanted characteristics of the system.

1.1.1 High-temperature

One of the most commonly referred definitions of "high-temperature" is taken from the US military standards. MIL-STD-883H define high-temperature to begin at 125 °C and defines environmental thermal stress test conditions ranging up to 175 °C–300 °C[9]. MIL-STD-202G extend the environmental test conditions up to 500 °C for electronic parts[10]. In addition, applications have their requirements for temperature compatibility. Common high-temperature applications include down-hole instrumentation in oil, gas, and geothermal wells, sensor and actuator systems in aerospace and space, power electronics in automotive (electric (EV) and hybrid electric (HEV)), safety systems in nuclear power plants, and thermoelectrical energy harvesting. An outline of the temperature requirement for some high-temperature applications is given in Fig. 1. This project aim was to investigate high-temperature electronics suitable for use at 250 °C or higher.

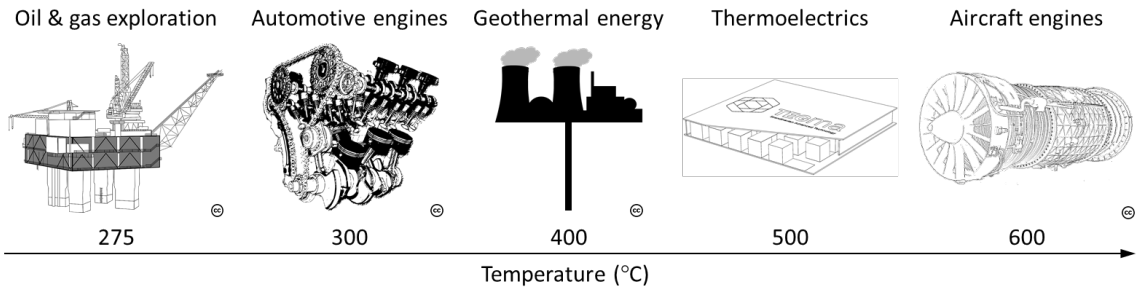

Fig. 1 Typical temperature requirement for common high-temperature applications[11]. Images were used under the Creative Commons agreement.

1.1.2 Thermoelectrics

Thermoelectric devices convert thermal energy into electrical energy, or *vice-versa*. When a thermoelectric material is heated, electrons (n-doped) and holes (p-doped) are activated through the Seebeck effect. That means that, if a thermal gradient is applied across the material, a charge density gradient across the material is also created, *i.e.,* a voltage gradient is created across the material. The sign of the created voltage gradient depends on the doping of the material; n- or p-doped, and the direction of the temperature gradient. The most common arrangement is to place solid pieces, or elements, with alternating n-doped and p-doped elements in a thermally parallel configuration and an electrically serial configuration, using interconnects, and connect them to a load. This creates a circuit where a current can flow. Such a device can convert heat flux ($\boldsymbol{q}$) into

electrical current (I) and transfer it to a distant location, *i.e.*, to a load. This device is called a thermoelectric module, or a simple form of a thermoelectric generator (TEG). When only two elements, one n-doped and one p-doped, are connected in such a configuration it is called a uni-couple. A uni-couple connected to a load is illustrated in Fig. 2.

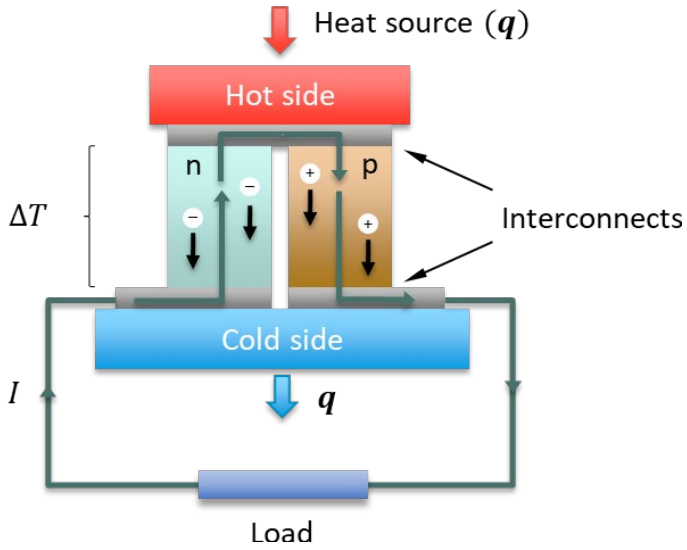

Fig. 2 Illustration of a thermoelectric uni-couple connected to a load that forms a device that can convert thermal energy into electrical energy and transfer it to a distant location (load).

The efficiency (η) of a thermoelectrical device is dependent on the temperature difference across the elements (ΔT) and a unitless quantity called the thermoelectric figure of merit (zT)[12]. The efficiency of a thermoelectrical device can be calculated according to

$$\eta = \frac{T_\mathrm{h} - T_\mathrm{c}}{T_\mathrm{h}} \frac{\sqrt{1+zT} - 1}{\sqrt{1+zT} + T_\mathrm{c}/T_\mathrm{h}} \tag{1}$$

where T_h and T_c are the local temperatures on the hot and cold sides of the thermoelectric material and zT is the figure of merit defined as:

$$zT = \frac{\sigma \alpha^2 T}{\lambda} \tag{2}$$

where λ is the thermal conductivity, σ is the electrical conductivity and α is the Seebeck coefficient. The efficiency as a function of temperature is presented in Fig. 3. One can see that a larger temperature difference across the thermoelectric material makes for a

more efficient device. In addition, a larger temperature difference also allows more heat energy to flow through the device according to Fourier's law:

$$\boldsymbol{q} = -\lambda \nabla T \tag{3}$$

where $\boldsymbol{q}$ is the heat flux and ∇T is the temperature gradient. In general, a large temperature gradient across a thermoelectric material allow more thermal energy to flow through it that can be efficiently converted and harvested. This is a simplification of how real thermoelectric devices work, but it is not the scope of this thesis to get deeper into such details. Readers are encouraged to start such knowledge exploration by themselves, *e.g.*, using the webpages at Northwestern University, Dept. of Materials Science and Engineering[13] which provide an excellent introduction to the field.

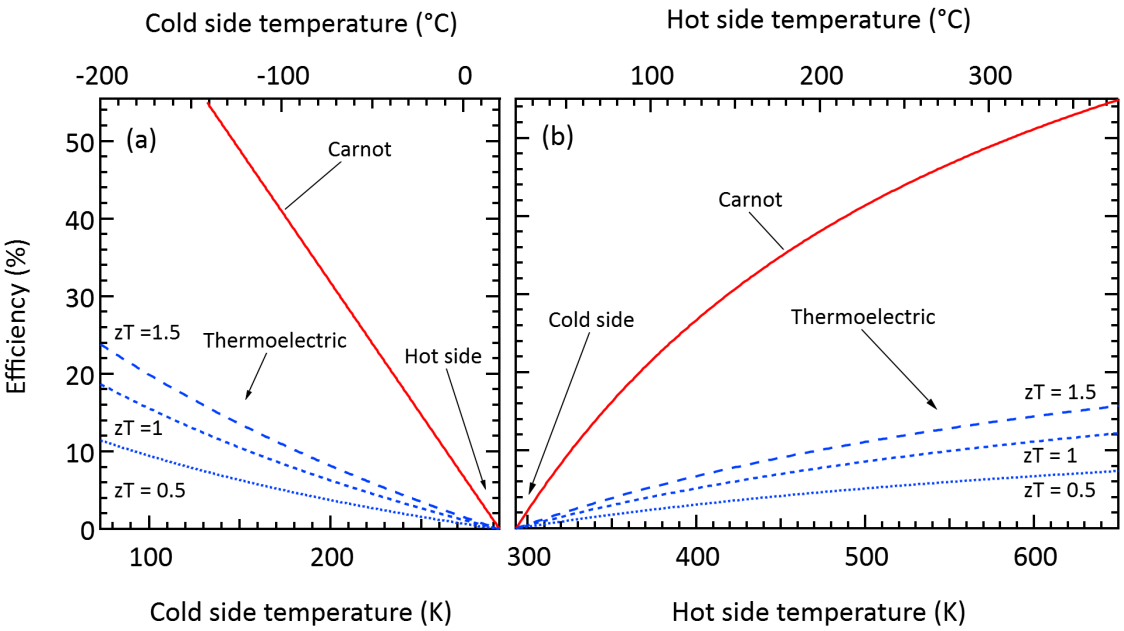

Fig. 3 A graph illustrating efficiency as a function of temperature. (a) show the efficiency as a function of cold side temperature while the hot side is kept at 20 °C. (b) show the efficiency as a function of hot side temperature while the cold side is kept at 20 °C. The efficiency increases with the increase in temperature difference between the hot and cold sides. The thermoelectric efficiency (dashed blue) is significantly lower than the theoretical limit of the Carnot cycle (red). The figure of merit, zT, was kept constant, *i.e.*, temperature independent material properties were assumed.

In simplified terms, the power output, P, is equal to the square of the generated voltage, U, and inversely proportional to the circuit resistance, R[14]:

$$P = \frac{U^2}{R} \tag{4}$$

The maximum generated power (P_{max}), with a matched load, is approximately[15]:

$$P_{max} = \frac{U^2}{4R_i} \tag{5}$$

where (R_i) is the internal resistance of the TEG. The voltage is proportional to the number of uni-couples (n), the temperature difference (ΔT) across the elements, and the difference in Seebeck coefficient ($\Delta\alpha$) between n- and p-doped elements[16]:

$$U \propto n\Delta T\Delta\alpha \tag{6}$$

Fig. 4 shows the voltage distribution as a function of the temperature distribution of a uni-couple ($n = 1$). Following the preceding formulae, the generated power can be expressed as:

$$P \propto \frac{(n\Delta T\Delta\alpha)^2}{R} \tag{7}$$

Therefore, it is important to apply as large temperature difference across thermoelectrical devices as possible. To achieve this one may cool the cold side or heat the hot side or do both. Cooling to a temperature significantly lower than ambient temperatures is often impractical, complex or expensive since it often requires cryogenic equipment, *e.g.,* vacuum chambers, and pumps. Since there exist many high-temperature sources with abundant heat in various places, it is often preferable to target thermoelectrics for high-temperature applications where electricity can be harvested. Examples of high-temperature heat sources include: engines, exhaust systems, incinerators, and molding processes. Materials properties are as a rule temperature dependent which makes different materials suitable for different temperature ranges. Two of the most common thermoelectric materials used for higher temperatures are Bi_3Te_2 and $CoSb_3$. Their thermoelectric figure of merit and efficiency as a function of temperature are shown in Fig. 5. The power output of two equivalent thermoelectric generators, one based on Bi_3Te_2 and the other based on $CoSb_3$ is shown in Fig. 6. The power output monotonically increases with increasing in hot side temperature. With a hot side temperature above 350 °C, the $CoSb_3$ surpass the Bi_3Te_2 module producing more power.

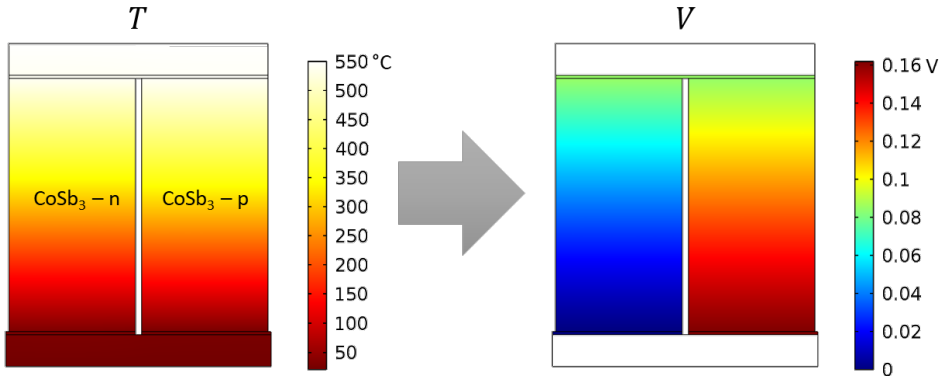

Fig. 4 Simulation results of a uni-couple showing the resulting voltage distribution (right) as a function an applied temperature difference (left).

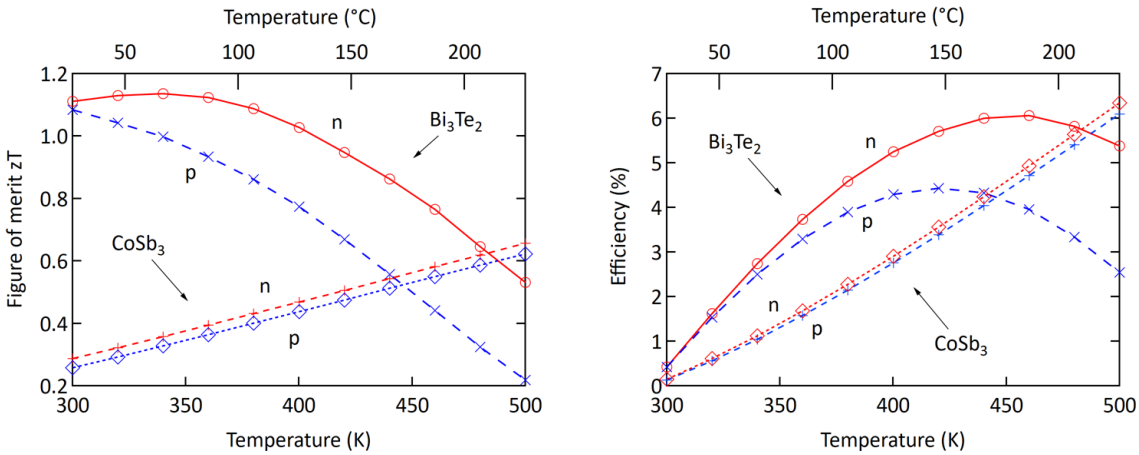

Fig. 5 Graph of the thermoelectric figure of merit and efficiency as a function of temperature, with the cold side of 20 °C, for two common thermoelectric materials: Bi_3Te_2 and $CoSb_3$[17]. The graphs illustrate that Bi_3Te_2 is suitable for use in a lower temperature range than $CoSb_3$ is.

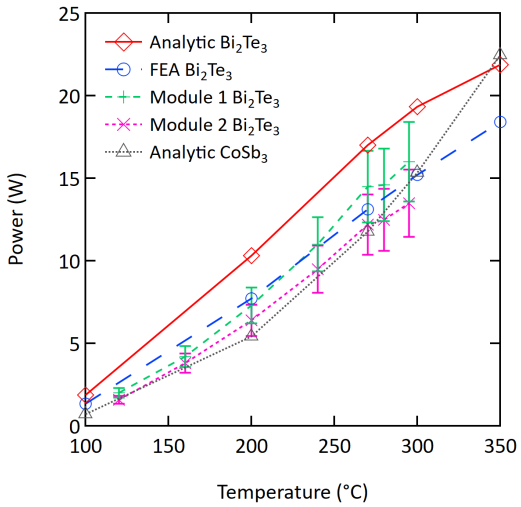

Fig. 6 Graph of the power output as a function of hot side temperature for a thermoelectric module with a fixed cold side temperature of 38.5 °C. Two models were developed in this thesis; an analytical and a finite element model. The graphs show a comparison between the models (analytic and FEA) and measurements on two equivalent thermoelectric generators (Module 1 & 2)[17].

1.1.3 Power electronics

In recent years, semiconductive components have been developed and demonstrated to operate at temperatures well above 200 °C, such as silicon on insulator (SOI), gallium arsenide (GaAs), gallium nitride (GaN), and silicon carbide (SiC). In particular, the wide-bandgap materials SiC and GaN have matured and have been successfully adopted and integrated into commercial power devices such as diodes, MOSFETs, BJTs, and HEMTs[18,19]. They offer high-temperature stability, fast switching and high-power handling with low losses[20,21]. Wide-bandgap power devices are typically attached to high-temperature compatible ceramic substrates, such as aluminum nitride (AlN), silicon nitride (Si_3N_4), or alumina (Al_2O_3)[21–23]. High-temperature compatible devices reduce the cooling needs of electronic systems since the components can be run at higher temperatures. Thus, the systems may be smaller, and cost can be reduced. Another benefit from such components is that they enable implementation of electronics in new environments and applications where space or cooling capacity are limited. High-temperature power electronics is needed in various application, *i.e.,* in DC/DC converters in electric (EV) and hybrid electric vehicles (HEV), and in motor drives for oil and gas exploration.

1.2 Electronics packaging

The purpose of electronics packaging is to facilitate that discrete electronic components are connected and operate properly in an electronic system. There are several levels of packaging, from adding metal layers on the electronic components to the final enclosure for assembled systems. Thus, many challenges need to be considered for packaging of electronic systems. The die-attach is of particular interest at high temperature since it forms a critical joint between the electronic components and the circuit board. All adjoined materials must be mechanically and chemically stable or evolve predictively at the expected operating conditions; including temperature, vibration, and humidity. The joints' main purpose is to secure that joined components are always mechanically attached to the circuit board. Often the die-attach also form an interconnect between an electronic device, *e.g.*, a transistor, diode MEMS, or similar. Thus, the electrical and thermal properties of a die-attach must also be apt for proper system behavior. Also, other conditions such as hermiticity, ductility, wettability, cost, availability, and process

implications must be considered before successful implementation of a packaging scheme can be achieved. Both metals and adhesives are commons for die-attach applications, though adhesives are not suitable for high-temperature application.

From a packaging point of view, the preferred environmental condition for an optimized TEG can be extremely demanding. An extreme thermal gradient, 100 °C/mm or more, is combined with a very high temperature, 300 °C or more on the hot side. This creates very high mechanical stress levels inside the interconnects, *i.e.*, the joints, that attach the elements to the circuit boards, which are typically in the form of metallized ceramic substrates. This is due to a mismatch in material properties of the joined components and the joint itself. Also, the high temperature rapidly accelerates degradation processes. Thus, there is a need to form strong, high-quality joints that are stable at high temperatures and have suitable material properties.

Power devices offer another challenge since they control high voltages (up to hundreds of kV) and high currents (up to hundreds of amperes) at high temperatures. This activates and accelerates other degradation mechanisms such as electromigration of interconnects[24,25] and diffusion of atoms[26]. Despite that wide-bandgap power devices are more efficient, with lower losses than corresponding Si devices due to fast switching and low on-resistance, they can still have significant power losses (in absolute terms). *I.e.,* local junction temperatures and the temperature at the die-attach can be very high causing large temperature gradients, up to 100 °C/mm, across the die-attach.

Both thermoelectric and power devices induce high stress levels in joints due to the mismatch in material properties of the joined materials as well as the local thermal gradient. This is illustrated in Fig. 7 which show the stress components in a Ni–Sn SLID joint between a $CoSb_3$ thermoelectric element and an Al_2O_3 substrate.

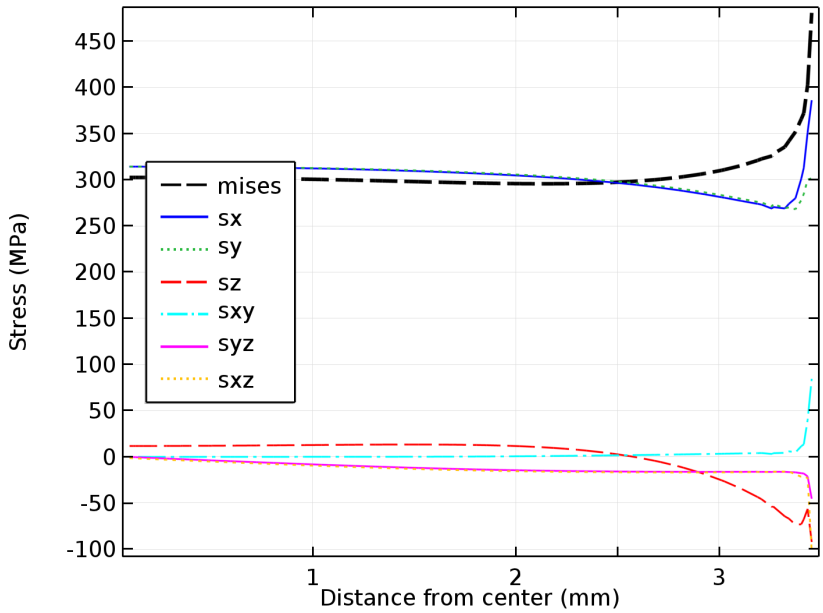

Fig. 7 Plot of the stress components in a Ni_3Sn_4 layer in a Ni–Sn SLID joint in a $CoSb_3$ based thermoelectric element attached to an Al_2O_3 ceramic substrate exposed to a temperature gradient of 84 °C/mm with the cold side kept at 25 °C[27]. The layer structure was: Al_2O_3 (635 µm) | Cu (10 µm) | Ni (2 µm) | Ni_3Sn_4 (4 µm) | Ni (2 µm) | TiN (700 nm) | $CoSb_3$ (5 mm).
Legend: mises show the equivalent stress according to the von Mises yield criterion, sx, sy, and sz are orthogonal normal stress components, and sxy, syz, and sxz are orthogonal shear stress components. The z-axis is normal to the joint plane, and the x- and y-axes are in the joint plane.

1.3 Die-attach techniques

Joining of materials or components is an ancient art emanating many thousands of years back in time[28–30]. In more recent time, joining metals has become an art of greatest importance for electronic systems, particularly in high-temperature electronics. Joining of metals has enabled man to create extraordinary things and devices such as the space shuttle and remarkable functionality in modern miniaturized electronics, such as the smartphone. Some of the most advanced forms of joining technologies today are die-attach technologies used in assemblies forming advanced and complex electronic systems. Joining is also known as bonding in electronic packaging. Electronic bonding technologies include[31–34]; soldering, brazing, welding, thermo-compression, ultra-sonic, diffusion bonding, transient liquid phase (TLP)/solid liquid inter-diffusion (SLID) and sintering.

1.3.1 Soldering and brazing

Soldering is the most common joining technology for electronics and is widely used in many other applications. Its main component is a filler material, the solder, which is typically a bi-metal system such as the lead–tin (Pb–Sn) system shown in Fig. 8 which has three phases (α, β, and L) and one eutectic point (e). The solder composition is usually near a eutectic composition to reduce the process temperature and to get a clear phase transformation from solid to liquid during heating. The solder is placed between two surfaces to be joined. The solder is heated until it melts (isothermally for eutectics) and wets both bond surfaces. By sequential cooling, the solder solidifies (again isothermally for eutectics) and creates a solid joint. *Off-eutectic* soldering is sometimes used. Off-eutectic solder alloys have a compositional offset from the eutectic composition. One benefit of using off-eutectic solder is that it gives more time applying the solder to the joint[35]. Plumber's solder is such a solder that utilizes this expanded timeframe for application (see Fig. 8). Off-eutectic compositions are also used to increase the melting point of the solder (high melting point solder in Fig. 8). One possible downside to off-eutectic solders is that, during joints formation the solder solidifies by a transformation through a two-phase state. This may introduce defects into the final joint. Significant volumetric changes during solidification can cause strain inside final joints which may impede on both joint quality and reliability. Another downside is squeeze-out caused by the existence of the liquid phase during soldering. As the liquid phase is pushed out from the joint region it may end up on other components or areas causing short-circuits (malfunctions) or contaminations (reliability). Some soldering material systems create intermetallic compounds (IMC) with adjoined materials that impede on the material properties of the final joint. IMC are often brittle and may have undesirable electrical properties which can make them unreliable. Two famous and detrimental IMCs are the Au_5Al_2 and $AuAl_2$ phases, also known as white and purple plague. Au_5Al_2 has a high electrical resistivity while $AuAl_2$ is brittle. They are often formed between Au wire bond on Al pads or *vice versa*. Thus, care should be taken when using Au based solder on Al metallization schemes (*e.g.*, in CMOS based technologies). Formation of intermetallics at interconnect interfaces with other metals is probably the main reason for the "bad reputation" IMC have within the field of packaging.

Soldering is typically characterized by relatively low process temperatures compared to other joining techniques. This is very beneficial for sensitive components, such as electronics, and that is why soldering is commonly used in electronics. The apparent downside is that higher temperatures quickly approach the melting point of the solder which makes the joint unreliable at higher temperatures.

Brazing is essentially similar in its characteristics as soldering, but it is carried out at an elevated process temperature, typically defined to be above 400–450 °C.

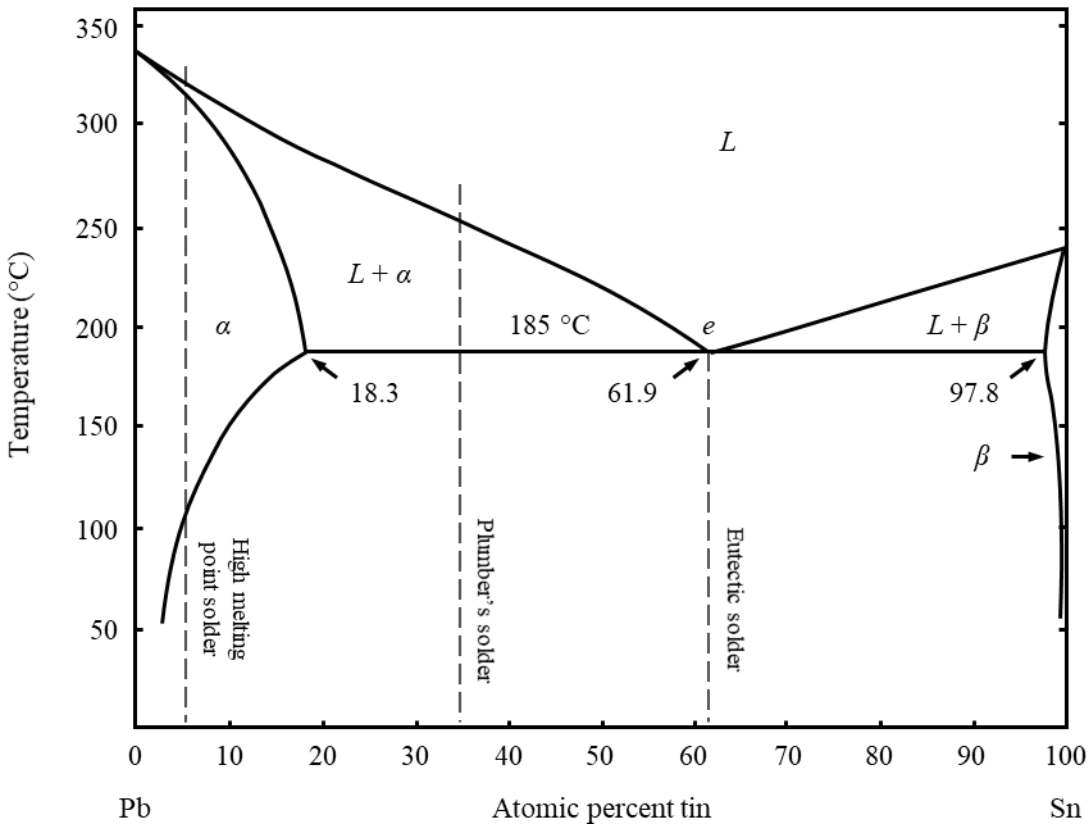

Fig. 8 The lead–tin (Pb–Sn) phase diagram with three different solder compositions marked out; one eutectic, and two non-eutectic (Plumber's solder and a high melting point solder). The phase diagram was adapted from Ref. [35,36].

1.3.2 Liquid solid diffusion (LSD) bonding

Liquid solid diffusion (LSD) bonding is a term introduced in this work to describe an alternative soldering technique. It is based on off-eutectic soldering in that the composition is off-eutectic. It differs in that by forming an off-eutectic compound that has enough solid phase in a partially liquid state (partially molten) to join two components mechanically. Regular off-eutectic solder, such as plumber's solder (see Fig. 8), behaves

like a paste in its partially liquid state ($L + \alpha$ in the phase diagram). *I.e.,* solid particles are suspended in a liquid melt at temperatures above the eutectic isotherm. Exchanging the geometrical location of the solid and liquid components in such a paste-like material could create a porous solid structure where pores are filled with the liquid phase. Both types of structures, solid particles in a suspension and a porous structure with liquid filled pores, can have the same composition while their mechanical properties would be significantly different.

LSD combines features from several other joining technologies. Two pieces of similar materials composition are brought together with a low melting point compound, *e.g.*, with a eutectic composition, and placed between the bond surfaces. The materials stack is then heated and wetting and cooling forms a joint, *i.e.,* soldering. Unlike regular soldering, there is excess seed material (solvent) available at the bond region creating a compositional transition of the solder joint. The structure is formed from a layered structure comprising basically 2D layers, *i.e.,* a large aspect ratio of the thickness *vs*. lateral size, that react and form a new 3D compound. The transition is similar to how SLID/TLP works, but unlike them, no stable phase, a solid solution or an intermetallic with a high melting point is reached. The process is finished before isothermal solidification is completed.

1.3.3 Welding

Welding is another very common joining technology. There are many different forms of welding, such as resistance welding, arc welding, gas welding, and laser welding[31]. They all have in common that the bond interface is heated above the melting point of at least one of the components. The surfaces are then pressed together and upon cooling the melt solidifies and creates a solid joint. Welding is typically characterized by its high process temperature and near monometallic joints. At high vacuum, another welding process may be achieved, but at a significantly reduced process temperature. It is called *cold welding* or *contact welding*. Two very flat and clean bond surfaces of similar material (preferably the same) are pressed together which initiates a solid interdiffusion process across the adjoined surfaces which creates a joint similar to regular welding joints. *Friction welding* and *explosive welding* are two other welding techniques where the interface surfaces

never melt during the bond process. Welding is commonly used in structural components, *e.g.*, as a hermetic seal of lids in electronics packages to large steel members in trusses.

1.3.4 Thermocompression and ultrasonic bonding

Thermocompression and *ultrasonic* bonding press two components of similar composition together while thermal or thermal and ultrasonic energy is transferred into the bond surfaces. This catalyzes the interdiffusion process between the bond surfaces creating a solid joint at a temperature significantly below the melting points of the constituting materials. In principle, it is similar to regular welding where the required energy to initiate bonding is supplied by a combination of heat, pressure, and vibrations instead of solely by heat.

1.3.5 Diffusion bonding

Diffusion bonding is a solid-state joining technology. Two components are pressed together forming an intimate contact between the components. Heat is applied, and solid interdiffusion creates a bond between the two adjoined surfaces. This process usually takes a long time or is performed at high temperatures.

1.3.6 Solid-liquid interdiffusion (SLID) bonding

Solid-liquid interdiffusion (SLID), or *transient liquid phase* (TLP), is another method to create metallic joints. A binary metallic system is often used where one element has a lower melting point than the other element. The bond surfaces are pressed together and heated until the low melting point metal melts and wets the bond surfaces. This initiate a solid-liquid interdiffusion process. Continued heating drives the diffusion process to create a new material compound by isothermal solidification. This compound can be either a solid solution or an intermetallic compound (IMC). The benefit of forming such IMCs is that some material systems have stable material phases which have a much higher melting point than the original low melting point material. Thus, the final material composition may be used for high-reliability or high-temperature applications[37].

1.3.7 Sintering

Sintering utilize small metal particles that are placed at bond surfaces of the same or similar material to form near mono-metallic joints. Micro- or nanosized particles are mixed into a paste containing volatile solvents, binder, dispersant, and thinner[21,38]. Applied heat and pressure drive a solid-state diffusion process which forms a solid joint and removes solvents[39]. The technology is categorized by forming monometallic joints of uniform, but porous, geometry at high pressure and relatively low temperature[40]. Like TLP/SLID, sintering creates joints at process temperatures significantly lower than the melting point of the final joint.

1.4 Objectives

The main objective of this project was to develop high-temperature compatible die-attach technologies for electronic systems. This objective was divided into two sub-objectives:

1. Develop a die-attach technology for electronic systems with a large mismatch in the coefficient of thermal expansion (CTE) for use in environments with temperatures up to 250 °C.
2. Develop a die-attach technology assembly of thermoelectric devices to be used in extreme environmental conditions with temperatures up to 550 °C.

Two different technologies to be investigated was defined by the project partners: Liquid solid diffusion (LSD) bonding and Ni–Sn solid-liquid interdiffusion (SLID) bonding.

LSD bonding was at an early idea stage when the project started. Thus, proof-of-concept experiments were necessary to confirm feasibility. It was essential to develop an understanding of how to fabricate the proposed materials and to characterize them before implementation into high-temperature electronics, such as the motor and controller system developed by the project partner TECHNI AS shown in Fig. 9.

The Ni–Sn system was and still is fairly unexplored for SLID bonding. It was important to demonstrate successful bonding creating the desired intermetallic phases. Joint quality and process scheme were also central for successful implementation in thermoelectric devices, such as the thermoelectric energy harvesting system developed by the project partner TEGma AS shown in Fig. 10.

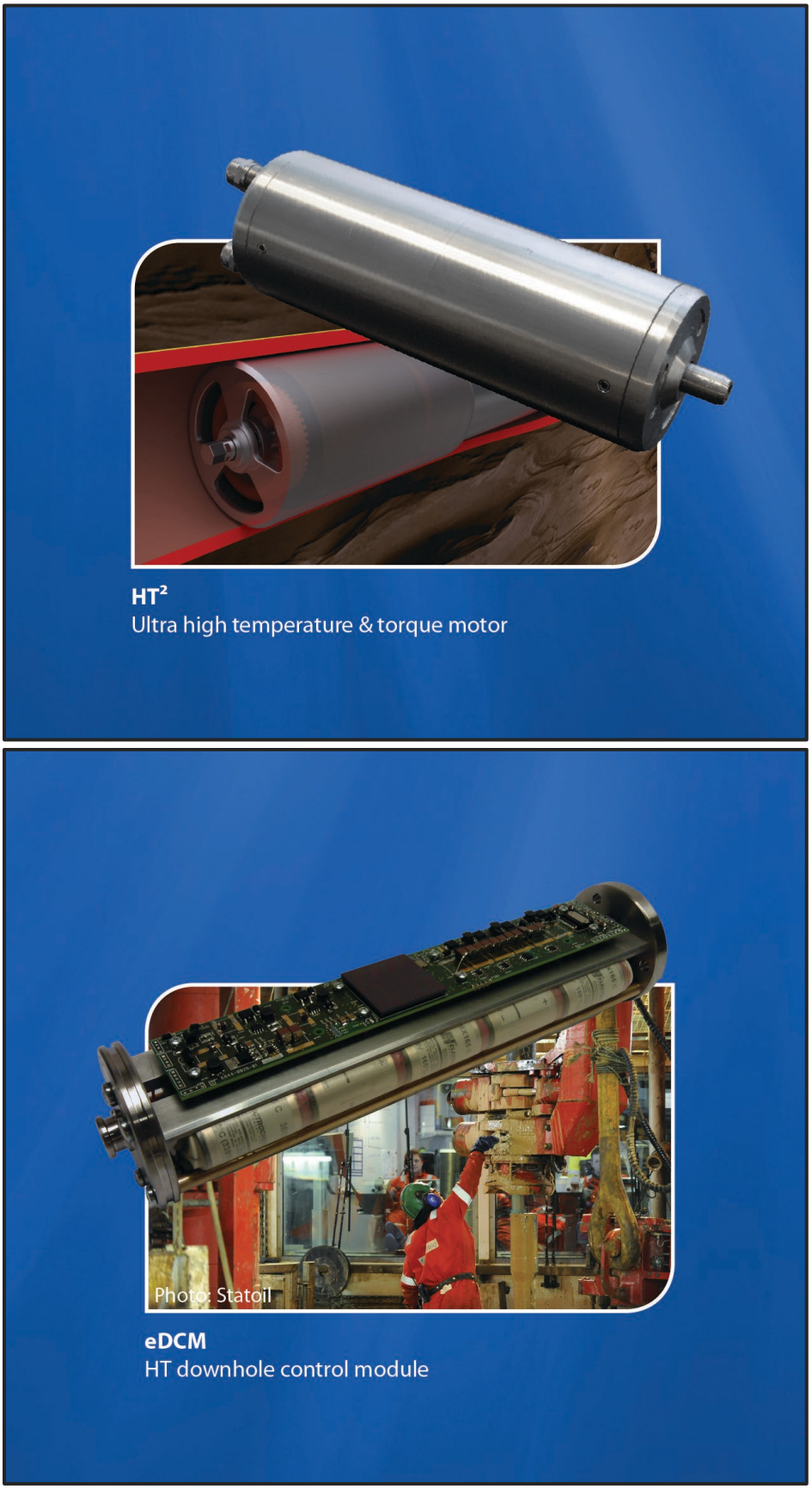

Fig. 9 High-temperature motor and controller developed by TECHNI AS, Borre, Norway.

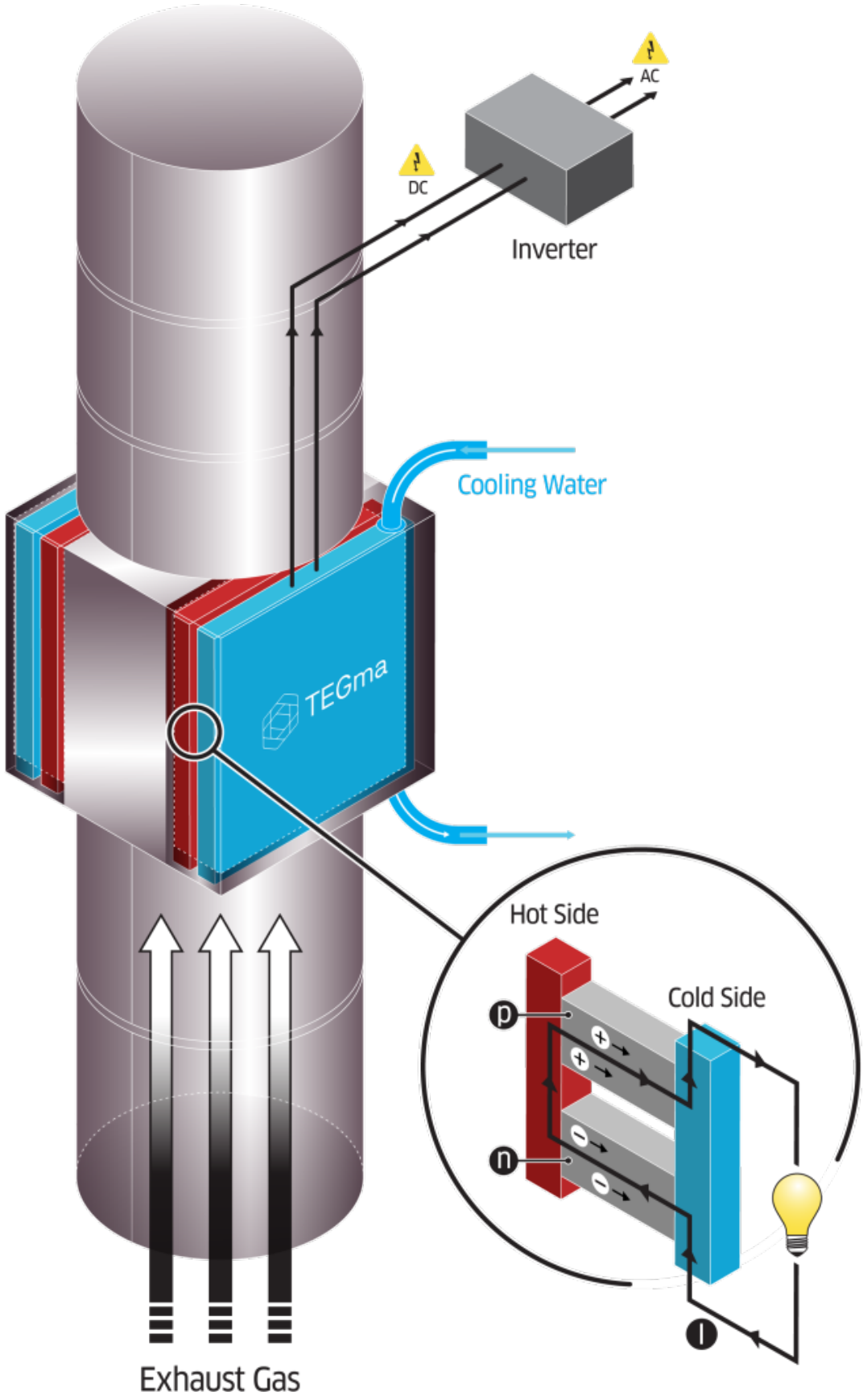

Fig. 10 Energy harvesting system developed by TEGma As, Drammen, Norway.

2 Methods

This chapter gives a brief review of the key methods and techniques used in this thesis. Unique methods developed for this thesis are given a more thorough description. In a broader sense than explicitly for high-temperature, these methods may also be suitable to use for other harsh environments. Careful considerations should be taken for the specific challenges of any particular environment at hand. Other harsh environments include; high-humidity, low-temperature (cryogenic), and high-stress/strain.

2.1 Liquid solid diffusion (LSD) bonding

2.1.1 Concept

Binary off-eutectic materials systems are partially solid and liquid when in the two-phase field region between the solidus and liquidus in the phase diagram[41]. During solidification of off-eutectic compounds, a paste-like mixture is formed in this field region, when the temperature is between the liquidus and solidus temperatures. This region is known as the 'mushy zone'[42,43]. This mushy state is caused by the mixture consisting of solid particles being suspended in a liquid phase or dendrites protruding into a liquid phase. This makes the compound easily reworkable, which is used in some applications such as soldering pipes with plumbers' solder. When reheated after complete solidification by cooling, it is often assumed that same paste-like structure will form. It was envisaged that it could be possible to switch place of the liquid and solid phases, forming a continuous and coherent porous structure with liquefied pores at elevated temperatures, instead of this mushy state. It was believed that diluting a eutectic or off-eutectic compound to a composition close to the maximum solubility limit at equilibrium and annealing it such

that phase segregation changes the microstructure and morphology of the joint, might be able to form such structures. The maximum solubility limit is defined by intersection of the solidus and the eutectic isotherm in the phase diagram, *i.e*. 18.3 at.% Sn in Pb and 2.7 at.% Pb in Sn in Fig. 8. When reheated, the segregated solute would react locally with the solvent. At the eutectic temperature, a liquid is formed at the interface between the two phases. The reaction continues until all the solute has been consumed, creating a liquid domain. The surrounding material then comprises a solid structure of a single phase, a solid solution, or an intermetallic compound. One may think of a porous metal foam structure like a sponge or sandstone, where the pores are filled with a liquid. The solid phase may be used to maintain structural integrity between two adjoined components at a temperature significantly above the eutectic melting point of the material system. Non-equlibrium states have not been evaluates in this thesis.

Another interesting effect that might happen is that forming of a liquid phase inside the joint could improve its thermal cycling characteristics. Materials defects like lattice defects and voids tend to accumulate at grain boundaries, triples points and at interfaces between dissimilar material phases. When such defects reach a critical size, they might compromise the integrity of the material, forming a crack initiation point. Since a liquid is formed at such interfaces between dissimilar materials with the LSD method; one might expect that these defects are dispersed into the melt. Upon solidification, large defects absorb into the melt. As the melt solidifies again new defects might emerge, but not as large defects. In a sense, this is like resetting the microstructure for each thermal cycle above the eutectic melting point. This is, of course, speculative, but it was one of the train-of-thoughts that fed the idea behind the LSD method. A partially melted compound was also expected to be softer, or more compliant, than a purely solid compound. Thus, when exposure to high-temperature imposes large deformations of the joint due to a mismatch in CTE, Youngs modulus and Poisson's ratio, a more compliant (flexible) material is likely to have a lower stress state inside the joint than its solid counterpart, as illustrated by Fig. 11. This figure shows a simplified case where mechanical properties and characteristics of a semi-solid (the joint) are not included. There will be interfacial reactions between the liquid and solid phases, and stress concentrations will likely appear at high curvature structures. The apparent downside is of course that the absolute structural load capacity of this semi-solid compound is likely weaker than a

corresponding completely solid phase, due to the difference in the solid fraction. The question is whether it is strong enough for its intended use, here as a die-attach for electronic components.

Other advantages of the LSD method are expected to be similar to the advantages of soldering such as a simple and fast process scheme, low bond line pressure, relatively easily repaired, high tolerance of rough and irregular bond surfaces, self-aligning, excellent joint quality. Apparent disadvantages include unexplored joining technology and uncertain high-temperature stability and joint strength.

The LSD method shares similarities with both off-eutectic bonding and the TLP and SLID type bonding technologies, as will be explained in the coming sections.

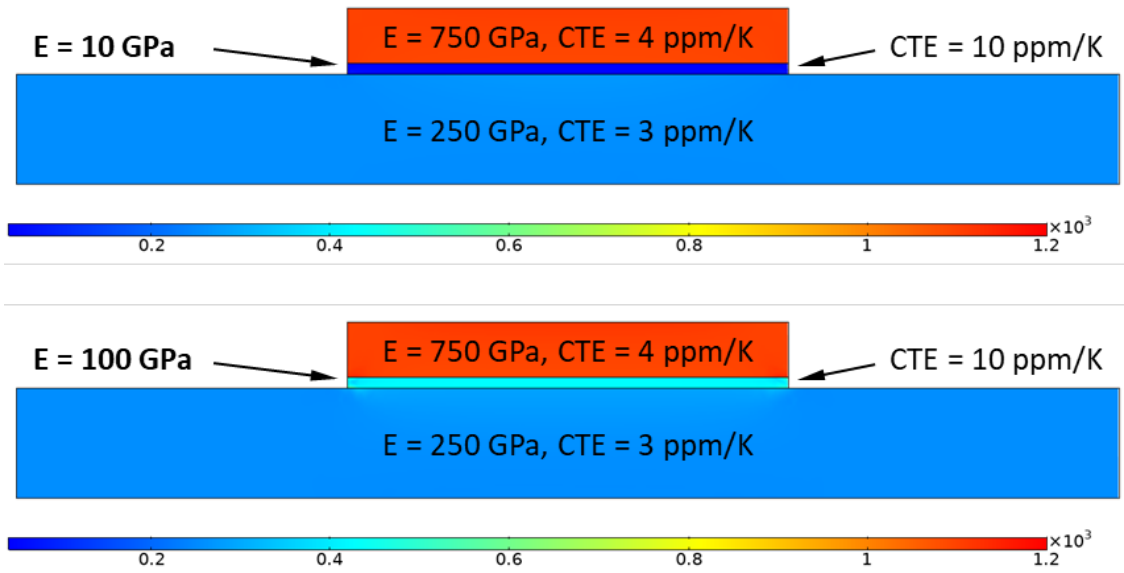

Fig. 11 Plot from a finite element analysis showing the stress field distribution in two identical systems consisting of a die, a joint, and a substrate. The stress is caused by dissimilar coefficients of thermal expansion when exposed to a thermal load. The only difference between the two models is the stiffness of the joint: 10 GPa *vs*. 100 GPa. The stress state is significantly lower in the softer joint (10 GPa).

2.1.2 Joint configuration

In its simplest form, the pre-joint system comprises two basic components: a substrate consisting of a compound with a high melting point, and an interlayer with a low melting point. The high melting point material (HMP) can be deposited onto another substrate, such as solder bumps on electronic circuit boards. The low melting point or melting point depressant material (MPD), may be in the form of a preform or can be deposited directly

onto the substrate. The main purpose of the MPD is to reduce the process temperature. It may be either a pure element or a compound; an alloy or intermetallic compound, with a relatively low melting point. Its liquid state enables low bond line pressures during bonding, like soldering and TLP bonding. The MPD is used as an interlayer between two adjoining layers comprising the HMP, such as depicted in Fig. 12. The HMP is the main component in the final joint. It makes up the solid structure in the final joint at elevated temperatures. The HMP is used as a seed layer during fabrication to dilute the solute concentration in the final joint, unlike regular off-eutectic bonding which uses an off-eutectic solder compound. The reaction between the HMP and MPD cause the joint to reach the desired composition and microstructure, and to transform a discretely layered structure HMP / MPD / HMP into one compound, a mixture of HMP and MPD.

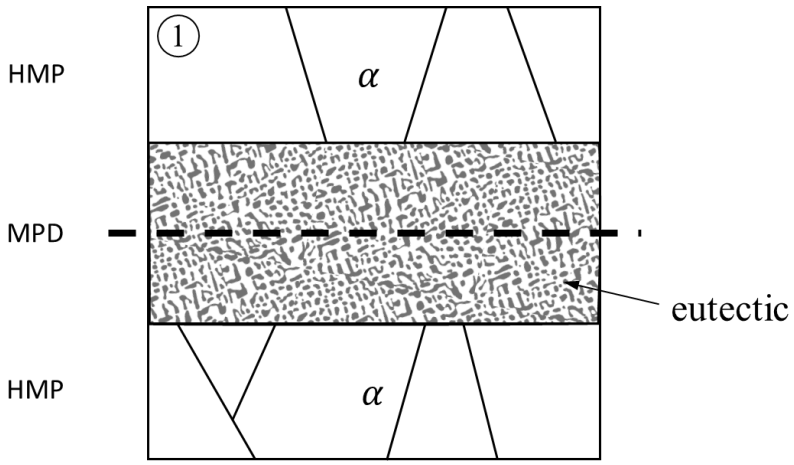

Fig. 12 Schematic illustration of a pre-joint configuration. A melting point depressant (MPD) material is represented by an interlayer of a eutectic composition comprising two phases; eutectic α and eutectic β. The interlayer is adjoined between two substrates of a high melting point material (HMP) made of a single phase, the α phase. The structure/microstructure corresponds to point one in Fig. 13 where the position of mark ① in the phase diagram represents the average composition in the center of the joint, indicated by a horizontal dashed line in the illustration.

2.1.3 Joint formation

This section describes how I interpret and believe LSD joints are formed. The joint formation can be divided into four different stages:

- Melting
- Dissolution
- Solidification
- Dehomogenization

The process flow and remelting are illustrated with a eutectic phase diagram in Fig. 13. A brief description of the different stages, as envisaged, is given in the following sections. The illustrations in the following sections are not to be interpreted as depictions of real microstructures. They are mere illustrations. Thus, crystals may have different shapes than indicated in the illustrations, *e.g.*, real crystals in real microstructures may have curved boundaries and rounded corners. Also, each numbered point in Fig. 13 represents the average composition in the center of the joint, as indicated by a horizontal dashed line in the illustration in Fig. 12. The concentration of each phase will vary through the joint as it evolves. Examples of the concentration distribution through the joint is given in Fig. 14 and Fig. 15. For a more detailed description on the evolution of the concentration distribution in a joint during solid-liquid interdiffusion, the reader is directed to Fig. 1 in Cook and Sorensen's review of TLP bonding[44], or Fig. 3 in Gale and Butts review on TLP bonding[45] or one of the articles by MacDonald and Eagar on TLP bonding[46,47].

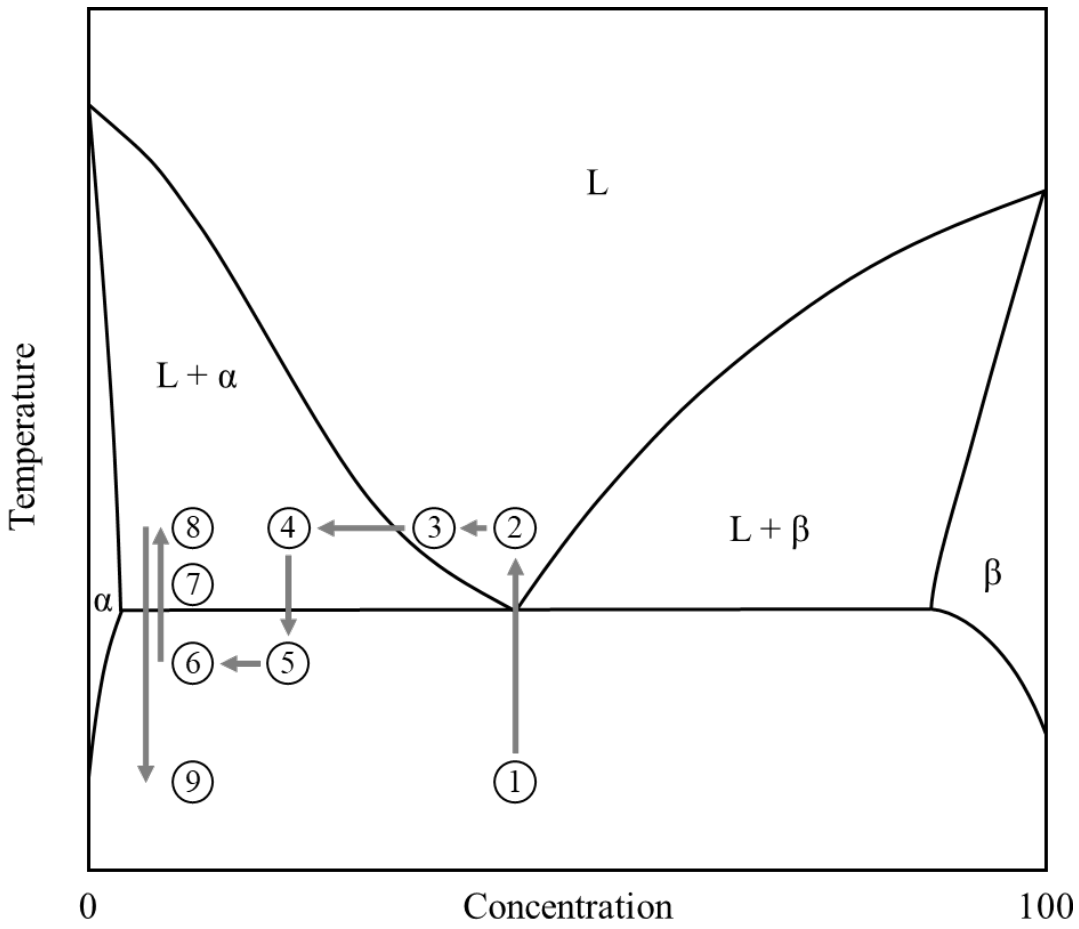

Fig. 13 Illustration of the process flow and remelting in a eutectic system. Each numbered point represents the average concentration in the center of the joint, as indicated by a dashed line in the illustration in Fig. 12.

Melting

During heating, solid–solid interdiffusion between the adjoined layers is first initiated, and dissolution of the high melting point material (HMP) starts. The bond region is heated up above the melting point of the MPD interlayer. The interlayer melts rapidly to form a liquid (L) which wets the adjoining bond layers (HMP), see Fig. 14. The liquid conforms with the surface roughness filling surface features and reducing void formation caused by rough interfaces.

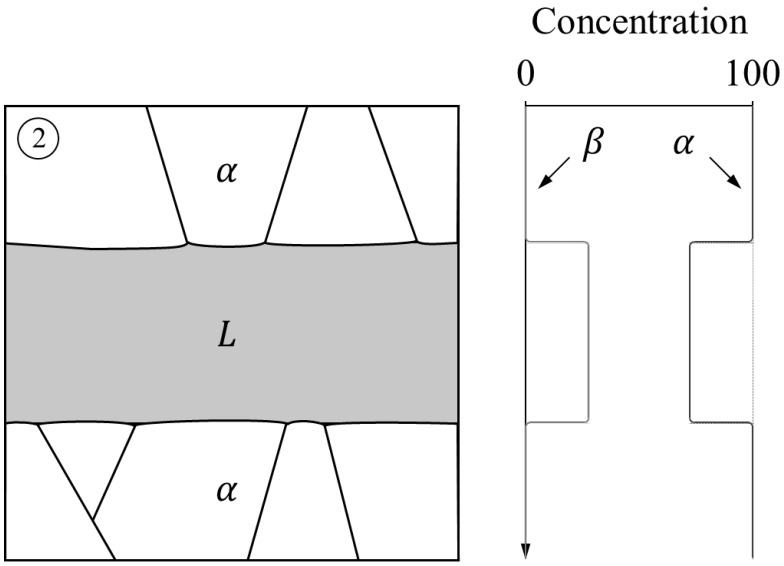

Fig. 14 Illustration of the joint after melting of the MPD, corresponding to point two Fig. 13. A liquid (L) phase is formed between the solid substrate surfaces. The concentration of each phase, α and β, through the joint, is indicated in the concentration graph to the right.

Dissolution

At temperatures above, or well above, the melting point of the MPD interlayer, the interlayer is completely melted. To conserve mass, rapid solid–liquid interdiffusion dissolves parts of the HMP layers, also known as melt back, corresponding to point three in Fig. 13 and Fig. 15. Continued dissolution of the HMP partially initiates the solidification process. Excess HMP beyond the solubility limit of the liquid will precipitate into crystals suspended in a liquid. These may be form either by homogenous or heterogeneous nucleation. This thesis has not studied the explicit mechanisms in detail. Crystal growth or dendrite structures start to form on the solid surfaces, see Fig. 16. The concentration of the liquid and solid compounds follows the liquidus and solidus (*cf.*

Cook and Sorensen[44]). The solid fraction in the semi-solid may be determined by the lever rule[41].

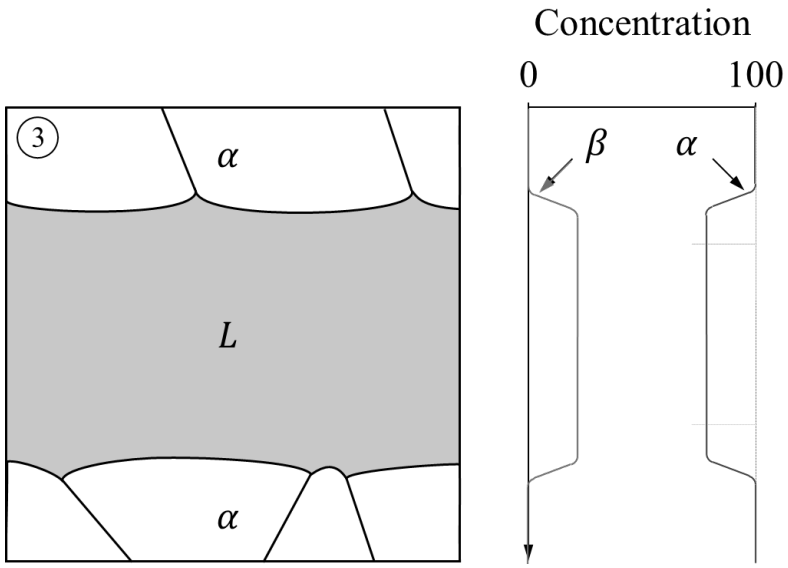

Fig. 15 Illustration of liquid growth, dissolution of the α phase into the melt (L), in the bond region consuming adjoin layers by solid-liquid interdiffusion, corresponding to point three in Fig. 13. The concentration of each phase, α and β, through the joint, is indicated in the concentration graphs to the right.

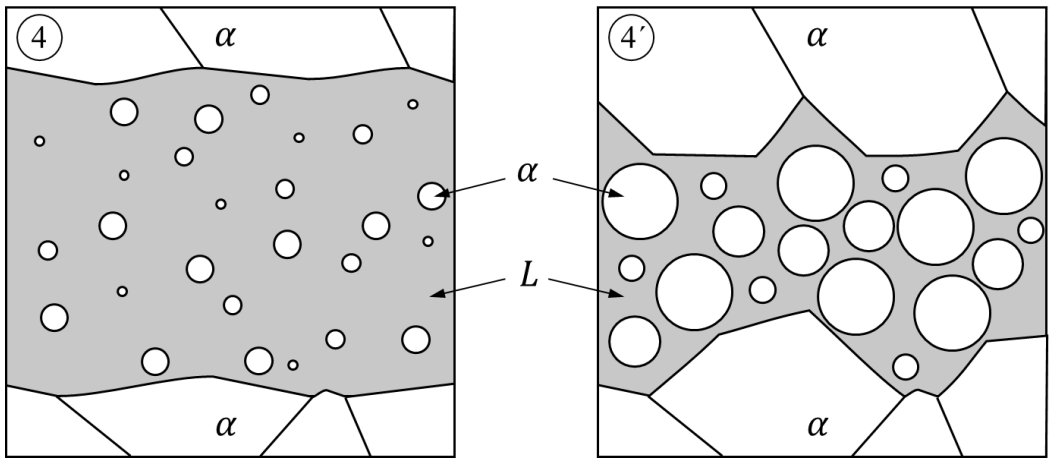

Fig. 16 Illustration of solid crystals (α) suspended in a liquid phase (L). Solid–liquid interdiffusion initiates nucleation and grain growth in the melt as well as crystal growth on the solid surfaces, corresponding to point four in Fig. 13.

Solidification

The joint region is then cooled to complete the solidification. This is unlike TLP type processes where isothermal solidification is utilized[44]. During cooling, more of the HMP

precipitate and the entire joint solidifies when the temperature is lowered below the solidus, *i.e.,* the eutectic isotherm. A mixture of two phases has now been created, as depicted in Fig. 17.

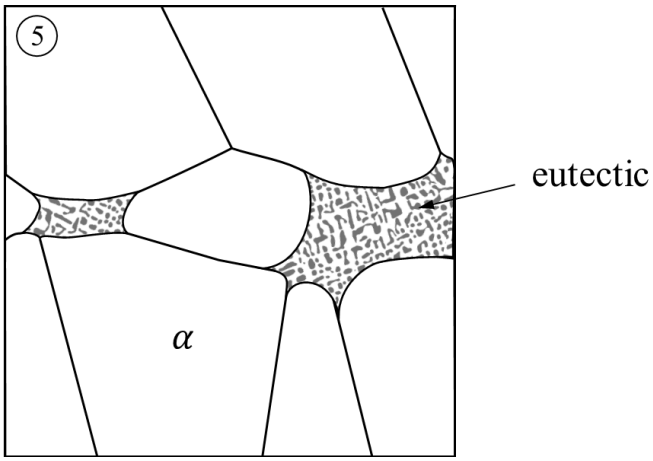

Fig. 17 Illustration of the microstructure of solidified off-eutectic joint, corresponding to point five in Fig. 13.

Dehomogenization

Continued heating cause additional HMP to dissolve into the joint region. This changes the composition of the mixture and completes the process. It also changes the microstructure of the joint. Besides grain growth, the heat also causes phase segregation of the two phases in the mixture (given enough time and heat). The phases locally relocate, and the solute accumulates at corners, edges, and boundaries between grains[48,49], as shown in Fig. 18. The diffusion process is driven by grain boundary segregation and grain boundary diffusion[26]. In contrast, a typical TLP type process aims to homogenize the joint to form a homogenous single-phase compound. The HMP form a porous structure with the MPD in the pores. The pores may open or closed.

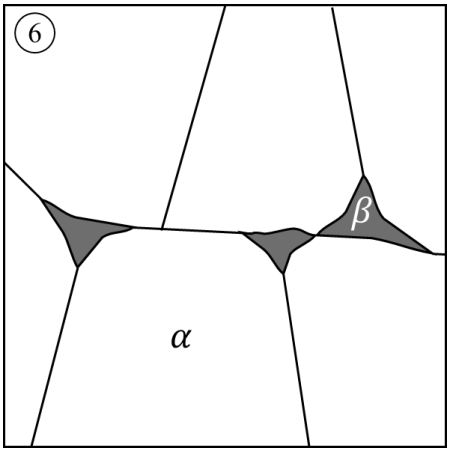

Fig. 18 Illustration of a dehomogenized joint with segregated phases/compounds, corresponding to point six in Fig. 13.

Incongruent re-melting and re-solidification

When a finished joint is reheated above the eutectic isotherm, the two phases begin to react at their interface. When enough volume of the two components has interdiffused and created an interlayer with a eutectic composition, a thin liquid phase is formed at this interface, as shown in Fig. 19. More and more of the minority phase, the solute, will react until all has diffused into the melt increasing its volume, *i.e.,* a liquid domain is formed. The remaining solid phase, the solvent, still forms a continuous and coherent solid structure through the joint. When the joint solidifies, a new morphology may form as illustrated by point mage nine in Fig. 13 and Fig. 20.

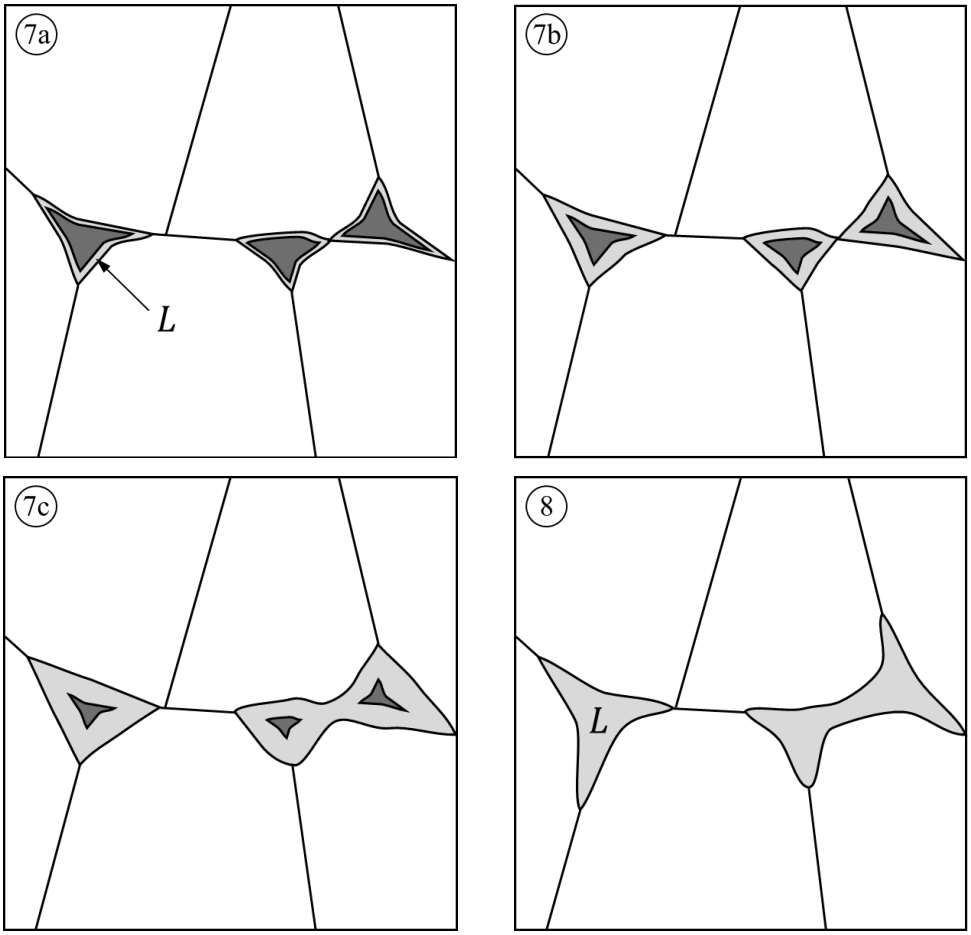

Fig. 19 Illustration of eutectic reaction at the interface between the two phases and the creation of a solid porous structure with liquefied pores, corresponding to points seven and eight in Fig. 13.

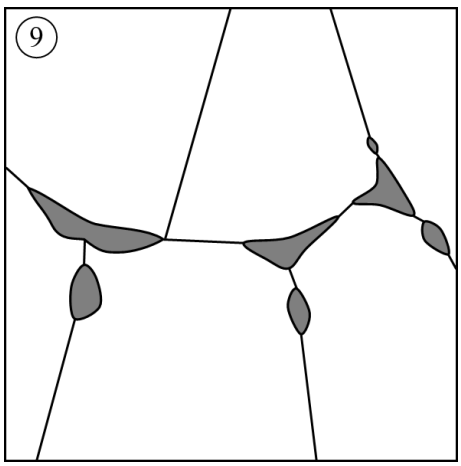

Fig. 20 Illustration of a new morphology formed by re-solidification after a re-melting step (Fig. 19), corresponding to point nine in Fig. 13.

2.1.3.1 Target composition

Following the preceding chapters, the target composition should be an off-eutectic composition near the maximum solubility limit of one phase in the other. This target composition (X_0) is marked with a dashed region in Fig. 21 illustrated by use of the Au–Ge system. It is expected that LSD joints can be used at temperatures above the eutectic melting point temperature. This thesis set off to investigate this hypothesis. Can such structures be created? Do they have sufficient structural integrity at high temperatures? Are they stable? Which material systems can be used?

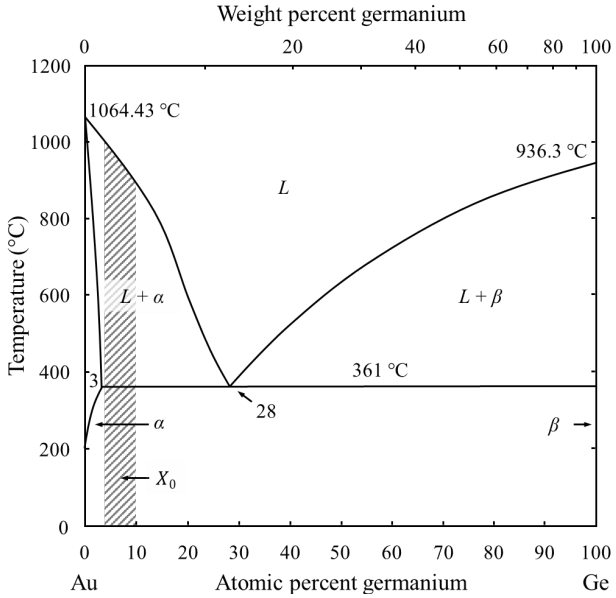

Fig. 21. The binary phase diagram of the Au–Ge system. The target off-eutectic composition, X_0, of the fabricated joints is marked with a dashed region. The phase diagram was adapted from Okamoto and Massalski[50]. The eutectic melting point varies slightly in the literature; 356–361 °C [51,52].

2.2 SLID bonding

Solid-liquid interdiffusion (SLID) bonding is also known as transient liquid phase (TLP) bonding. As pointed out by MacDonald and Eagar[46], the SLID process is a subordinated version of the TLP process. Bernstein[53] and Bernstein and Bartholomew[54] introduced the SLID process to fabricate electronic joints comprising intermetallic compounds by using the same TLP principles to form the joints. TLP type joints have been fabricated since ancient times. In *A search for structure*, Cyril Stanley Smith proposes that granules were attached to the dagger of the Egyptian pharaoh Tutankhamun (*ca.* 1323 B.C.) by use of a TLP type process[28]. A photo of the dagger taken at the *The Discovery of King Tut*

exhibition in New York City is shown in Fig. 22. Smith proposed that the small gold granules on the handle were attached by TLP type techniques described by the German monk Theophilus (*ca.* 1125 A.D.)[29] and Cellini (1568)[55]. Detailed recipes on TLP processes are also found in the eight-century *Mappae Clavicula*[30]. In more recent times, TLP is commonly accredited to Littledale who was granted a patent in 1933 on a TLP type process for joining jewellery[56]. In 1959 Lynch *et al*. published a scientific paper on the method[57].

Fig. 22 Photograph of the dagger found around the hips of the Egyptian pharaoh Tutankhamun. Granules on the dagger were likely attached a TLP type process *ca.* 3342 years ago. Photo: Courtesy of Mary Harrsch[58].

2.2.1 Concept

As mentioned in the previous chapter, TLP and SLID type joints have been thoroughly explored over the years. Thus, a brief introduction to the technology is given here. Interested readers are directed to one of many excellent papers on the topic, *e.g.*, Refs. [37,44–47,53,53,59–61]. SLID joints are formed by interdiffusion of dissimilar materials that react with each other and form new materials phases that have different properties than their parent materials. Using materials systems that have materials or compounds with a low melting point combined with seed (solute) materials that form phases with high melting points, allows the formation of joints that can be used at temperatures significantly above the process temperature required to melt the low melting point material. This makes SLID

bonding particularly interesting for high-temperature applications. Other advantages using SLID type joints include relatively low bond line pressure, compliant with rough bond surfaces (local topology), flux-less, similar materials properties as the base materials, good joint quality, and very strong joints (up to 150–200 MPa). The disadvantages include flat and well-aligned bond surfaces (non-local *e.g.* bowing), time-consuming bond process, lack of reparability, and IMC may reduce strength and ductility.

2.2.2 Joint configuration

The pre-joint configuration is similar to that of LSD joints. SLID joints are formed by interposing a melting point depressant material (MDP) between the two components to be joined together, see Fig. 12. The bond surface of the components comprises a high melting point material (HMP) with which the MDP reacts by diffusion, thus forming a new material. It is also possible to use pastes where particles of both the HMP and MDP are mixed. The paste then replaces the MDP-layer in Fig. 12. The paste reduces the diffusion length, which reduces the time to complete the joint. The downside of pastes is that they may introduce voids into joints caused by solvents or other constituents in the paste.

2.2.3 Joint formation

Like LSD, the formation of SLID joints can be divided into different stages[44–46,53,60]. In this work, these stages are defined as:

- Melting
- Dissolution
- Isothermal solidification
- Homogenization

The process flow is illustrated with a eutectic phase diagram in Fig. 23.

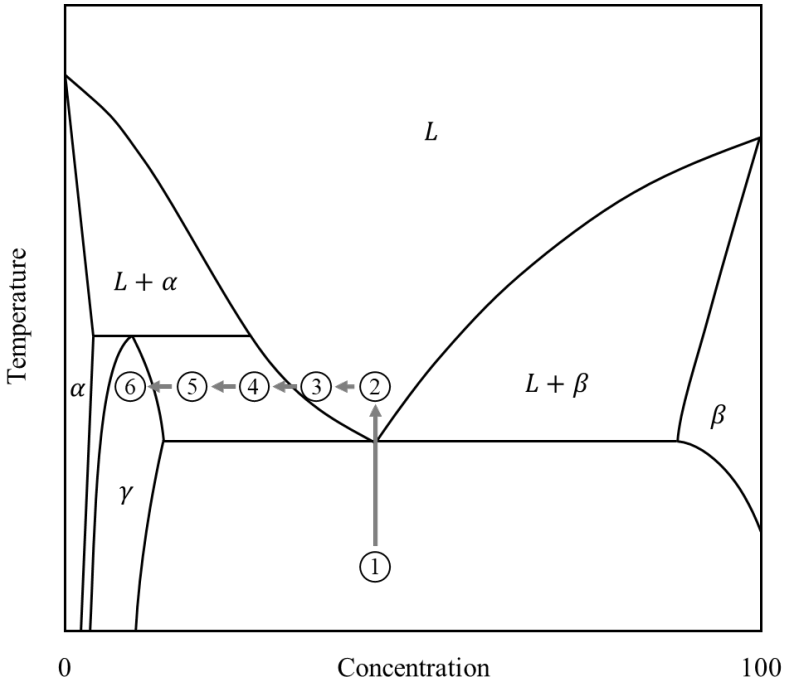

Fig. 23 Illustration of a SLID process flow in a eutectic system. Each numbered point represents the average concentration in the center of the joint, as indicated by a dashed line in the illustration in Fig. 12

Melting

Melting is essentially the same as for LSD and regular soldering, *cf.* the chapter on the formation of LSD joints (2.1.3).

Dissolution

As with LSD, the solid-liquid interdiffusion between the melt and solid seed layers (HMP) cause an intermetallic compound (IMC) to form at the interphase between the solid and liquid phases, and nucleation of crystals of the same IMC form in the melt, illustrated by the left part in Fig. 24. As time progresses, the intermetallic layer precipitates grow, and solidification of the liquid is started, see the right part of Fig. 24. This growth may be as a layer or by a formation of idiomorphic crystals, also known as scallops.

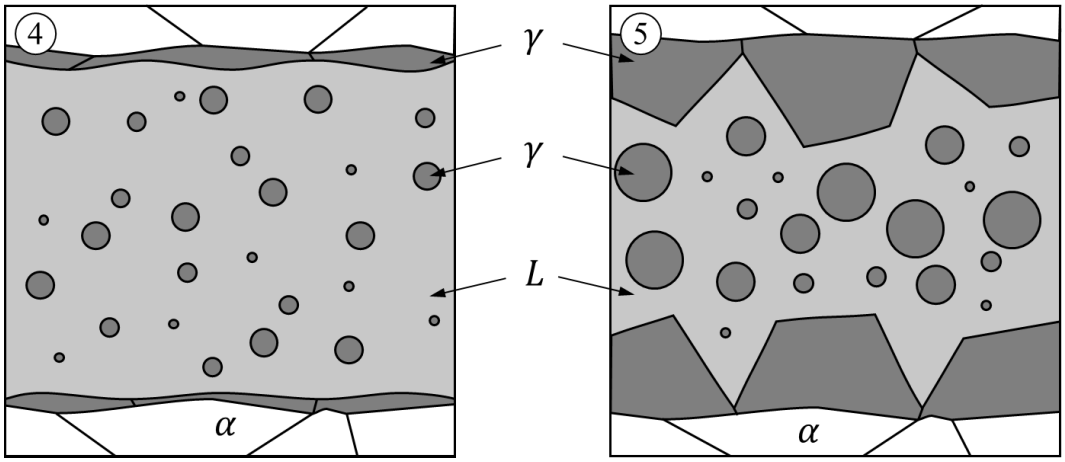

Fig. 24 Illustration of solid intermetallic crystals (γ) suspended in a liquid (L) during solid-liquid interdiffusion and crystal growth, corresponding to point four and five in Fig. 23. Idiomorphic crystals of the γ phase grow outward from the solid surface.

Isothermal solidification

The solid-liquid interdiffusion process is continued until all liquid has reacted with the solid HMP layer and solidified, see Fig. 25. The joint is now completely solid comprising a single phase or layers of intermetallic phases. There is a concentration gradient of the solute phase through the joint, with a higher concentration of the solute in the center than in the seed layers (solvent). This concentration gradient is often unwanted since the joint may evolve further during usage in an application. This can make the joint unpredictable, changing its characteristics during evolution. Thus, a homogenization step is often required to finalize the joint.

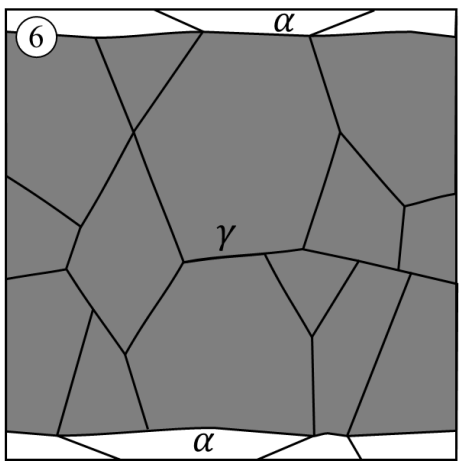

Fig. 25 Illustration of a solidified SLID joint. Most of the joint has been transformed into the intermetallic γ phase by isothermal solidification.

Homogenization

The joint is heat treated to complete the diffusion process. Heat is applied until there is a homogenous single-phase joint essentially free from concentration gradients. If there is excess seed material (solvent), the final joint will have a layered structure as in Fig. 26.

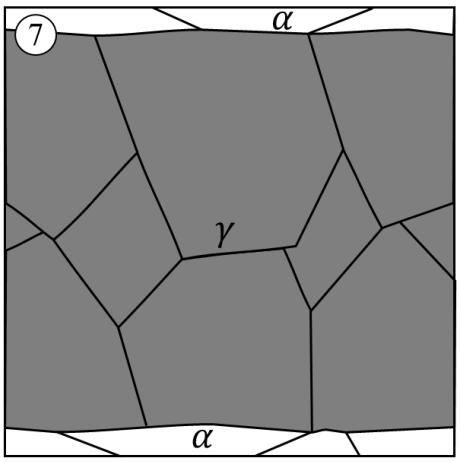

Fig. 26 Illustrations of a homogenized and finished SLID joint. Some excess α-phase remains after all β-phase have reacted with the α-phase forming a new intermetallic γ-phase.

2.3 Materials

The main goal of this project was to investigate die-attach technologies for high-temperature electronic applications. The focus has been on the die-attach itself; microstructure and morphology, joint quality, defects, electromechanical characteristics, stability, and evolution. To facilitate investigations, different types of test structures were used in this work. The purposes of the different test structures are summarized in Table 1, and their materials configurations are shown in Table 2. Initially, thermoelectric elements were used (test structure **0**) and intended to be used for subsequent test structures with SLID type joints. Due to long lead times and inadequate materials quality of the thermoelectric element, such test structures were abandoned. *E.g.*, the mechanical strength of the joints was significantly stronger than the strength of the thermoelectrical elements themselves. Therefore, it was not possible to measure the shear strength of the joints, since the elements fractured prematurely at low loads. Nor did the elements survive sample preparation for cross-sectioning. Thus, it was not feasible to use them for characterization of the fabricated joints themselves.

Table 1 Purpose of the test vehicles used in this work.

	Purpose
0	Evaluate Ni–Sn SLID joint quality when joining thermoelectric elements ($CoSb_3$) to ceramic substrates (Al_2O_3) and study stress fields in joints by finite element analysis (FEA).
I	Evaluate Ni–Sn SLID joint quality and composition as a function of different process parameters.
II	Evaluate the effective detachment temperature of Au–Ge LSD joints and investigate wetting and the eutectic reaction of a thin Ge layer on a thin Au layer (2-3 µm) substrate and die.
III	Eutectic Au–Ge preform replaced the thin Ge layer in test structure **II**.
IV	Bonding with eutectic Au–Ge preform and thick Au layer (22 µm) on a substrate and die.
V	Perform electrical characterization and investigation on microstructural evolution at high-temperature storage in Au–Ge LSD joints.
VI	Join a high-temperature compatible device (SiC) with a high-temperature compatible substrate (Si_3N_4) using Au–Ge LSD bonding and evaluate the shear strength at high temperature.
VII	Evaluation of a Bi_2Te_3 based thermoelectric module at high temperatures compared with a $CoSb_3$ based module.

Table 2 Material configurations for the test vehicles, defined in Table 1, used in the experiments.

	Die-attach	**Materials stack before bonding** **Layer thickness (µm)**			**Publ.**
		Substrate	**Preform**	**Die**	
I	SLID Ni–Sn	Si | TiW | Ni | Sn 525 | 0.15 | 3 | 2	-	Sn | Ni | TiW | Si 2 | 3 | 0.15 | 525	7
II	Off-eutectic Au–Ge	Si | TiW | Au 525 | 0.15 | 2.8	-	Ge | Au | TiW | Si 0.4 | 2.8 | 0.15 | 525	-
III	Off-eutectic Au–Ge	Si | TiW | Au 525 | 0.15 | 2.8	$Au_{72}Ge_{28}$ 25	Au | TiW | Si 2.8 | 0.15 | 525	5
IV	Off-eutectic Au–Ge	Si | SiO_2 | Ti | Au 525 | 0.3 | 0.03 | 22	$Au_{72}Ge_{28}$ 35	Au | Ti | SiO_2 | Si 22 | 0.03 | 0.3 | 525	3
V	Off-eutectic Au–Ge	Ti | Au 0.03 | 22	$Au_{72}Ge_{28}$ 35	Au | Ti 22 | 0.03	1,3
VI	Off-eutectic Au–Ge	SiC | Ni | Au 330 | 0.3 | 5	$Au_{72}Ge_{28}$ 35	Au | Ni–P | Cu | Si_3Ni_4 | Cu | Ni–P 5 | 3 | 150 | 635 | 150 | 3	2

2.3.1 Die and substrate

A die, also called a chip, is a piece of semiconductor material that is used to create electronic components. Components include integrated circuits (IC), transistors, diodes, and micro-electro-mechanical system (MEMS). Si is by far the most commonly used semiconducor material. The silicon on insulator (SOI) concept is a Si device. It has a buried silicon dioxide (SiO_2) layer between a silicon device layer (active) and a silicon wafer (passive bulk), which makes it more robust and more reliable, especially at higher temperatures. Thus, it is a natural choice to evaluate a die-attach in a system that comprises Si dice. Si wafers are also readily available, and an inexpensive material

compared with wide-bandgap materials. Therefore, investigations were done on systems including Si as the structural component, test structure **I**-**IV**

The die and substrate were omitted from test structure **V** to create a joint free from thermomechanical stress imposed on the joint by the die and substrate due to dissimilar material properties; *i.e.,* the coefficient of thermal expansion (CTE), Young's modulus, and Poisson's' ratio.

SiC is a preferred choice for high-temperature power electronics applications[7,19,62,63]. Ceramic substrates are the preferred choice for high-temperature applications due to their robustness, stability, and thermomechanical material properties. The substrate, or circuit board, is the backbone of electronic systems. It is the base onto which other components are attached and connected into a system. The substrate shall provide electrical isolation, structural support, and transport excess heat from the system. Thus, in test structure **VI**, SiC dice were attached to ceramic Si_3N_4 substrates. The substrates had thick active metal brazed (AMB) conductors of Cu on them.

2.3.2 Metallization scheme

The different metal layers between dice and substrates have different purposes or functions. The main functions are:

- Adhesion layer – Ensure adequate adhesion to the die or substrate.
- Diffusion barrier – Prevent diffusion between different adjacent layers in the layer structure.
- Wetting layer – A surface layer which provides good wetting properties with the used die-attach material. Often referred to as top metallization.
- Conductive layer – Provides the electrical connection between discrete components on the circuit board.

Sometimes one layer can be used for more than one function. *E.g.*, Au can be both an excellent wetting layer and a conductive layer and Ti may be used as both an adhesion layer and as a diffusion barrier.

As can be seen in Table 2, three different metallization schemes were used in the test structures. $Ti_{10}W_{90}$ was used in the initial test structures, **I** to **III**, to create a combined adhesion layer and diffusion barrier. Ti was used because of its well-known good adhesion properties to Si[64,65] and W is known to be a good diffusion barrier[31,66,67]. Due to delamination issues, W was omitted from the layer in test structure **IV**, and SiO_2 was included to improve adhesion properties. Ni was used as a combined adhesion layer and diffusion barrier in test structure **VI**. In test structure **I** Sn was used as the wetting layer (top metallization), while Au was used as the top metallization in test structures **II**–**VI**. The relatively poor adhesion of test structure **IV** was used to enable lift-off the metallization to be used in a structure without die and substrate, *i.e.,* test structure **IV**.

2.3.2.1 Layer thickness

When designing joints formed by SLID or LSD bonding, it is important to design the layer thickness so that the desired composition or phase may be formed. One simple approach to do this is to calculate the number of atoms of each element in the metallization on the bond surfaces and preforms before joining commences. For single element layers, one can calculate the volume of each bond layer and then calculate the number atoms (N_n) in each layer by

$$N_n = \frac{\rho_n a_n t_n}{M_n} = \frac{\rho_n V_n}{M_n} \tag{8}$$

where ρ_n is the density, a_n is the footprint area of the layer, t_n is the thickness of the layer, V_n is the volume, and M_n is the atomic weight of element n. The atomic concentration X_n of element n at thermodynamic equilibrium is the number of atoms of that element divided by all atoms in the compound, $\sum_i N_i$, according to

$$X_n = \frac{N_n}{\sum_i N_i} \tag{9}$$

When using a eutectic preform during joining, one can decompose each elemental component in the preform into an equivalent volume. For binary compounds comprising elements A and B, this may be done by calculating their relative volumetric ratio (γ) by

$$\gamma = X_{\mathrm{B}} \frac{\rho_{\mathrm{A}} M_{\mathrm{B}}}{\rho_{\mathrm{B}} M_{\mathrm{A}}} \tag{10}$$

where X_{B} is the atomic concentration of component B in the preform, $\rho_{\mathrm{A,B}}$ is the density and $M_{\mathrm{A,B}}$ is the atomic weight of elements A and B. The equivalent layer thickness may then be calculated according to

$$t'_{\mathrm{B}} = \frac{t_{preform}}{1 - \gamma^{-1}} \tag{11}$$

$$t'_{\mathrm{A}} = t_{preform} - t'_{\mathrm{B}} \tag{12}$$

The required thickness of the melting point depressant (MPD) and seed layers on dice, substrates, and in preforms may be determined using this technique. An illustration of the equivalent layers of a seed layer / preform (MPD) / seed layer structure is shown in Fig. 27.

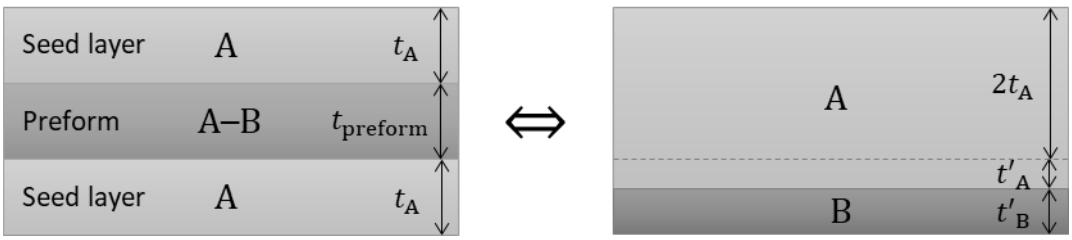

Fig. 27 Schematic illustration of a seed layer / preform / seed layer configuration (left) and its corresponding decomposition into two equivalent layers (right).

2.3.2.2 Preforms

Eutectic Au–Ge preforms were used in test structure **III-VI**. The thickness varied from 25 µm to 37 µm between different acquired foils. Both sheets, 50 mm by 50 mm, and 1 mm wide tapes were used. Cross-sections of preforms showing the microstructure can be seen in Fig. 28. The composition was measured to be between 28-39 at.% Ge.

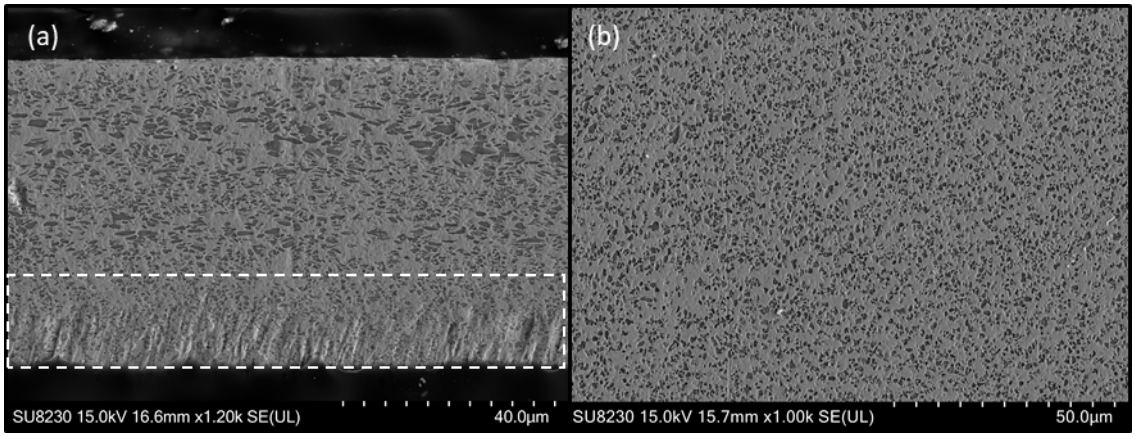

Fig. 28 SEM images of cross-sections of virgin preforms used in this study. (a) shows a cross-plane section. The dashed box marks a region with smeared material from sample preparation. (b) shows an in-plane section. Dark grey is Ge, and the lighter grey is Au.

2.3.3 Die-attach

2.3.3.1 Au–Ge LSD

Both the Au–Ge and the Au–Si systems are good candidates for initial investigations of the LSD method because of their simple phase diagrams with large two-phase fields regions. Both phase diagrams comprise a deep eutectic point and a wide compositional range in the two phase-field state. *I.e.,* when an off-eutectic compound is in a partially melted state, a significant fraction may be in a solid state at temperatures significantly above the eutectic isotherm, within a reasonably large compositional range. Both systems have also shown excellent high-temperature performance of the eutectic composition demonstrating significant shear strength capacity at high temperatures[5,68,69] (up to 300 °C) and excellent thermal cycling capacity[70,71] (-40 °C to 300 °C) which makes them good candidates for high-temperature applications. The Au–Ge was chosen primarily because of previous experience with it and that preforms were easily available for initial testing, which showed promising results. Also, a review on eutectic Au–Ge joints showed great high-temperature compatibility up to around 300 °C[72] which made the Au–Ge system a suitable candidate for this work.

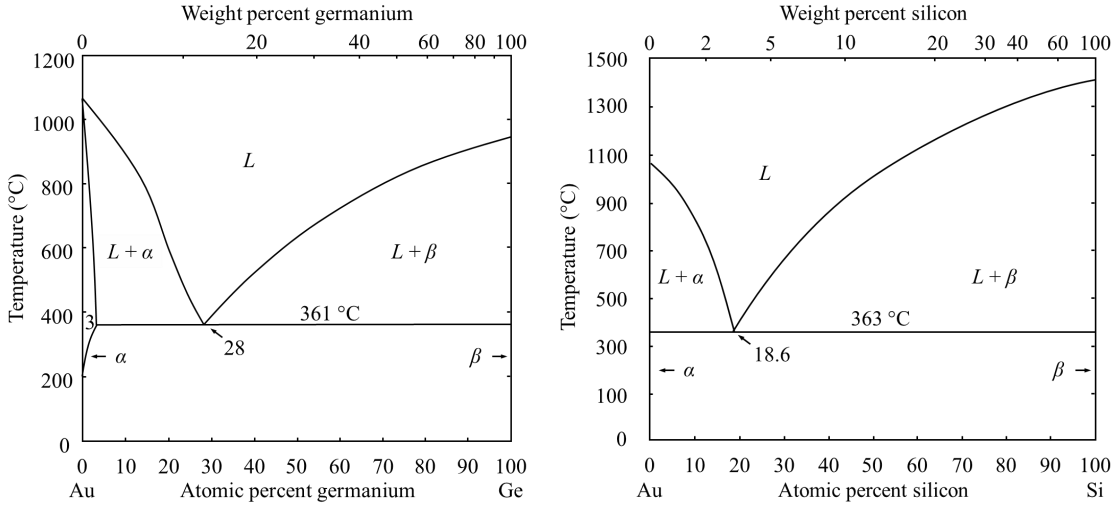

Fig. 29 The gold–germanium (Au–Ge) and gold–silicon (Au–Si) systems. Both have a deep eutectic point and large two-phase field regions ($L + \alpha$ and $L + \beta$). The phase diagrams were adapted from Okamoto and Massalski[50,73].

2.3.3.2 Ni–Sn SLID

The binary Ni–Sn system was chosen as a suitable candidate to form reliable high-temperature compatible joints for thermoelectric modules[74]. Ni and Sn are relatively inexpensive materials which makes them interesting for high-volume applications. The Ni–Sn system also has three intermetallic phases that all have a high melting point, see Fig. 30. This makes them possible candidates for high-temperature applications. Their thermomechanical material properties are also a good match to common thermoelectric materials as can be seen in Table 3. Sufficient sources of material data were not found for the Ni_3Sn_2 and Ni_3Sn phases. Thus, they were excluded from Table 3.

Table 3 Critical materials properties for high-temperature application of Ni and the Ni_3Sn_4 phase compared with two common thermoelectric materials; $CoSb_3$ and Bi_2Te_3.

Material	**Coefficient of thermal expansion (CTE) ppm/K**	**Youngs modulus GPa**	**Poisson's ratio**
Ni	13.4–16.1[75,76]	180–225[75]	0.29–0.32[75]
Ni_3Sn_4	13.4–21[76,77]	127.7–138.9[77]	0.315–0.345[77]
$CoSb_3$	9.1–13.5[78]	133–148[79]	0.20–0.25[79]
Bi_2Te_3	12.1–16.7[80]	37.1–52.5[81]	0.21–0.37[81]

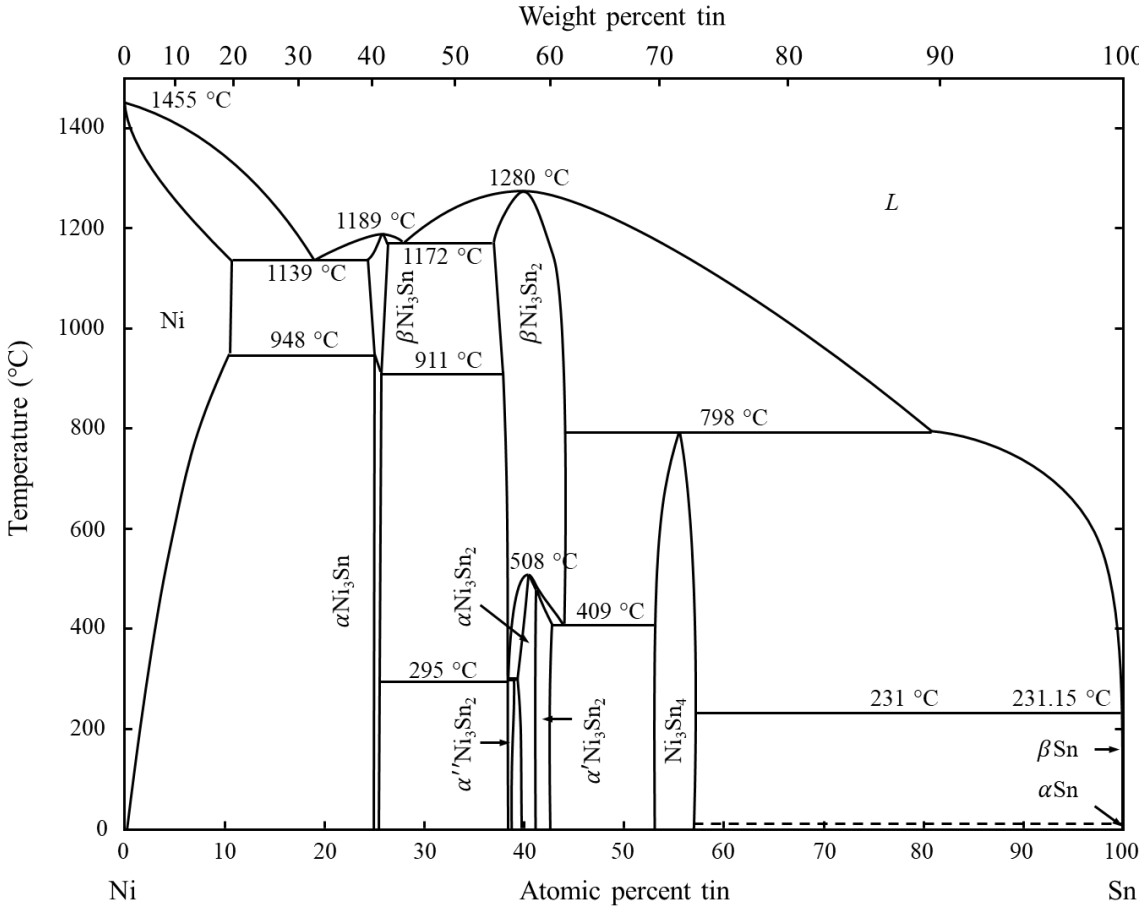

Fig. 30 The nickel–tin (Ni–Sn) system. The phase diagram was adapted from Okamoto and Massalski[82].

2.4 Process and fabrication methods

Two different types of samples were fabricated; dice joined to substrates (test structures **I**–**IV** and **VI**), and metal foils joined together (test structure **V**). The dice and preforms were manually placed onto substrates. Test structures **I**–**II** had a top metallization layer (Sn or Ge) that was used to form a MPD layer during bonding, see Fig. 31. This layer was replaced in test structures **III**–**VI** where a piece of preform (MPD) was placed between components to be joined, see Fig. 32. In test structure **V**, spacers were used to create samples with a uniform thickness, see Fig. 33. A force was used to apply a pressure on the bond line to secure a good thermomechanical contact between the adjoined components.

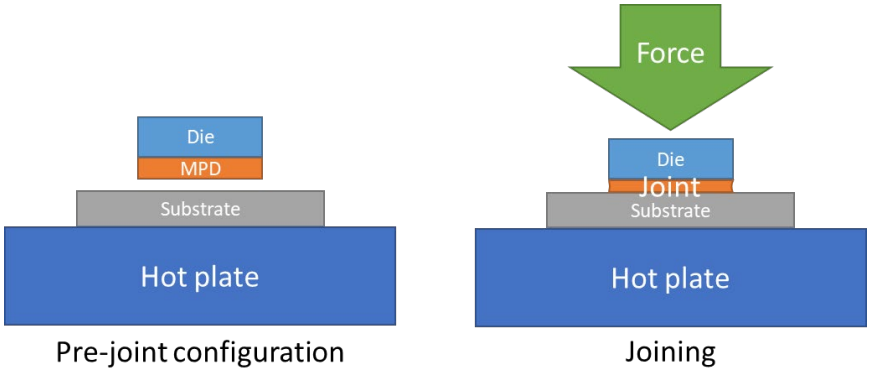

Fig. 31 Schematic illustration of materials stack and joining process for test structures **I** and **II**. The melting point depressant material (MPD) is plated onto the die.

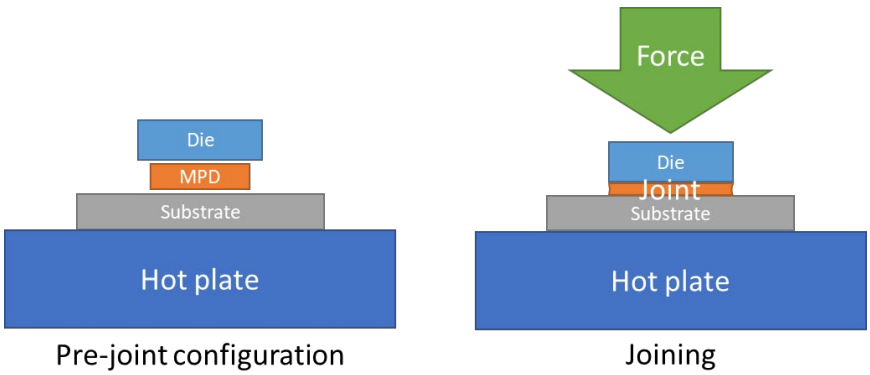

Fig. 32 Schematic illustration of materials stack and joining process for test structures **III**, **IV**, and **VI**. The melting point depressant material (MPD) is in the form of a preform.

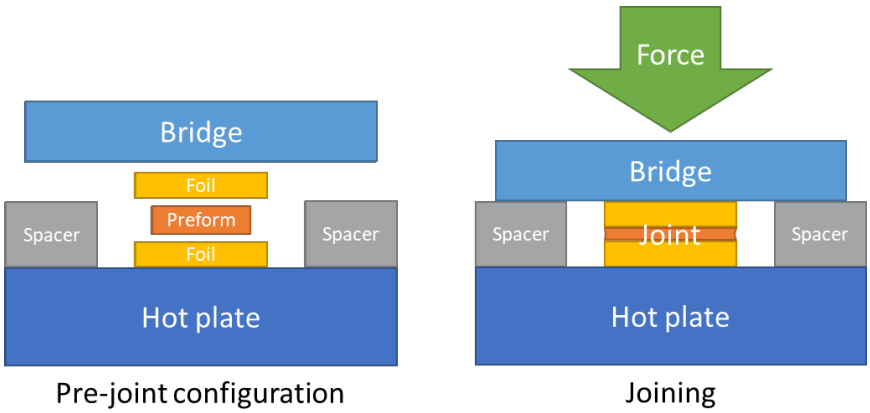

Fig. 33 Schematic illustration of materials stack and joining process for test structure **V**. The structure is without Si substrates, and the melting point depressant material (MPD) is in the form of a preform.

2.4.1 Cleaning procedure

A cleaning procedure was performed on all dice, substrate, and foils from all test structures before joining was started. First, hydrochloric acid (HCl, 10%) was used to remove any surface oxide or tough stains and coatings that may have formed during storage prior to joining. This is particularly important to the Sn top metallization layer on

test structure **I** since Sn oxidizes when exposed to the atmosphere. Secondly, they were immediately washed with acetone, isopropanol and deionized (DI) water in that sequence. Finally, the pieces were dried by blowing dry nitrogen on them. Typically, joining was commenced within a few minutes after the cleaning procedure was finished.

2.4.2 Temperature profile

The temperature profile used to fabricate joints may have a great impact on the quality of the final joints. A too cold or too brief process may lead to unfinished or incomplete joints where the desired microstructure and composition have not had time to be formed. The heating rate may influence the formation of idiomorphic structures (scallops) and voids, and cooling will affect the solidification stage. Thus, various bonding profiles were used in this study. Examples of one rapid and one slower temperature profile are shown in Fig. 34.

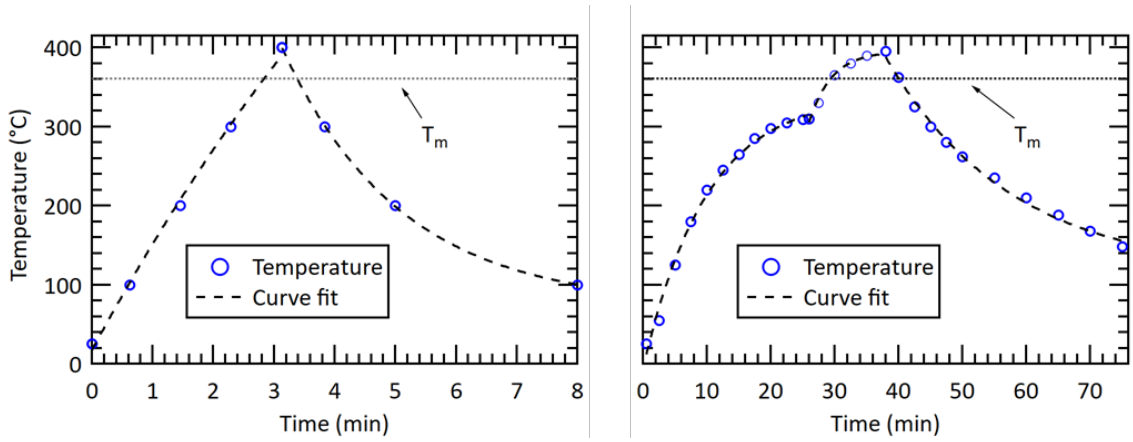

Fig. 34 Examples of bond profiles used to fabricate samples. A rapid bond profile is shown to the left and a slower bond profile including a bakeout step is shown to the right.

2.4.3 Atmosphere and wetting

The atmosphere wherein the joining process is executed may be of crucial importance to the joint quality. It is often necessary to avoid atmospheric oxygen to prevent oxidation of the bond surfaces during bonding. This may affect the wetting properties and prevent interdiffusion between the adjoined layers. Early tests on both Ni–Sn SLID and Au–Ge joints showed that exposure to oxygen should be minimized, as could be expected since both Sn and Ge can form oxides. Thus, all processes were performed in either vacuum (~1 mTorr) or dry nitrogen (~1 atm).

2.4.4 Pressure

The bond line pressure is sometimes of outmost importance to be able to form high quality joints (*cf.* sintering, thermocompression bonding, and contact melting). Both soldering and SLID type joints are created by a process that forms a temporary liquid phase at the bond line which may comply well with rough and uneven surfaces. Thus, they are less sensitive to the bond line pressure than other technologies. Nonetheless, care should be taken such that the pressure is not to low nor too high. A too low pressure for a thin liquid phase may cause wetting issues and heat transfer problems through the system. A too high pressure combined with rapid heating rate may cause a thick liquid film to be squeezed out from the joint. The squeeze out may hit neighboring structures contaminating them, or too much of the material is ejected from the joint such that the desired composition cannot be formed. A mechanical clamp or spring ball plungers were used to apply the force on the systems during bonding. Three different sizes of the spring plungers were used with a combined nominal force range of 0.5–29 N. They are shown in Fig. 36, and characterization results from the smallest spring plunger is shown in Fig. 37. The applied force was adjusted by fine-tuning the gap between ball and the base plate on the fixture (Fig. 36(b)) using blade measures with a 50 µm incremental thickness step of the blades. The clamp provided a force roughly between 5–15 N.

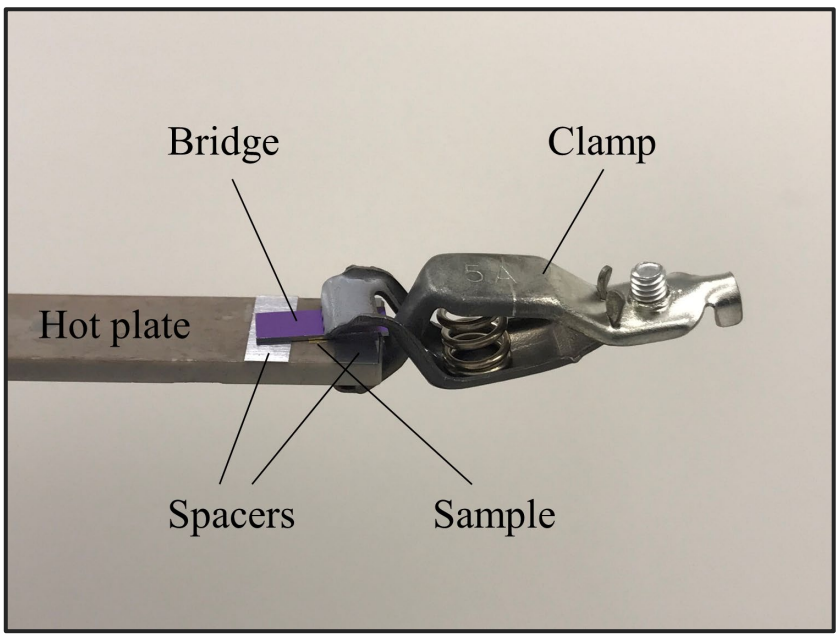

Fig. 35 A clamp was used apply a force on the materials stack during fabrication of samples. Here it is used during fabrication of sample using spacers on opposite sides of a stack of Au foil / Au–Ge preform / Au foil (test structure **V**)

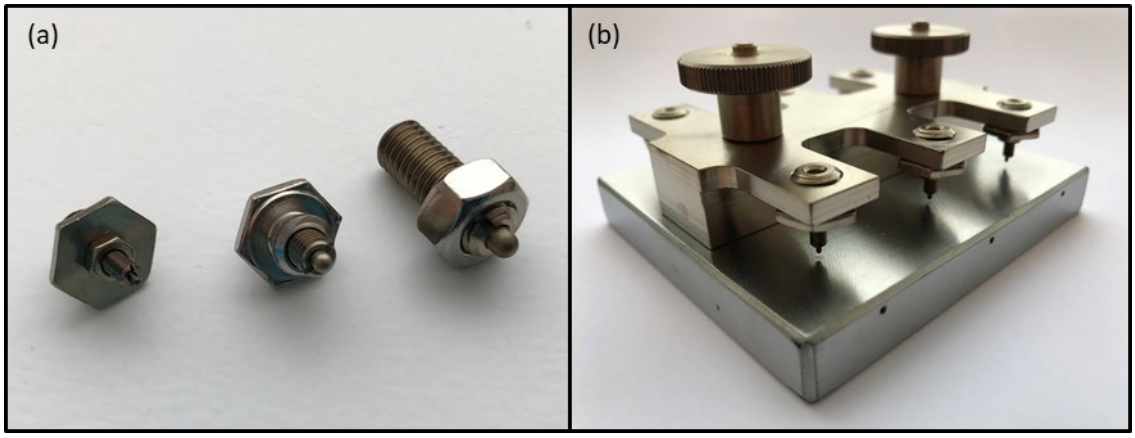

Fig. 36 Spring ball plungers (a) and fixture (b) used to fabricate test structures.

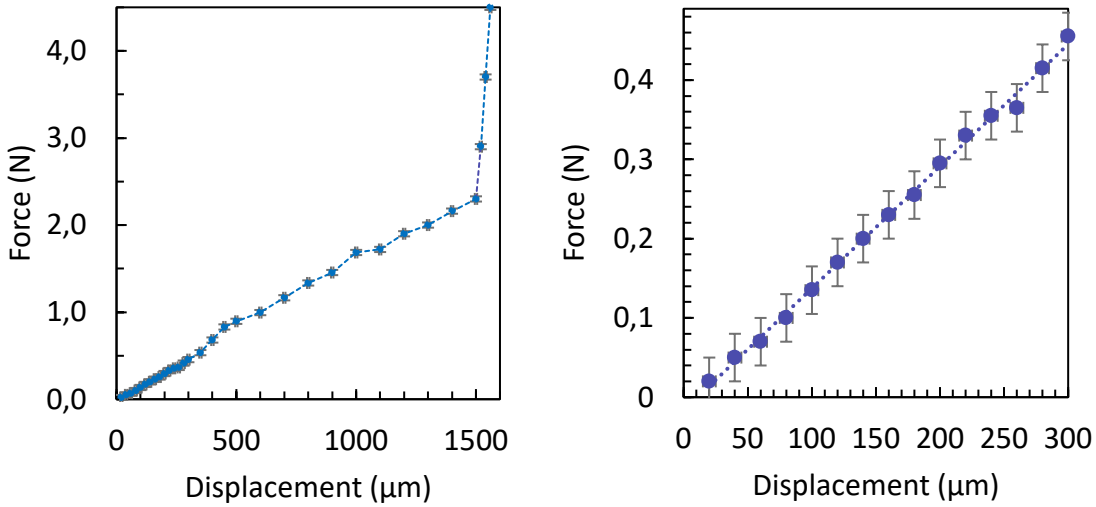

Fig. 37 Characterization results for the smallest spring plunger. The graph to the left shows the entire springe range, while the graph to the right shows a magnified section of the small displacement region.

2.5 Characterization

2.5.1 Sample preparation and microstructure analysis

Sample preparation for microstructural analysis was mainly done by making cross-sections of samples and analyzing them with different microscope techniques. Cross-sections were, in general, prepared in two orthogonal orientations relative to the fabricated joints to analyzed, see Fig. 38.

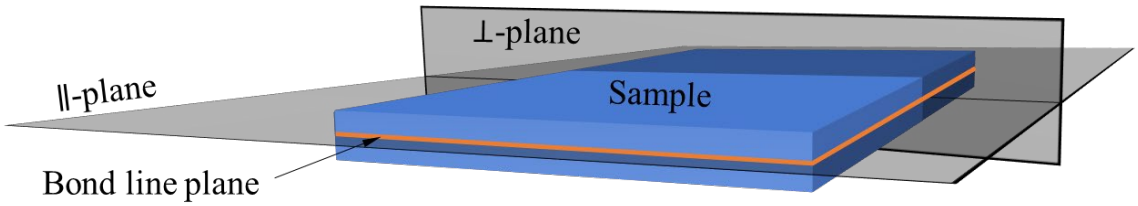

Fig. 38. Illustration defining the nomenclature used in this thesis for the cross-section planes prepared in analyzed samples.

Cross-sections were prepared with two different methods. The first method was to mold samples into epoxy and then ground and polish them until the cross-section region of interest was exposed, and there were no visible scratches from grinding left. Then, ion milling was used to prepare the final surface for analysis. The ion-milling step is crucial for several subsequent characterization procedures. If done correctly, this procedure creates excellent surfaces that are free of smearing artifacts which may conceal voids, cracks or other small features, and it exposes clear grain structures for electron backscatter diffraction (EBSD) analysis. If analysis in a SEM is commenced immediately after ion-milling is finished, this method very effectively reveals the microstructure of the sample. Grains, boundaries, phases, and orientations can easily be seen with the different detectors. *E.g.*, it is easy to see grains with all the available detectors in the SEM; upper and lower secondary electron detector, and upper and lower backscatter detectors. If samples are exposed too long in air between preparation and analysis, grains can typically only be seen indirectly by the backscatter detector. Care should also be taken such that unnecessary heating does not occur during ion-milling, since it may cause changes in the microstructure of the sample, *i.e.,* ion-milling should be kept brief, and most of the surface preparation should be done by careful grinding and polishing.

The second method also used ion-milling to expose a fresh surface for examination. First, samples were cut close to the desired location of the final cross-section. This was done by using a dicing machine or manually by cutting with a scalpel, knife or similar. Then, samples were aligned in a fixture with a hard metal screen that was withdrawn 25–100 µm from the newly cut edge. The screen secured that the ion beam could only remove material from the sample not shielded by the screen. Thus, a clean straight line along an orthogonal plane was achieved. This method can be very quick and effective. There are two apparent downsides of this method. First, since the exposure time to the ion beam can be quite long, tens of minutes to one or two hours, there is heating of the sample. The temperature

was estimated to reach above 100 °C during milling. Second, there may be traces of redeposition of removed material back onto the surface. Thus, both these effects must be considered during analysis using this preparation method.

2.5.2 Composition analysis

Energy dispersive X-ray spectroscopy (EDX or EDS) was used to analyze the composition of the different materials components in the studied samples. Accelerated electrons in the scanning electron microscope (SEM) penetrate the surface of the specimen under examination. These electrons interact with the specimen, and the SEM captures them and creates an image accordingly. X-rays generated from these interactions are used in energy dispersive X-ray spectroscopy (EDX) to determine qualitatively which elements comprise the specimens and to quantitively measure the chemical composition. Thus, it is important to know the interaction volume of these electrons during analysis to be able to correctly interpret the results. *E.g.*, the interaction volume, or rather electron range (R_0) can be estimated by the Kanaya-Okayama depth penetration formula:

$$R_0 = \frac{0.0276A}{Z^{0.89}} E_0^{1.67} \tag{13}$$

where A is the atomic weight, Z is the atomic number, and E_0 is the beam energy. Monte Carlo simulations are useful to investigate the electron trajectories within the exposed material. Monte Carlo simulations calculate the elastic and inelastic interaction of the incoming electrons with the irradiated material. Calculated electron trajectories in Ge for nine different beam energies are shown in Fig. 39 and trajectories for 13 keV electrons in nine different materials are shown in Fig. 40. One can clearly see that the interaction volume varies greatly depending on the both material and beam energy. To be able to make accurate quantitative compositional measurements one must have control of the microstructure as well as the interaction volume. Thus, small features may not always be quantified by EDX.

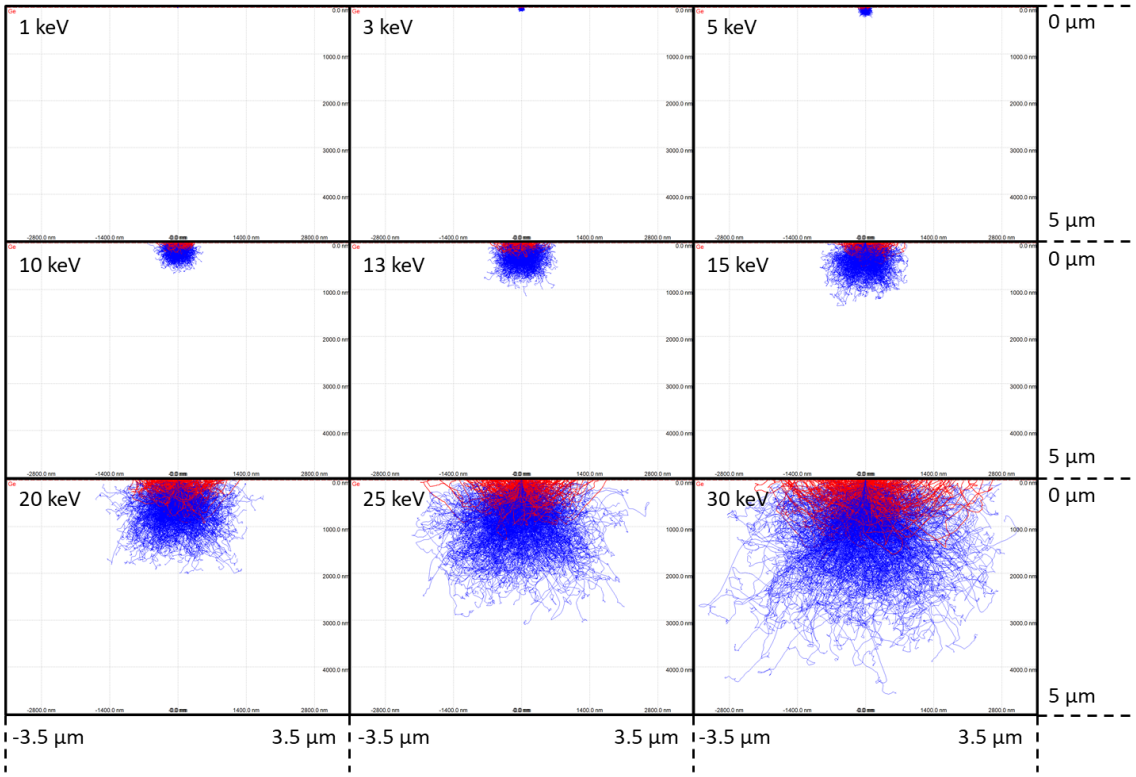

Fig. 39 Electron trajectories with nine different beam energies in Ge illustrating the interaction volume during analysis. The red lines show backscattered electrons.

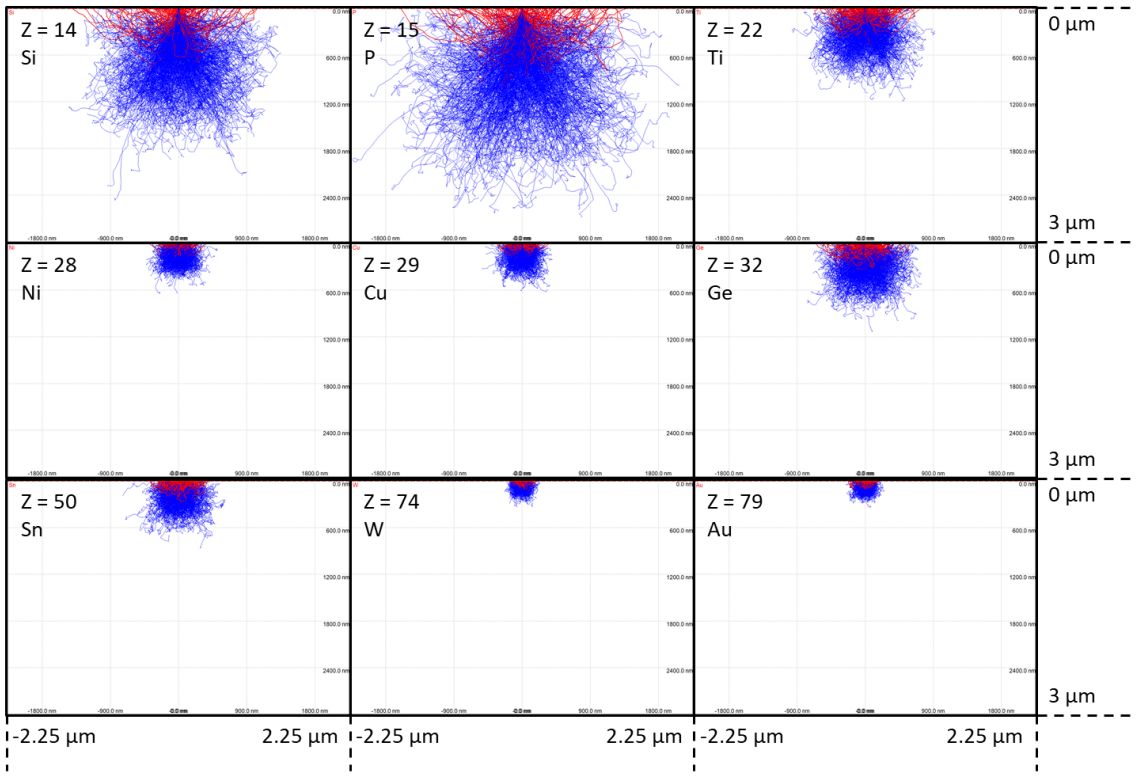

Fig. 40 Electron trajectories in nine different materials using 13 keV electron energies illustrating the interaction volume during analysis. The red lines show backscattered electrons.

2.5.3 Shear testing and failure analysis

Shear testing is one of the most widely used tests to characterize electronic joints. Despite this, shear testing is relatively seldom performed at high temperature, *e.g.*, at the operation temperature. Material properties often change as a function of temperature. *E.g.*, their mechanical properties may be significantly degraded at high temperature. The alignment, *i.e.* how parallel the contact surfaces of the shear tool and sample are, may also be critical for the results as illustrated by Fig. 38 as it may also shift the failure mode and impede on the measured strength, see Fig. 41 and Fig. 42. Thus, care should be taken when performing shear testing and subsequent failure analysis.

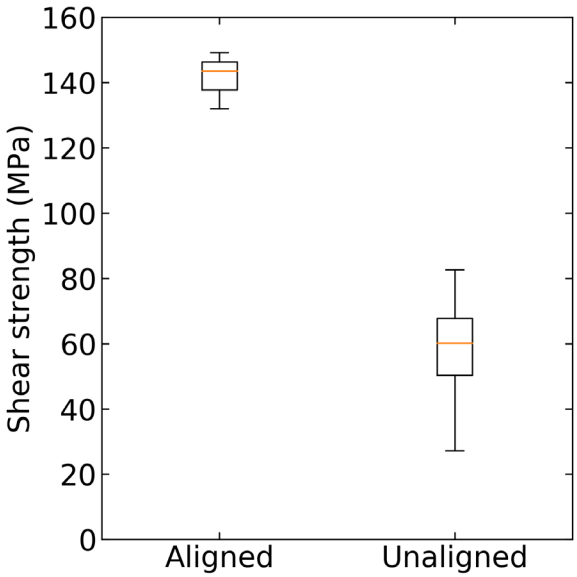

Fig. 41 Shear strength results for two identical sample groups made from test structure **VI** (SiC die joined with Au–Ge to Si_3N_4 substrate) illustrating the importance of proper alignment (parallelity of contact surfaces on shear tool and sample) during shear testing.

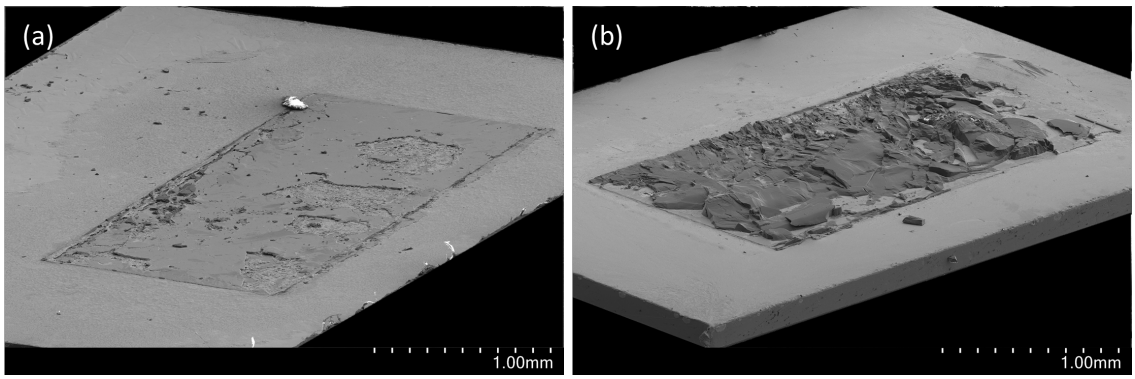

Fig. 42 Two different failure modes of two identical samples (test structure **VI)** caused by the alignment of the shear tool during shear testing. (a) Aligned (tool and sample contact surfaces are parallel) shows a mainly adhesive fracture mode while the misaligned (tool and sample contact surfaces are not parallel) sample (b) shows a cohesive fracture in the die.

Performing fracture analysis is important to understand where and why samples fail. It is the weakest link in the system that is prone to fail first. This study has used multiple tools to investigate fractures, such as optical microscope, interferometer, profilometer, SEM, and EDX. Combining several of these tools may reveal which type of fracture and in which material or layer it is located. It is common to categorize fracture as cohesive (within one material), adhesive (between two materials) or a mixture of cohesive and adhesive fracture. One example illustrating how the different techniques can be used together to investigate a fracture is shown in Fig. 43.

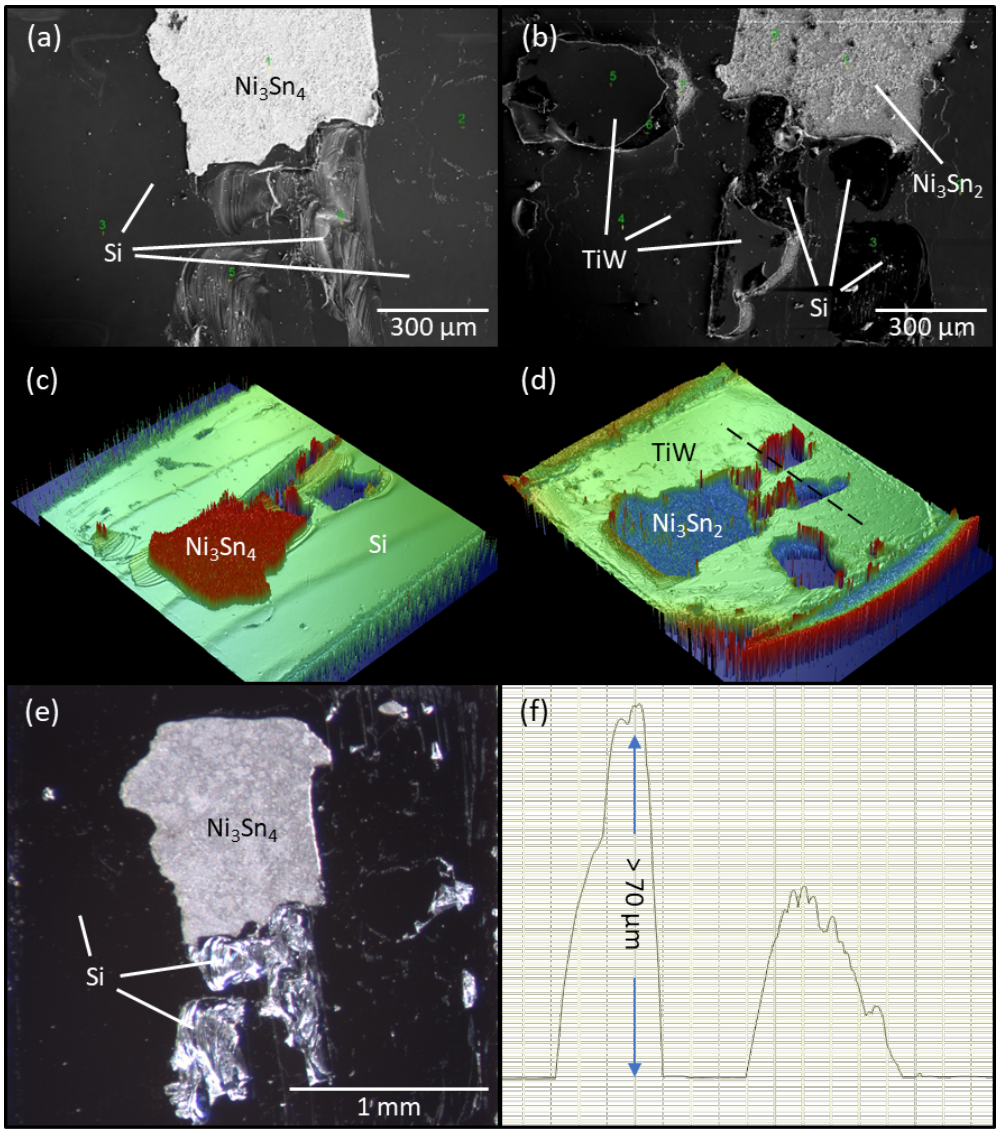

Fig. 43 Images from fracture analysis on one Ni–Sn SLID sample. (a) SEM micrograph of the die side of the fracture surface, (b) SEM micrograph of the substrate side of the fracture surface, (c) white light interferometry (WLI) of die, (d) WLI of the substrate, (e) optical micrograph of die, and (e) height profile from profilometer along the dashed line in (d). EDX was used to determine Si, Ni_3Sn_4, Ni_3Sn_2, and TiW.

2.5.4 Finite element analysis

Finite element analysis (FEA) is a powerful tool to investigate and develop an understanding of the physics at play during experimental work and to assist interpretation of experimental results. Simulations can be used to predict results, define requirements and boundary conditions for experiments. That is, FEA has been used to understand limitations and expectation of experiments and provide valuable insight to practicality of envisaged experiments. COMSOL Multiphysics was used for various finite element modeling during the project. Models include the ones published in Article 6 and Article 8, and models shown in Fig. 4, Fig. 11, and Fig. 46. Other examples include an electrical resistance model of an idealized LSD microstructure, deformation analysis of a metalized substrate, intrinsic stress inside $CoSb_3$ element exposed to a thermal gradient, a shear tool temperature impedance model, thermal-stress models of joints, validity checks of plain strain and plain stress conditions, thermal resistance evaluations, conjugate-flow, thermoelectric module concepts, and other models.

2.5.5 High-temperature shear testing

Measuring the local temperature inside the joint is troublesome. It may be both impractical or inappropriate to insert a temperature probe inside the joint itself, as it may affect the thermomechanical properties of the joint. Placing a probe on the substrate surface will give an offset reading that is hard to correlate with the real local temperature inside the joint. Instead, eutectic Au–Ge ($Au_{72}Ge_{28}$) with a well-defined melting point (361 °C) was used together with video recordings to calibrate a finite element model (FEM). Shear testing at high-temperature is a transient physics problem. The sample quickly reaches roughly the same temperature as the hot plate. When the colder tool head contacts the die, the joint temperature drops to an unknown temperature. Using video to record melting and solidification of the eutectic Au–Ge when the tool head makes contact with the die, it was possible to trim the thermal properties of the FEM to correlate accurately with the dynamics observed in the recordings. Fig. 44 shows a sample during calibration experiments and a section of the developed FEM. The force-time graphs (Fig. 45) from testing were used to define the duration of contact between the tool head and die in the FEM. The results from the FEA is presented in Article 2[83]. They show a

significant temperature drop locally in the joint caused by heat transfer from the die to the tool head as shown in Fig. 46.

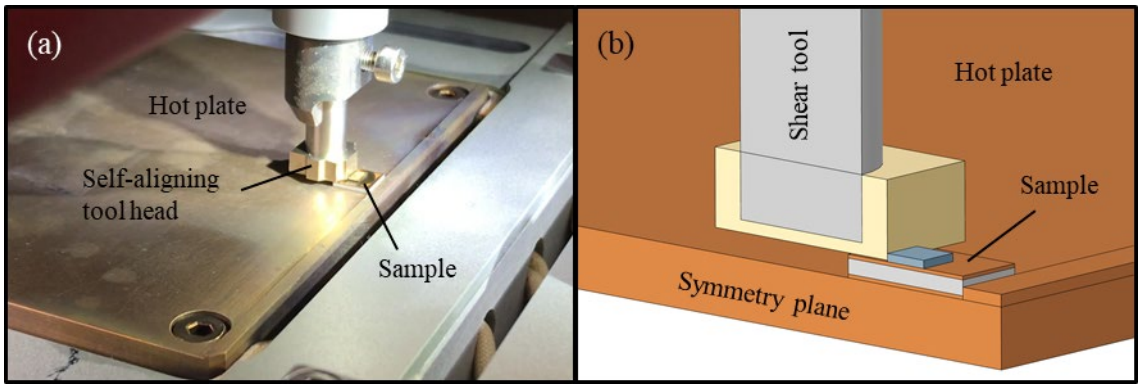

Fig. 44 High-temperature shear testing. A sample is placed onto a hot plate, and the self-aligning shear tool makes contact and applies a force to the die until it shears off. (a) Photograph from calibration experiments. (b) Section showing the shear tool in contact with the die on the sample placed onto the hot plate in the finite element model.

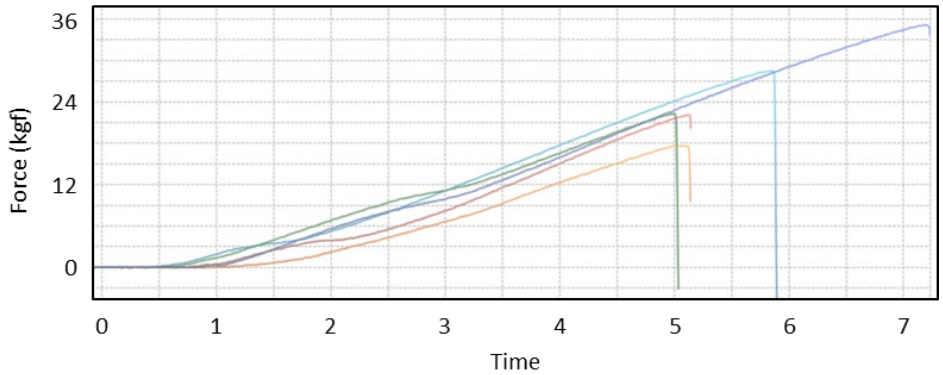

Fig. 45 Graph showing the applied force as a function of time from high-temperature shear tests. Used to calibrate a finite element model.

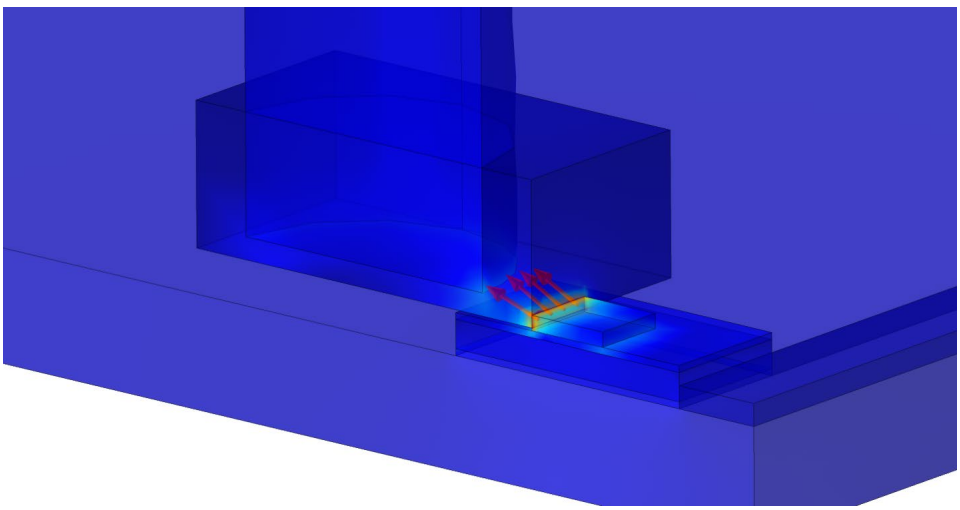

Fig. 46 Plot from finite element analysis (FEA) of the heat flux density showing significant heat transfer from the die to the tool head (red arrows).

2.5.6 Detachment temperature

An experiment to measure the effective melting point, or detachment temperature, of LSD joints, was devised. Samples were clamped onto a hot plate in a vertical orientation, see Fig. 47. Weights were hung from the attached die, and the temperature was then raised until the die sheared off. LSD joints should be able to carry a larger weight than equivalent eutectic Au–Ge joints at the same temperature and should be able to be exposed to temperatures above the eutectic melting point without dice shearing off. The tests were performed both in a vacuum (Fig. 48) and in the air. Reference samples were fabricated by using dice and substrates from the same wafers as the LSD samples but using a bigger preform and such that the joints got a near eutectic composition, with a Ge concentration between 25–28 at.%. The reference samples were used to verify that the experimental setup worked as intended. A 5-gram weight, creating a 8 kPa shear load, was enough to shear off the reference samples when the temperature reached 330–350 °C.

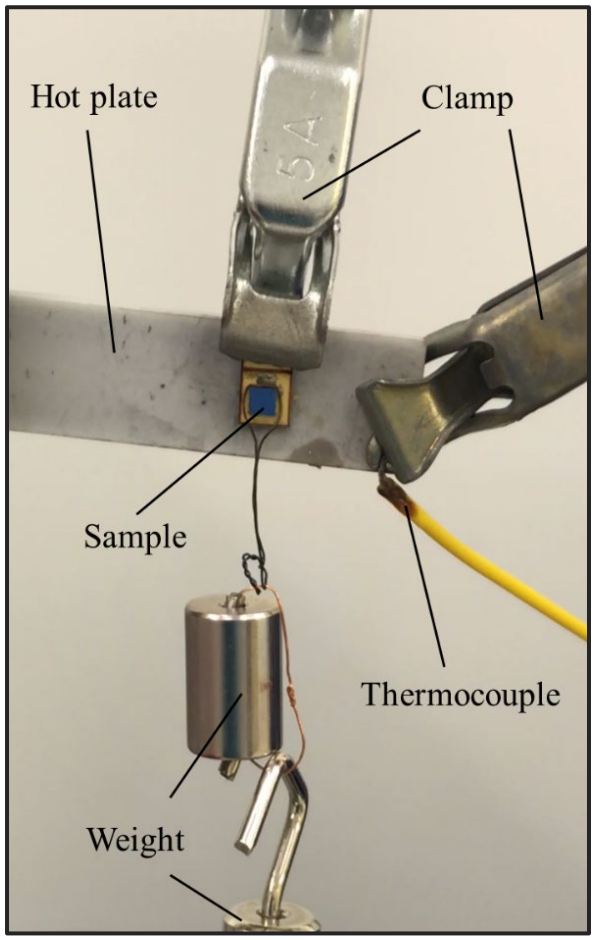

Fig. 47 Experimental setup used to measure the effective melting point of fabricated LSD joints. Weights are hanging from the die while the sample is heated until the die is sheared off.

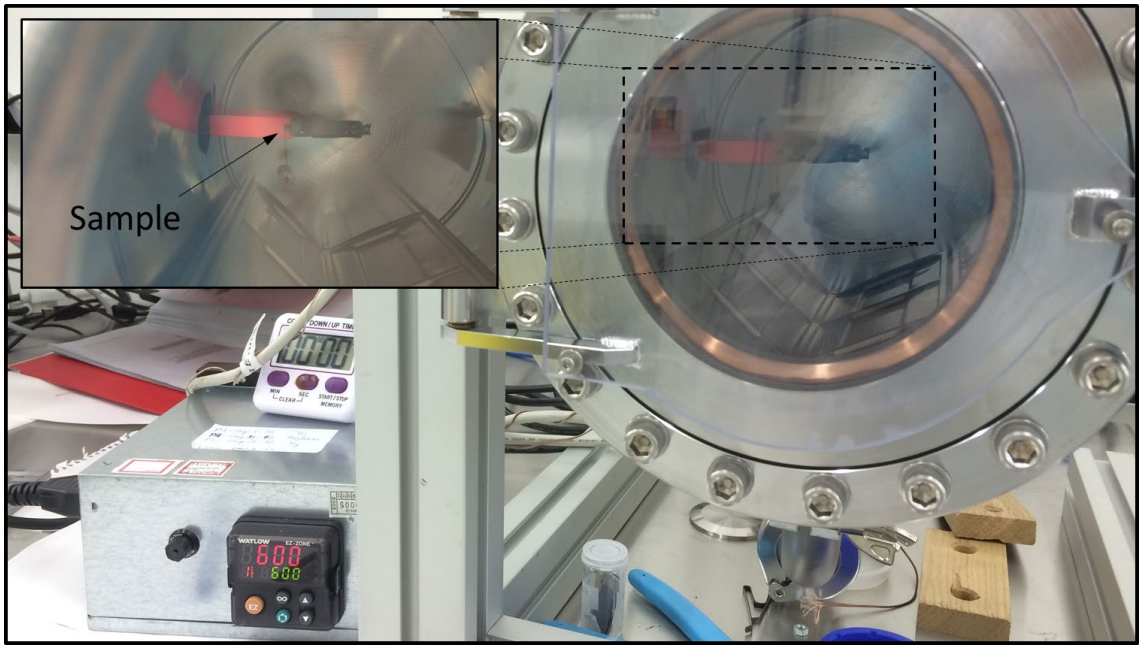

Fig. 48 Ongoing test of the effective melting point on a sample (test structure **III**) in a vacuum chamber. The hot plate temperature is approximately 600 °C, and it is glowing red hot. The inset shows a clearer view of the sample on the red-hot heater.

2.5.7 Electrical resistivity

An electrical resistance measurement setup was devised to capture the partial melting process as LSD samples were exposed to a temperature above the eutectic melting point. When a material melts, there is an abrupt change in the electrical resistivity[84,85]. This is illustrated by the measurements on a eutectic Au–Ge preform sample shown in Fig. 49. Samples from test structure **V** were fabricated and cut into long narrow strips with an aspect ratio of roughly 10:1. A 4-point DC measurement setup was used to measure the resistance. The resistivity was then calculated using the dimensions of the samples and the distance between the probes. Results from a measurement sequence are shown in Fig. 50. As can be seen in the figure the measurements were noisy at high temperature. Thus, a new measurement system was developed by Christian Bjørge Thoresen using a lock-in amplifier that reduced the noise significantly which can be seen in Article 3[86]. The circuit diagram of that system is shown in Fig. 51.

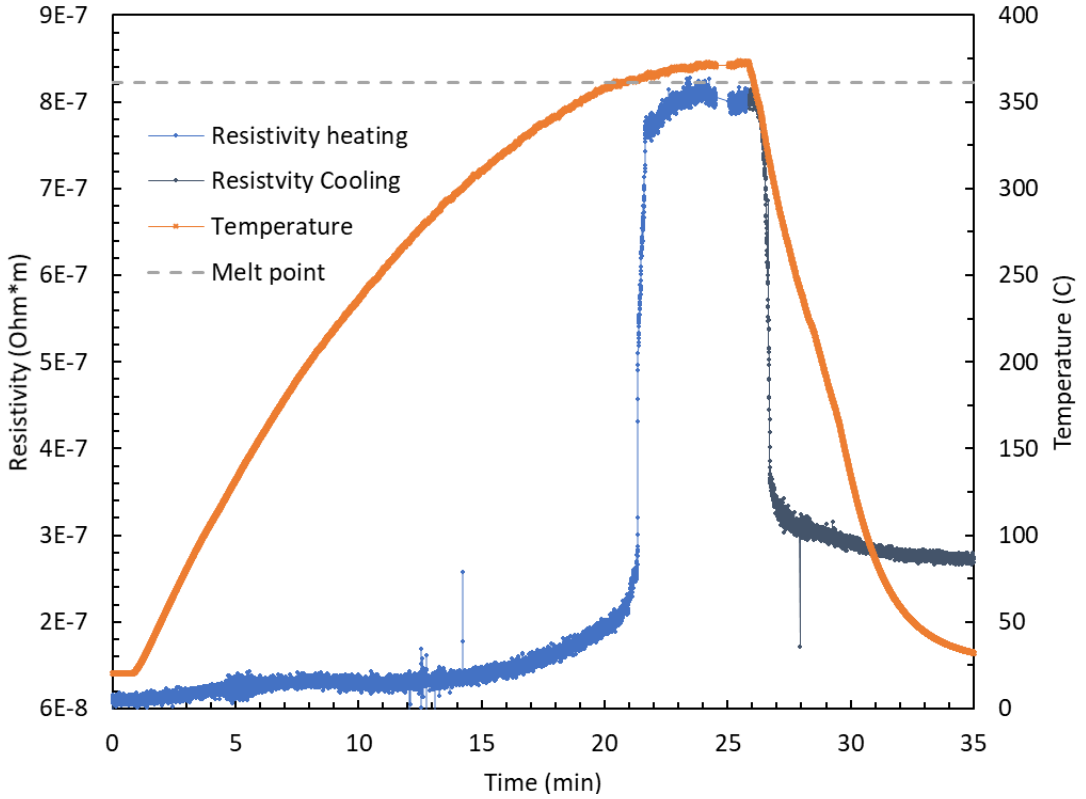

Fig. 49 Resistivity as a function of time of a reference sample, a eutectic Au–Ge preform. There is a clear abrupt change in the resistivity as the sample melts and solidifies.

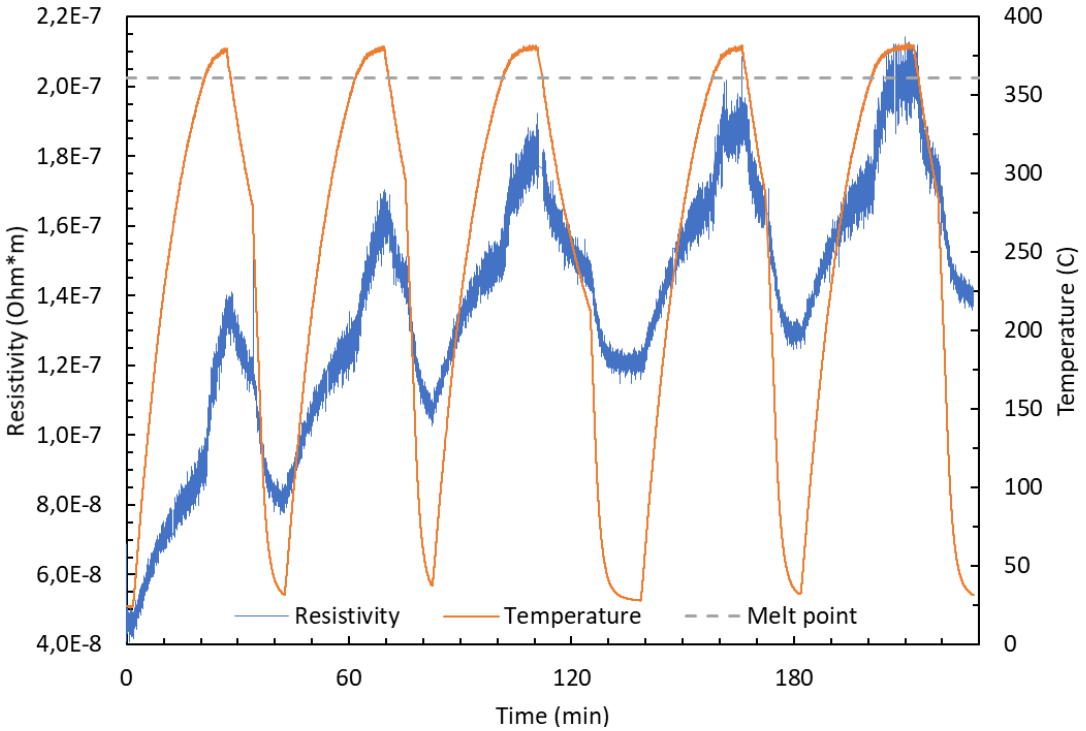

Fig. 50 Resistivity as function of time of one LSD sample exposed to five thermal cycles up to approximately 380 °C. Each time the temperature passes the eutectic melting point, there is an abrupt change in resistivity of the sample. The resistivity appears to increase asymptotically towards a finite value.

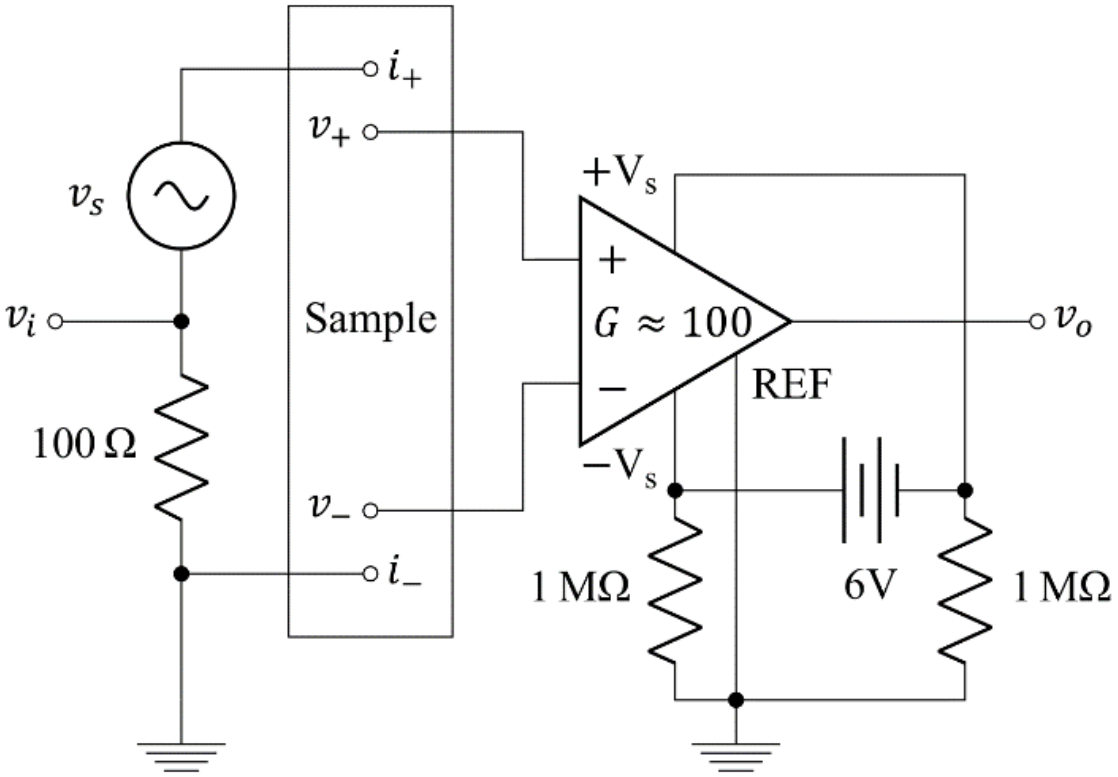

Fig. 51 Circuit diagram of the 4-point measurement setup used to measure the electrical resistivity of off-eutectic Au–Ge joints[86].

2.6 Equipment

The equipment used in this thesis is listed in Table 4.

Table 4 Equipment used in this thesis.

Application	Type	Model	Location
Analysis	Interferometer	Wyko NT9100	USN, Borre, NO
Analysis	IR-camera	Pixel link PL-B74EF	USN, Borre, NO
Analysis	Profilometer	DETAK 150	USN, Borre, NO
Analysis	Optical microscope	Leica DM4000M	USN, Borre, NO
Analysis	Optical microscope	Zeiss V12	USN, Borre, NO
Analysis	Optical microscope	Neophot 32	USN, Borre, NO
Analysis	Thickness gauge	Heidenhain MT 60M, Microbas	USN, Borre, NO
Analysis	Probe station	Micromanipulator Company	USN, Borre, NO
Analysis	SEM	Hitachi SU 3500	USN, Borre, NO
Analysis	SEM	Hitachi SU 8230	USN, Borre, NO
Analysis	EDX	Oxford X-MAX 150	USN, Borre, NO
Analysis	EDX	Oxford X-MAX 50	USN, Borre, NO
Analysis	EBSD	Oxford Nordlys Nano	USN, Borre, NO
Analysis	Microtomography	ID19 beamline	ESRF, Grenoble, FR
Characterization	Shear tester	Delvotec 5600	USN, Borre, NO
Characterization	Shear tester	XYZTEC Condor Sigma	XYZTec, Panningen, NL
Characterization	Thermal chamber	Lenton WHT6/30	USN, Borre, NO
Characterization	Data acquisition	Keysight 34972A, 34901A	USN, Borre, NO
Fabrication	Thermal evaporator	Moorfield Minilab T25M	USN, Borre, NO
Fabrication	Electroplating	USN custom made setup for Ni	USN, Borre, NO
Fabrication	Electroplating	USN custom made setup for Sn & Cu	USN, Borre, NO
Fabrication	e-beam	AJA Int. Phase II J. A300 A3CV & CTM	USN, Borre, NO
Fabrication	Sputtering	AJA Int. Phase II J. Telemark 294	USN, Borre, NO
Fabrication	Vacuum bonder	USN custom made setup	USN, Borre, NO
Fabrication	Vacuum bonder	Budatec VS160UG	USN, Borre, NO
Fabrication	Dicing saw	Disco DAD-2H/6T	USN, Borre, NO
Fabrication	Dicing saw	Disco 321	USN, Borre, NO
Fabrication	Dicing saw	Disco DAD 3220	USN, Borre, NO
Fabrication	Laser cutter	Rofin PL E 25 SHG CL	UiO, Oslo, NO
Preparation	Grinding	Struers	USN, Borre, NO
Preparation	Polishing	Struers DP10	USN, Borre, NO
Preparation	Ion-milling	Hitachi IM4000	USN, Borre, NO

3 Summary and outlook

The main objective of this thesis was to develop a reliable die-attach for high-temperature compatible electronics, such as thermoelectrics and power electronics. Two similar die-attach techniques were investigated; liquid solid diffusion (LSD) bonding using Au-rich off-eutectic Au–Ge, and solid-liquid interdiffusion (SLID) bonding using the Ni–Sn system.

The main conclusions of this work are given in the conclusion sections of the individual articles generated through this thesis. This chapter provides a summary of the most central elements and results of this thesis and provides a brief outlook.

3.1 Au–Ge LSD bonding

The main objective of the research performed on this technology was to confirm or falsify the LSD concept as a possible joining technology for use at temperatures when the joint is in a partially liquid state, *i.e.*, a semi-solid. This thesis has not been able to falsify the concept. All results point towards that it still seems feasible to use LSD joints at high-temperatures, *i.e.,* when joints are in a partially liquid state. The main results that supports this are the high-temperature shear strength capacity quantified with test system **VI**[83], the increased detachment temperature measured on test systems **III-VI**[86,87], the abrupt change in electrical resistivity that confirmed partial melting at high temperatures in test structure **V**[86], and the microstructure that exhibited single phase (Au) columnar-like features forming a solid connection with a very high melting point, through the joints, found in test structure **V**[88].

The detachment tests were used as a proof-of-concept setup for the LSD concept. The hypothesis was that eutectic joints and off-eutectic LSD joints should have a different effective melting point. Eutectic joints should lose their mechanical integrity at a temperature slightly below the eutectic melting point, while, the off-eutectic LSD joint structure should be able to keep the die attached to the substrate to a temperature well above the eutectic melting point. The highest recorded effective melting point, or detachment temperature, was at 600 °C. This was a non-destructive test that was aborted since 600 °C was the maximum limit of the hot plate used. This result is marked in the phase diagram in Fig. 52 visualizing that the joint was well inside the two-phase field region ($L + \alpha$).

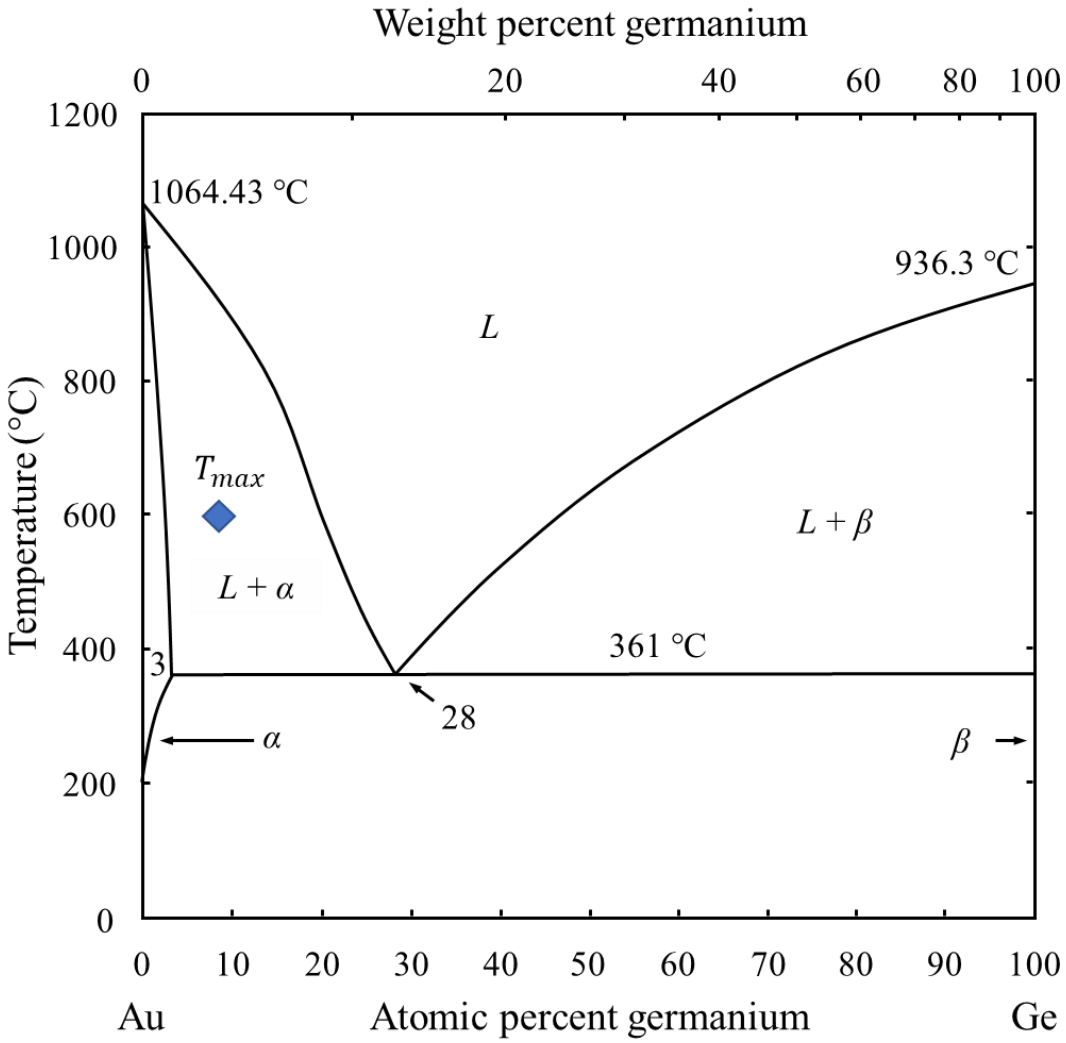

Fig. 52 The Au–Ge phase diagram with the highest recorded detachment temperature, T_{max}, indicated with a blue diamond. This was done on test structure **III** (Si / Au–Ge LSD / Si) with a $Au_{92}Ge_8$ joint composition. The test was nondestructive, *i.e.,* the joint was intact after the hot plate reached its maximum temperature at 600 °C[87]. The applied shear load was 27 kPa. The phase diagram was adapted from Okamoto and Massalski[50].

Shear testing at high temperature later revealed joints with remarkable strength of about 40 MPa when tested at temperatures around 400 °C, see Fig. 53. This is roughly up to twice as strong as regular Sn–Pb and SAC solders characterized at room temperature, and about ten times the room-temperature requirement for such die-attaches of the same size according to the US Military standard[9]. The corresponding fracture analysis revealed fracture surfaces that apparently had been in a partially liquid state, see Fig. 54. The partial melting was also confirmed by measuring the electrical resistivity of LSD joints. An abrupt change is resistivity was measured when the temperature passed the eutectic melting point as can be seen in Fig. 55.

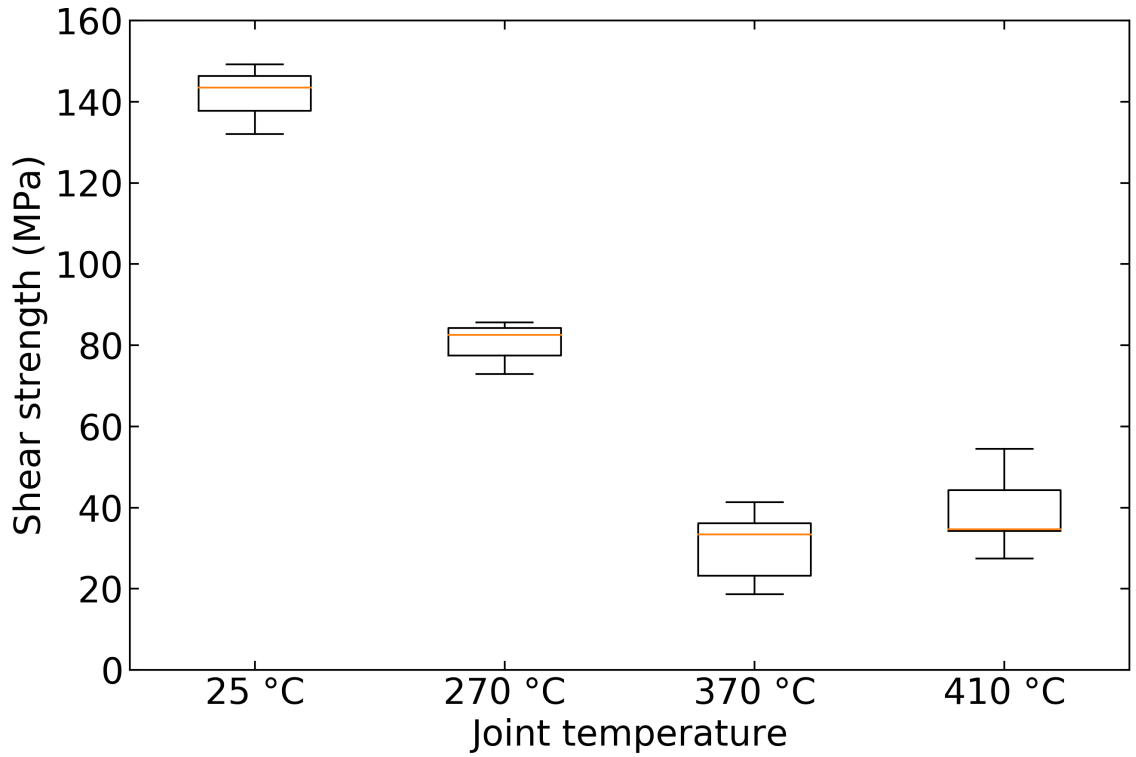

Fig. 53 Shear strength of AuGe LSD joint as a function of joint temperature for test structure **VI**[83]; SiC / Au–Ge LSD / Si_3N_4. The shear strength at 410 °C demonstrates that Au–Ge LSD joints have the potential to be used at temperatures higher than their eutectic melting point. The US Military standard MIL-STD-883H requirement for similar joints is 3.9 MPa[9]. The recorded shear strength is roughly at least ten times stronger than the requirement.

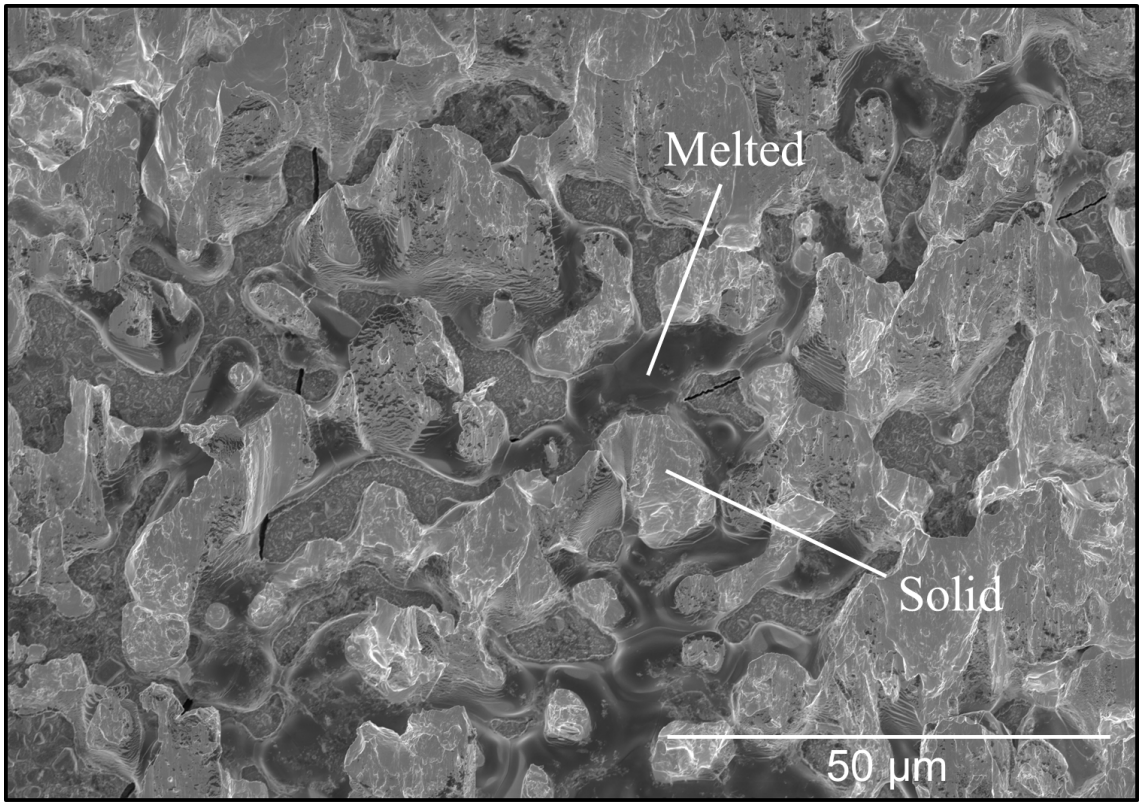

Fig. 54 SEM micrograph of a section from a fracture surface after shear testing at 370 °C with test structure **VI**. Rough columnar features intermixed with smooth regions demonstrate that the joint has been partially melted.

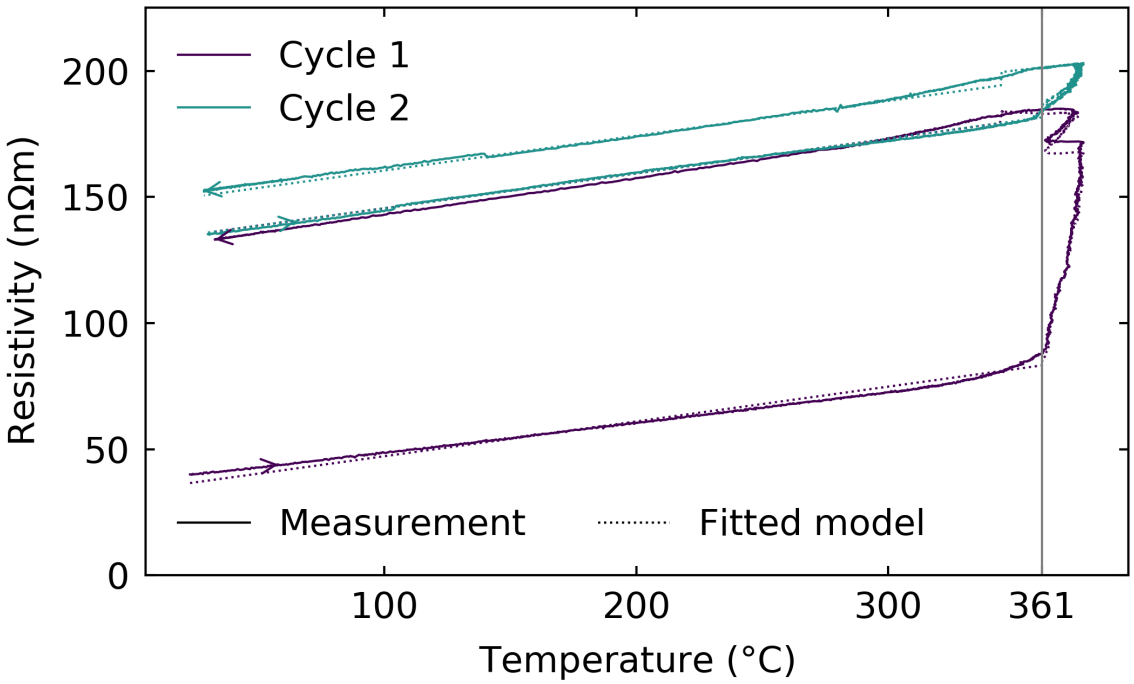

Fig. 55 Graph of the electrical resistivity of a Au–Ge LSD joint as a function of temperature, measured on test structure **V** (Au / Au–Ge LSD / Au). An abrupt change in the resistivity was recorded at the onset of melting at 361 °C, confirming a melting process.

Studies of the microstructure revealed an inhomogeneous microstructure. Cross-sections disclosed joints with columnar-like structures of Au protruding through a hypereutectic (Ge-rich) Au–Ge mixture at the joint center, *i.e.,* at the original bond line. An illustration of this microstructure is shown in Fig. 56. Two cross-sections taken in two orthogonal directions of joints show these columnar structures in Fig. 57. The same type of columnar Au structures were found in fracture surfaces, Fig. 58 and Fig. 63(b), inside virgin joints, Fig. 63(a), and on the surface of wetting samples Fig. 63(c). The results support an explanation that these solid single-phase structures, with a high melting point, provide the measured shear strength capacity of the LSD joints at temperatures above the eutectic melting point. In Fig. 57(b) light band is visible at the joint centre in the Au column indicating nucleation of Au in the melt.

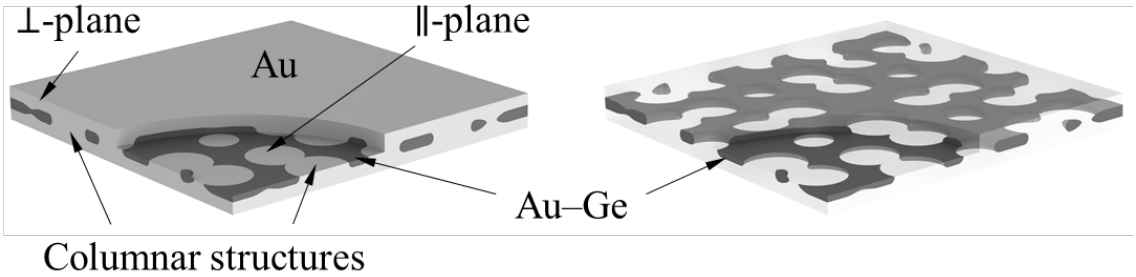

Fig. 56 3D illustration of how the Au-phase (light) and the Au–Ge mixture (dark) are distributed inside the fabricated joints. Columnar-like structures of Au extend through the eutectic Au–Ge layer. The Au-phase has been made semi-transparent in the image to the right to provide a clearer view of the eutectic Au–Ge mixture.

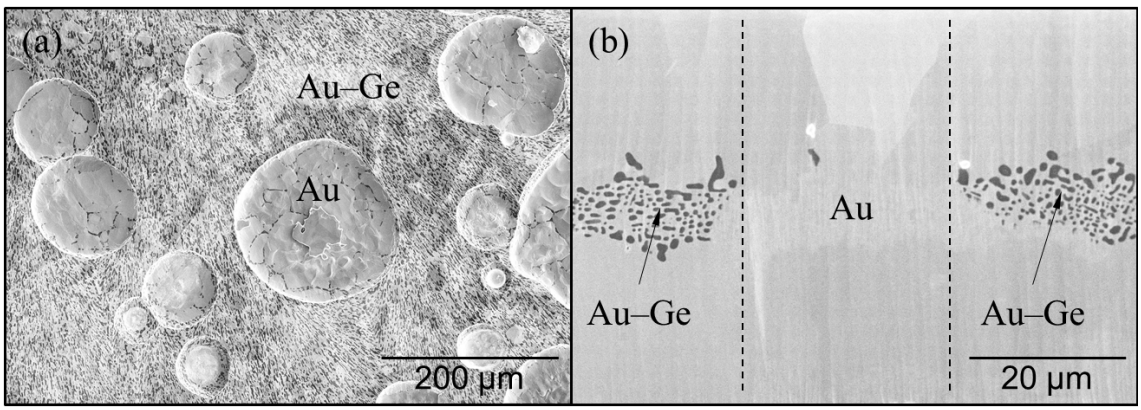

Fig. 57 SEM micrographs of cross-sections with columnar type structures of Au protruding through a eutectic Au–Ge layer. (a) is a section in the ∥-plane and (b) is in the ⊥-plane direction.

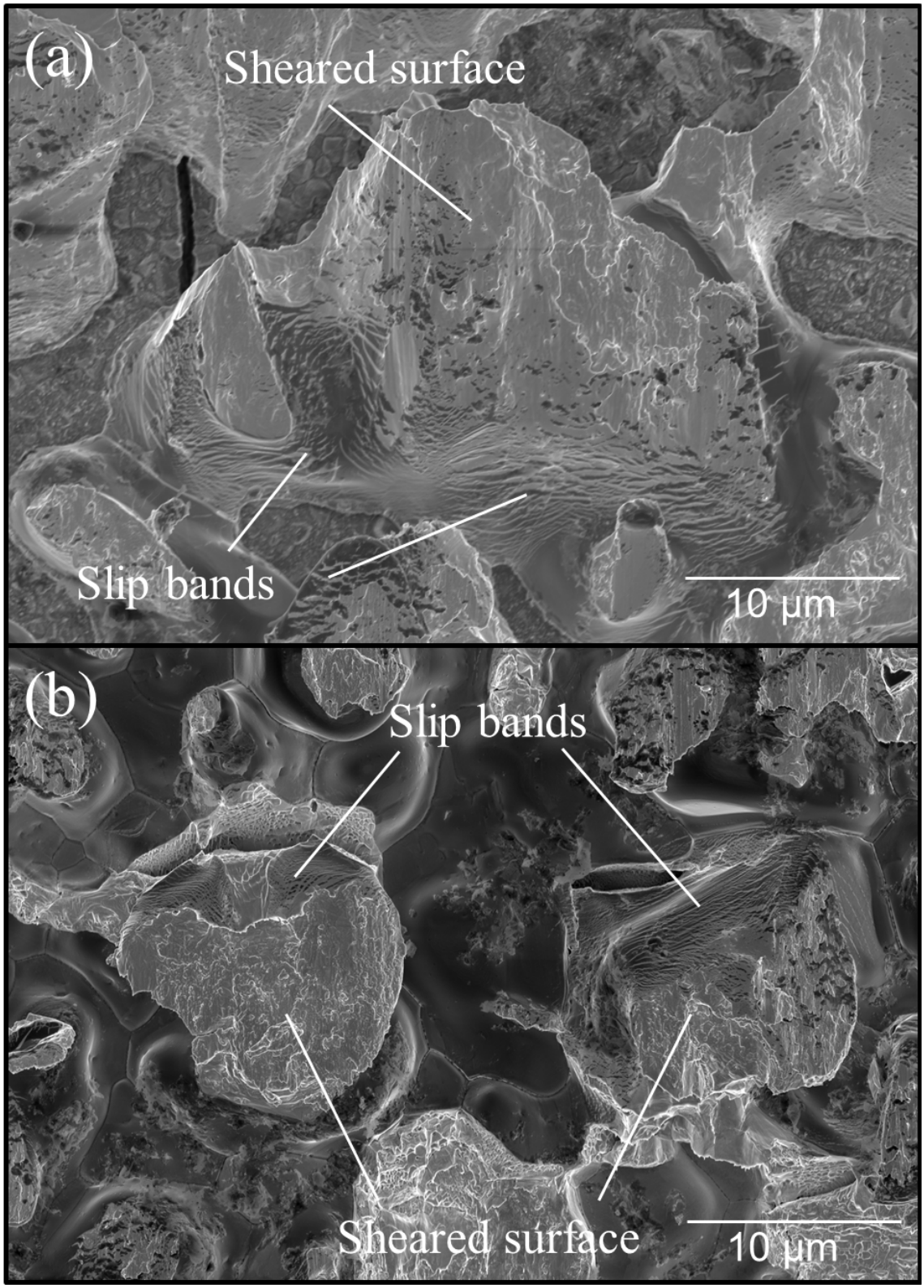

Fig. 58 SEM micrograph of columnar type structures of Au on both the substrate side (a) and the die side (b) of a fracture surface. They are located in a hypoeutectic (Au-rich) Au–Ge region and are surrounded by a compound that has clearly been in a liquid state with a free surface upon solidification. The columnar structures show ductile fracture features such as slip bands, necking and a shear surface indicating that they were in a solid state upon fracture.

3.1.1 Recommendations

The work can provide some initial guidelines for fabrication of the Au–Ge LSD joints:

- The bond line pressure should be high enough such that thermomechanical contact between components is achieved. The pressure should not be too high (several MPa) when using thick preforms and a fast heating process to avoid squeeze out.
- The bond surfaces need to be clean and free from oxides before joining.
- Joining should all be done in an inert atmosphere or in a vacuum to avoid atmospheric oxygen.
- The peak temperature during bonding has little effect on the joint quality, as long as melting of the MPD is achieved.
- Annealing below the eutectic melting point seems not to affect the overall inhomogeneous microstructure significantly. The microstructure coarsens but is otherwise stable. Annealing above the eutectic melting point rapidly transforms the microstructure. The eutectic mixture disappears and forms larger explicit Ge domains in a Au matrix.

Proposed next steps include:

- Design and fabricate a system with an improved diffusion barrier such that there is no flow of elements through the barrier. Then perform the high-temperature shear strength capacity high-temperature storage test again.
- Replace the thick preform with a eutectic paste or a Ge layer (attempted in test structure **II**) to form the MPD compound. This may enable the use of thinner Au layers on the die and substrate.
- Perform thermal cycling tests with a peak temperature above the eutectic melting point.

3.2 Ni–Sn SLID bonding

The main objective for Ni–Sn SLID joints was to investigate if it was possible to form high-quality joints comprising a stable IMC, preferably the Ni_3Sn phase next to the primary Ni phase, forming a Ni | Ni_3Sn | Ni joint. The results have shown a rapid formation of idiomorphic Ni_3Sn_4 crystals at the interface between the Ni and Sn layers.

These crystals impede the creation of high-quality joints, see Fig. 59[89]. These needle-like structures, or scallops, protrude into the melted Sn from each side of the melt until they meet in the middle. These structures were studied in more detail by Lis *et al.*[90]. They showed that these structures developed at 200 °C, 250 °C, and 300 °C. This creates solid structures that lock the relative position of the components to be joined. They work as spacers and fix the joint thickness. When the joint evolves into the Ni–Sn IMC phases, there is a volumetric contraction of the joint material. The contraction can be up to about 17 vol.% transforming Sn(l) and Ni(s) into Ni_3Sn(s). Since these spacers restrict the joint to contract, voids form in the center as the material evolves as can be seen in Fig. 60. Despite the severe voiding, the shear strength was significant as illustrated by Fig. 61, which shows the measured shear strength of the samples fabricated in this work. These samples struggled with a weak adhesion layer, and only partial bonding could be achieved (see Fig. 43). A deeper analysis calculating a more realistic shear strength using only the bonded area revealed a shear strength capacity up to 230 MPa. The kinetics of Ni–Sn system is slow compared to both Cu–Sn[91,92] and Au–Sn[93].

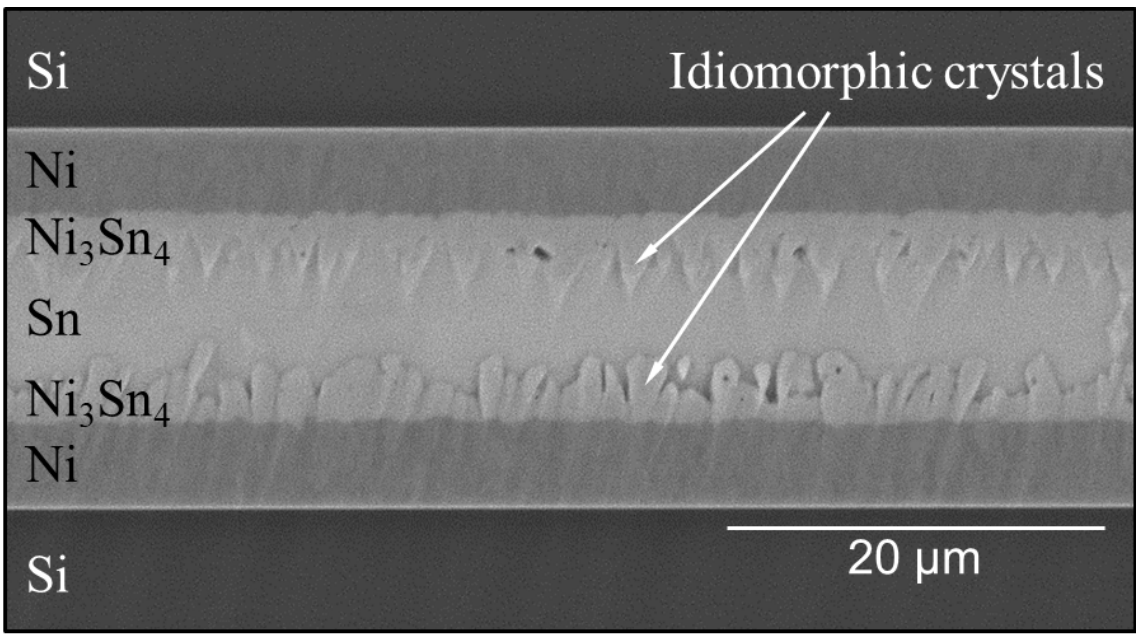

Fig. 59 SEM micrograph showing idiomorphic Ni_3Sn_4 crystals (scallops) that grow at the Ni / Sn interface. This ⊥-plane cross-section is from a sample exposed to 250 °C for 5 min. Test structure **I**.

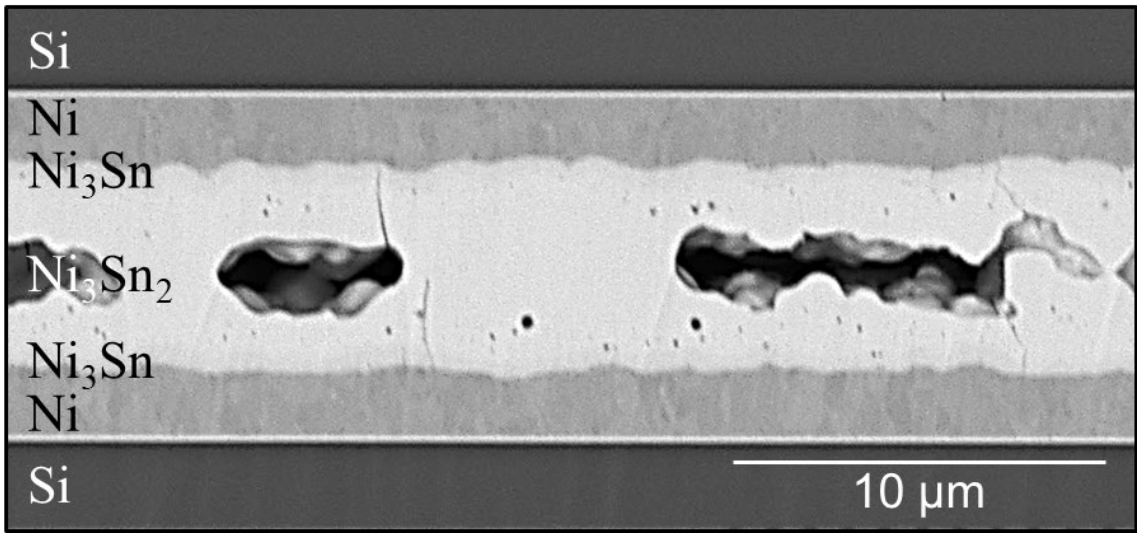

Fig. 60 SEM micrograph of severe voiding in Ni–Sn SLID joints caused by volumetric contraction during solidification. Test structure **I**.

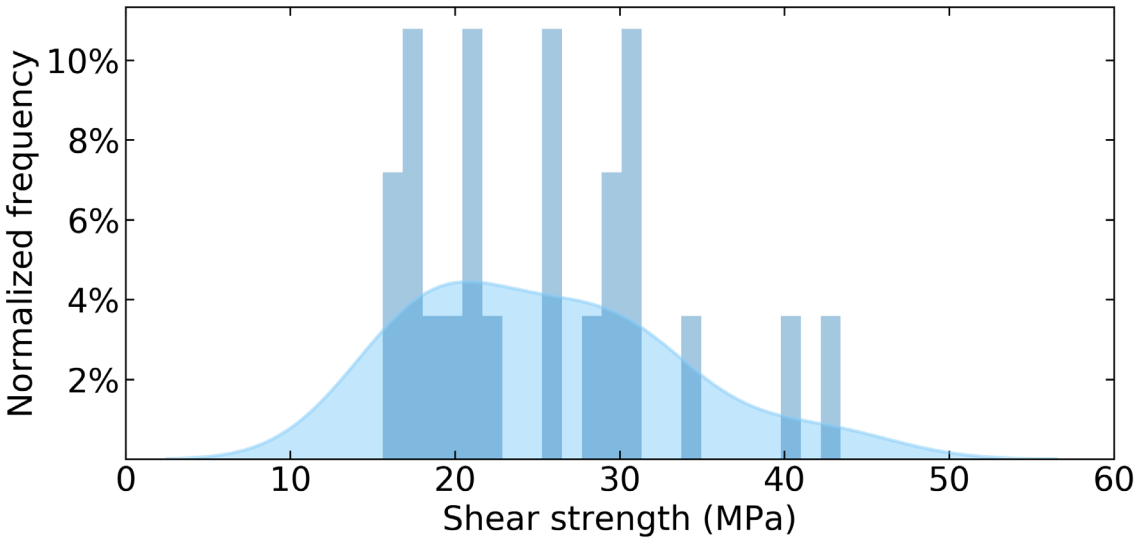

Fig. 61 Histogram and density plot of the measured nominal shear strength of Ni–Sn SLID joints. Test structure **I**.

3.2.1 Recommendations

This work and other recent studies on the Ni–Sn system point towards the same issues. Joints typically have inadequate quality and require long process times to complete homogenization[90–92,94–96]. Thus, the Ni–Sn system does not seem directly feasible to form high-quality joints within a reasonable amount of time, without a thorough revaluation of the system outline. There might be remedies that can improve its deficiencies.

Proposed next steps include:

- Evaluate the possibility to add a third element into the Ni–Sn system to stabilize or avoid the formation of idiomorphic structures.
- Investigate joint formation using a very thin (< 1 μm) Sn layer reducing the effect of constrained volumetric contraction.
- Replace the layered Ni | Sn | Ni structure with Ni–Sn paste to reduce the diffusion length and distribute the volumetric contraction into three dimensions.

3.3 Outlook

The outlook for high-temperature electronics looks promising. There are plenty of challenges to overcome, but in recent years, technology developments and new approaches attack the high-temperature challenge from new directions at a high pace. One of the main challenges that requires attention is to define and qualify a feasible and complete materials scheme suitable for use with wide bandgap materials and ceramic substrates. Individual components such as semiconductors, adhesion layers, diffusion barriers, conductors, and passivations already exist. Nevertheless, all components are not necessarily compatible with each other. Thus, one needs to find the correct combination of existing components and develop the missing pieces before a complete scheme can be defined. I believe that it is just a matter of time before adequate system solutions compatible with 300 °C or more are introduced into various electronic applications.

References

1. Au, K. Y., Che, F. X., Wai, E. & Ching, L. Extremely High Temperature and High Pressure (x-HTHP) Endurable SOI Device and Sensor Packaging for Harsh Environment Applications. 1107–1112 (2017). doi:10.1109/ECTC.2017.30

2. Yu, F. *et al.* Reliability of Ag Sintering for Power Semiconductor Die Attach in High-Temperature Applications. **32**, 7083–7095 (2017).

3. Hu, T. & Chen, H. Fabrication of Cu@Sn Core-Shell Structure Preform and Application in High Temperature Bonding. in *Materials Science and Technology* 951–956 (2016).

4. Yoon, S. W., Glover, M. D. & Shiozaki, K. Nickel-tin transient liquid phase bonding toward high-temperature operational power electronics in electrified vehicles. *IEEE Trans. Power Electron.* **28**, 2448–2456 (2013).

5. Chidambaram, V., Yeung, H. B. & Shan, G. Reliability of Au-Ge and Au-Si eutectic solder alloys for high-temperature electronics. *J. Electron. Mater.* **41**, 2107–2117 (2012).

6. Zheng, P. High Temperature Electronics Packaging Processes and Materials Development. (Ph.D. dissertation, Dept. Electr. Comput. Eng., Auburn Univ., Auburn, AL, 2010).

7. Kisiel, R. & Szczepański, Z. Die-attachment solutions for SiC power devices. *Microelectron. Reliab.* **49**, 627–629 (2009).

8. Hu, T., Chen, H., Li, M. & Zhao, Z. Cu@Sn Core-Shell Structure Powder Preform for High-Temperature Applications Based on Transient Liquid Phase Bonding. *IEEE Trans. Power Electron.* **32**, 441–451 (2017).

9. Test Method Standard - Microcircuits. *MIL-STD-883H* 729 (2010).

10. Test Method Standard - Electronic and electrical component parts. *MIL-STD-202G* 193 (2002).

11. Tollefsen, T. A. Electronic packaging for high temperature applications. (Ph.D. dissertation, Dept. Micro and Nano Systems Technology, Vestfold Univ. College, 2013).

12. Incropera, F. P., Bergman, T. L., Lavine, A. S. & DeWitt, D. P. *Fundamentals of Heat and Mass Transfer*. *Wiley* (2011). doi:10.1073/pnas.0703993104

13. Thermoelectrics. Available at: http://thermoelectrics.matsci.northwestern.edu/. (Accessed: 1st January 2019)

14. Freunek, M., Müller, M., Ungan, T., Walker, W. & Reindl, L. M. New physical model for thermoelectric generators. *J. Electron. Mater.* **38**, 1214–1220 (2009).

15. Rowe, D. M. & Min, G. Evaluation of thermoelectric modules for power generation. *J. Power Sources* **73**, 193–198 (1998).

16. Rowe, D. M. & Min, G. Design theory of thermoelectric modules for electrical power generation. *IEE Proc. - Sci. Meas. Technol.* **143**, 351 (1996).

17. Larsson, A., Tollefsen, T. A., Løvvik, O. M. & Aasmundtveit, K. E. Thermoelectric Module for High Temperature Application. in *Intersoc. Conf. Therm. Thermo-mech. Phenom. Electron. Sys. (ITHERM)* 719–25 (IEEE, 2017). doi:10.1109/ITHERM.2017.7992557

18. Roccaforte, F. *et al.* Emerging trends in wide band gap semiconductors (SiC and GaN) technology for power devices. *Microelectron. Eng.* **187**–**188**, 66–77 (2018).

19. Kargarrazi, S., Elahiphanah, H., Saggini, S., Senesky, D. & Zetterling, C.-M.

Letters 500 °C SiC PWM Integrated Circuit. *IEEE Trans. Power Electron.* **34**, 1997–2001 (2019).

20. Roccaforte, F. *et al.* Applied Surface Science Surface and interface issues in wide band gap semiconductor electronics. *Appl. Surf. Sci.* **256**, 5727–5735 (2010).

21. Manikam, V. R. & Cheong, K. Y. Die Attach Materials for High Temperature Applications: A Review. *Components, Packag. Manuf. Technol. IEEE Trans.* **1**, 457–478 (2011).

22. Murayama, N., Hirao, K., Sando, M., Tsuchiya, T. & Yamaguchi, H. High-temperature electro-ceramics and their application to SiC power modules. *Ceram. Int.* **44**, 3523–3530 (2018).

23. Sabbah, W., Azzopardi, S., Buttay, C., Meuret, R. & Woirgard, E. Study of die attach technologies for high temperature power electronics: Silver sintering and gold-germanium alloy. *Microelectron. Reliab.* **53**, 1617–1621 (2013).

24. Alam, M. O., Bailey, C., Wu, B. Y., Yang, D. & Chan, Y. C. High current density induced damage mechanisms in electronic solder joints: A state-of-the-art review. *Proc. Int. Symp. High Density Packag. Microsyst. Integr. 2007, HDP'07* 3–9 (2007). doi:10.1109/HDP.2007.4283569

25. Lall, P., Deshpande, S., Nguyen, L., Instruments, T. & Clara, S. Study of Electromigration in Cu and Ag Wirebonds Operating at High Current in Extreme Environments. in *Intersoc. Conf. Therm. Thermo-mech. Phenom. Electron. Sys. (ITHERM)* 10 (IEEE, 2017).

26. Mehrer, H. *Diffusion in Solids*. (Springer-Verlag Berlin Heidelberg, 2007).

27. Larsson, A., Tollefsen, T. A., Løvvik, O. M. & Aasmundtveit, K. E. Ni–Sn Solid-Liquid Interdiffusion (SLID) Bonding for Thermo-Electric Elements in Extreme Environments – FEA of the joint stress. in *Microelectronics Packaging Conference (EMPC)* 1–6 (IEEE, 2015).

28. Smith, C. S. *A search for structure*. (MIT Pr, 1981).

29. Hawthorne, J. G. & Smith, C. S. *On Divers Arts, The Treatise of Theophilus*. (Univ. Chicago, 1963).

30. Smith, C. S. & Hawthorne, J. G. Mappae Clavicula - A little key to the world of medeval techniques. *Trans. Am. Philisophical Soc.* **64**, 75 (1974).

31. Humpston, G. & Jacobson, D. M. *Principles of Soldering*. (ASM International, 2004).

32. Ulrich, R. K. & Brown, W. D. *Advanced electronic packaging*. (John Wiley & Sons, Inc., 2006).

33. Aasmundtveit, K. E., Luu, T.-T., Nguyen, H.-V., Larsson, A. & Tollefsen, T. A. Intermetallic bonding for High-Temperature Microelectronics and Microsystems: Solid-Liquid Interdiffusion Bonding. in *Intermetallic compounds - Formation and applications* (ed. Aliofkhazrai, M.) 43–72 (IntechOpen, 2018).

34. Manikam, V. R. & Cheong, K. Y. Die attach materials for high temperature applications: a review. *Components, Packag. Manuf. Technol. IEEE Trans.* **1**, 457–478 (2011).

35. Campbell, F. C. *Phase Diagrams - Understanding the Basics*. (ASM International, 2012).

36. Campbell, F. C. *Elements of Metallurgy and Engineering Alloys*. (ASM International, 2008).

37. Tollefsen, T. A. *et al.* Au-Sn SLID Bonding: A Reliable HT Interconnect and Die Attach Technology. *Metall. Mater. Trans. B* **44**, 406–413 (2013).

38. Chen, G., Feng, S.-T., Li, X., Lu, G.-Q. & Mei, Y.-H. Characterizations of Rapid Sintered Nanosilver Joint for Attaching Power Chips. *Materials (Basel).* **9**, 564 (2016).

39. Siow, K. S. Are sintered silver joints ready for use as interconnect material in microelectronic packaging? *J. Electron. Mater.* **43**, 947–961 (2014).

40. Paknejad, S. A. & Mannan, S. H. Review of silver nanoparticle based die attach materials for high power/temperature applications. *Microelectron. Reliab.* **70**, 1–11 (2017).

41. Okamoto, H. *Desk Handbook: Phase Diagrams for Binary Alloys*. (ASM International, 2010).

42. Dantzig, J. A. & Rappaz, M. *Solidification*. (CRC Press, 2009).

43. Glicksman, M. E. *Principles of Solidification*. (Springer, 2011). doi:10.1007/978-1-4419-7344-3

44. Cook, G. O. & Sorensen, C. D. Overview of transient liquid phase and partial transient liquid phase bonding. *J. Mater. Sci.* **46**, 5305–5323 (2011).

45. Gale, W. F. & Butts, D. A. Transient liquid phase bonding. *Sci. Technol. Weld. Join.* **9**, 283–300 (2004).

46. MacDonald, W. D. & Eagar, T. W. Transient liquid phase bonding processes. *Met. Sci. Join.* 93–100 (1992).

47. MacDonald, W. D. & Eagar, T. W. Isothermal Solidification Kinetics of Diffusion Brazing. *Metall. Mater. Trans. A* **29A**, 315–325 (1998).

48. Verhoeven, J. D. *Fundamentals of Physical Metallurgy*. (John Wiley & Sons, Inc., 1975). doi:169-215

49. Paul, A., Laurila, T., Vuorinen, V. & Divinski, S. V. *Thermodynamics, diffusion and the kirkendall effect in solids*. *Thermodynamics, Diffusion and the Kirkendall Effect in Solids* **9783319074**, (Springer, 2014).

50. Okamoto, H. & Massalski, T. B. The Au–Ge (Gold-Germanium) System. *Bull. Alloy Phase Diagrams* **5**, 601–610 (1984).

51. Elliott, R. P. & Shunk, F. A. The Au-Ge System (Gold-Germanium). *Bull. Alloy Phase Diagrams* **1**, 51–54 (1980).

52. Wang, J., Leinenbach, C. & Roth, M. Thermodynamic modeling of the Au-Ge-Sn ternary system. *J. Alloy. Compd.* **481**, 830–836 (2009).

53. Bernstein, L. Semiconductor Joining by the Solid-Liquid-Interdiffusion (SLID) Process. *J. Electrochem. Soc.* **113**, 1282–1289 (1966).

54. Bernstein, L. & Bartholomew, H. Applications of Solid-Liquid Interdiffusion (SLID) Bonding in Integrated-Circuit Fabrication. *Trans. Metall. Soc. Aime* **236**, 405–412 (1966).

55. Cellini, B. *Due Trattati, uno intorno alle otto principali arti del l'oreficeria. L'altro in material dell'arte della scultura*. (1568).

56. Littledale, H. A. P. Improvments in Hard Soldering Mixtures and Hard Soldering. 5 (1934).

57. Lynch, J. F., Feinstein, L. & Huggins, R. A. Brazing by the diffusion controlled formation of a liquid intermediate phase. *Weld. J.* **38**, 85–9 (1959).

58. Harrsch, M. The gold dagger of King Tutankhamun. Available at: https://www.flickr.com/photos/mharrsch/33516468980. (Accessed: 12th March 2019)

59. MacDonald, W. D. & Eagar, T. W. Transient Liquid Phase Bonding. *Annu. Rev. Mater. Sci.* **22**, 23–46 (1992).

60. Tuah-Poku, I., Dollar, M. & Massalski, T. A study of the transient liquid phase bonding process applied to a Ag/Cu/Ag sandwich joint. *Metall. Trans. A* **19**, 675–686 (1988).

61. Tollefsen, T. A., Larsson, A., Løvvik, O. M. & Aasmundtveit, K. Au-sn SLID bonding - Properties and possibilities. *Metall. Mater. Trans. B Process Metall. Mater. Process. Sci.* **43**, 397–405 (2012).

62. Navarro, L. A. *et al.* Thermomechanical assessment of die-attach materials for wide bandgap semiconductor devices and harsh environment applications. *IEEE Trans. Power Electron.* **29**, 2261–2271 (2014).

63. Murayama, N., Hirao, K., Sando, M., Tsuchiya, T. & Yamaguchi, H. High-temperature electro-ceramics and their application to SiC power modules. *Ceram. Int.* **44**, 3523–3530 (2018).

64. Kinbara, A., Kusano, E., Kamiya, T., Kondo, I. & Takenaka, O. Evaluation of adhesion strength of Ti films on Si(100) by the internal stress method. *Thin Solid Films* **317**, 165–168 (1998).

65. Roshanghias, A., Khatibi, G., Pelzer, R. & Steinbrenner, J. Surface & Coatings Technology On the effects of thickness on adhesion of TiW diffusion barrier coatings in silicon integrated circuits. *Surf. Coat. Technol.* **259**, 386–392 (2014).

66. Lang, F., Yamaguchi, H., Ohashi, H. & Sato, H. Improvement in joint reliability of SiC power devices by a diffusion barrier between Au-Ge solder and Cu/Ni(P)-metalized ceramic substrates. *J. Electron. Mater.* **40**, 1563–1571 (2011).

67. Nowicki, R. S. Diffusion barriers between gold and semiconductors. *Gold Bull.* **15**, 21–24 (1982).

68. Drevin-Bazin, A., Lacroix, F. & Barbot, J. F. SiC die attach for high-temperature applications. *J. Electron. Mater.* **43**, 695–701 (2014).

69. Tanimoto, S., Matsui, K., Murakami, Y., Yamaguchi, H. & Okumura, H. Assessment of Au-Ge Die Attachment for an Extended Junction Temperature Range in Power Applications. in *IMAPS Int. Conf. High Temp. Election. (HiTEC)* 32–39 (IMAPS, 2010).

70. Tanimoto, S., Watanabe, K., Tanisawa, H., Matsui, K. & Sato, S. Packaging techniques for compact SiC power modules operable in an extended Tj range. in *Electrochem. Soc. Meet., 224th* 1 (The Electrochemical Society, 2013).

71. Tanimoto, S., Tanisawa, H., Watanabe, K., Matsui, K. & Sato, S. Power Module Package Structure Capable of Surviving Greater ΔTj Thermal Cycles. *Mater. Sci. Forum* **740–742**, 1040–1043 (2013).

72. Larsson, A., Tollefsen, T. A., Løvvik, O. M. & Aasmundtveit, K. E. *A Review of*

Eutectic Au-Ge Solder Joints. (2019). doi:10.1007/s11661-019-05356-0

73. Okamoto, H. & Massalski, T. B. The Au-Si (Gold-Silicon) system. *Bull. Alloy Phase Diagrams* **4**, 190–8 (1983).

74. Li, C. C. *et al.* Development of interconnection materials for Bi2Te3 and PbTe thermoelectric module by using SLID technique. in *Proceedings - Electronic Components and Technology Conference* 1470–1476 (2015). doi:10.1109/ECTC.2015.7159791

75. King, J. A. *Materials Handbook for Hybrid Microelectronics*. (Artech House, Inc., 1988).

76. Jiang, N., Clum, J. ., Chromik, R. . & Cotts, E. . Thermal expansion of several Sn-based intermetallic compounds. *Scr. Mater.* **37**, 1851–1854 (1997).

77. Fields, R. J. & Low III, S. R. Physical And Mechanical Properties Of Intermetallic Compounds Commonly Found In Solder Joints. in *Metal Science of Joining* (1991).

78. Rogl, G. *et al.* Thermal expansion of skutterudites. *J. Appl. Phys.* **107**, 1–10 (2010).

79. Zhang, L. *et al.* Mechanical properties of filled antimonide skutterudites. *Mater. Sci. Eng. B Solid-State Mater. Adv. Technol.* **170**, 26–31 (2010).

80. Pavlova, L. M., Shtern, Y. I. & Mironov, R. E. Thermal expansion of bismuth telluride [3]. *Br. J. Appl. Phys.* **49**, 369–79 (2011).

81. Feng, S., Li, S. & Fu, H. First-principle calculation and quasi-harmonic Debye model prediction for elastic and thermodynamic properties of Bi2Te3. *Comput. Mater. Sci.* **82**, 45–49 (2014).

82. Okamoto, H. Ni-Sn (Nickel-Tin). *J. Phase Equilibria Diffus.* **29**, 297–298 (2008).

83. Larsson, A., Tollefsen, T. A. & Aasmundtveit, K. E. Shear strength of off-eutectic Au–Ge joints at high-temperature. *Microelectron. Reliab.* **99**, 31–43 (2019).

84. Ho, C. Y. *et al.* Electrical Resistivity of Ten Selected Binary Alloy Systems. *Journal of Physical and Chemical Reference Data* **12**, 183–322 (1983).

85. Matula, R. A. Electrical resistivity of Copper, Gold, Palladium, and Silver.pdf. *J. Phys. Chem. Ref. Data* **8**, 1147–1298 (1979).

86. Larsson, A. & Thoresen, C. B. Off-Eutectic Au – Ge Die-Attach — Microstructure, Mechanical Strength, and Electrical Resistivity. *IEEE Trans. Components, Packag. Manuf. Technol.* 11 (2019). doi:10.1109/TCPMT.2019.2926528

87. Larsson, A., Tollefsen, T. A., Løvvik, O. M. & Aasmundtveit, K. E. Liquid Solid Diffusion (LSD) Bonding - A novel joining technology. in *European Microelectronics Packaging Conference (EMPC)* 1–3 (IMAPS, 2017).

88. Larsson, A. & Aasmundtveit, K. E. *On the microstructure of off-eutectic Au–Ge joints — A hightemperature joint*. (2019).

89. Larsson, A., Tollefsen, T. A., Løvvik, O. M. & Aasmundtveit, K. E. Ni–Sn solid liquid interdiffusion (SLID) bonding – Process , bond characteristics and strength. in *6th Electronic System-Integration Technology Conference (ESTC)* (IEEE, 2016).

90. Lis, A., Kenel, C. & Leinenbach, C. Characteristics of Reactive Ni3Sn4 Formation and Growth in Ni-Sn Interlayer Systems. *Metall. Mater. Trans. A* **47**, 2596–2608 (2016).

91. Bader, S., Gust, W. & Hieber, H. Rapid formation of intermetallic compounds by interdiffusion in the Cu-Sn and Ni-Sn systems. *Acta Metall. Mater.* **43**, 329–337 (1995).

92. Lee, B. S., Hyun, S. K. & Yoon, J. W. Cu–Sn and Ni–Sn transient liquid phase bonding for die-attach technology applications in high-temperature power electronics packaging. *J. Mater. Sci. Mater. Electron.* **28**, 7827–7833 (2017).

93. Tollefsen, T. A. A. *et al.* High temperature interconnect and die attach technology: Au-Sn SLID bonding. *IEEE Trans. Components, Packag. Manuf. Technol.* **3**, 904–

914 (2013).

94. Chu, K., Sohn, Y. & Moon, C. A comparative study of Cn / Sn / Cu and Ni / Sn / Ni solder joints for low temperature stable transient liquid phase bonding. *Scr. Mater.* **109**, 113–117 (2015).

95. Zhong, Y. *et al.* Low Temperature Ni/Sn/Ni Transient Liquid Phase Bonding for High Temperature Packaging Applications by Imposing Temperature Gradient. *2017 IEEE 67th Electron. Components Technol. Conf.* 411–416 (2017). doi:10.1109/ECTC.2017.267

96. Yang, H. W., Yu, H. Y. & Kao, C. R. Critical Factors Affecting Structural Transformations in 3D IC Micro Joints. 3–8 (2017). doi:10.1109/ECTC.2017.98

Appendix

X-ray tomography

Three samples were examined at the microtomography beamline (ID19) at the European synchrotron radiation facility (ESRF) in Grenoble, France[2]. Unfortunately, no conclusive results could be drawn from these trials within the time frame of this project. The resulting images produced are presented in Fig. 62. A few interesting observations can be done.

The Au–Ge sample in Fig. 62(a) clearly demonstrates an inhomogeneous microstructure. Comparing a section from this plot with a fracture surface of another similar sample and the surface from a wetting sample (eutectic Au–Ge on a Au surface) reveals apparent similarities in the observed microstructure, as can be seen in Fig. 63. If the light and darks phases in Fig. 63(a) are Au and a eutectic Au–Ge mixture respectively, one can see that Au structures protrude through a eutectic Au–Ge mixture in all three samples. This is consistent with the results reported in Article 1. Further investigations of the Au–Ge sample in Fig. 62(a) also show that there are large structures of Au (turquoise/yellow) extending through the eutectic Au–Ge mixture (blue). This is also consistent with the high-temperature shear test results disclosed in Article 2.

[2] This work was done by: Dag. W. Breiby (NTNU) facilitating experiments, Vincent Fernandez (ESRF) performing the measurements, Elvia Anabela Chavez Panduro (NTNU) and Kim Robert Tekseth (NTNU) both post-processing data.

In Fig. 62(c) a vast network of dendritic structures can be seen. Comparing this plot with the corresponding ⊥-plane cross-section (Fig. 64) and matching these with each other, one can see that the dendritic structure (turquoise/green/yellow/red) is unreacted Sn and the other phase (deep blue) is voids.

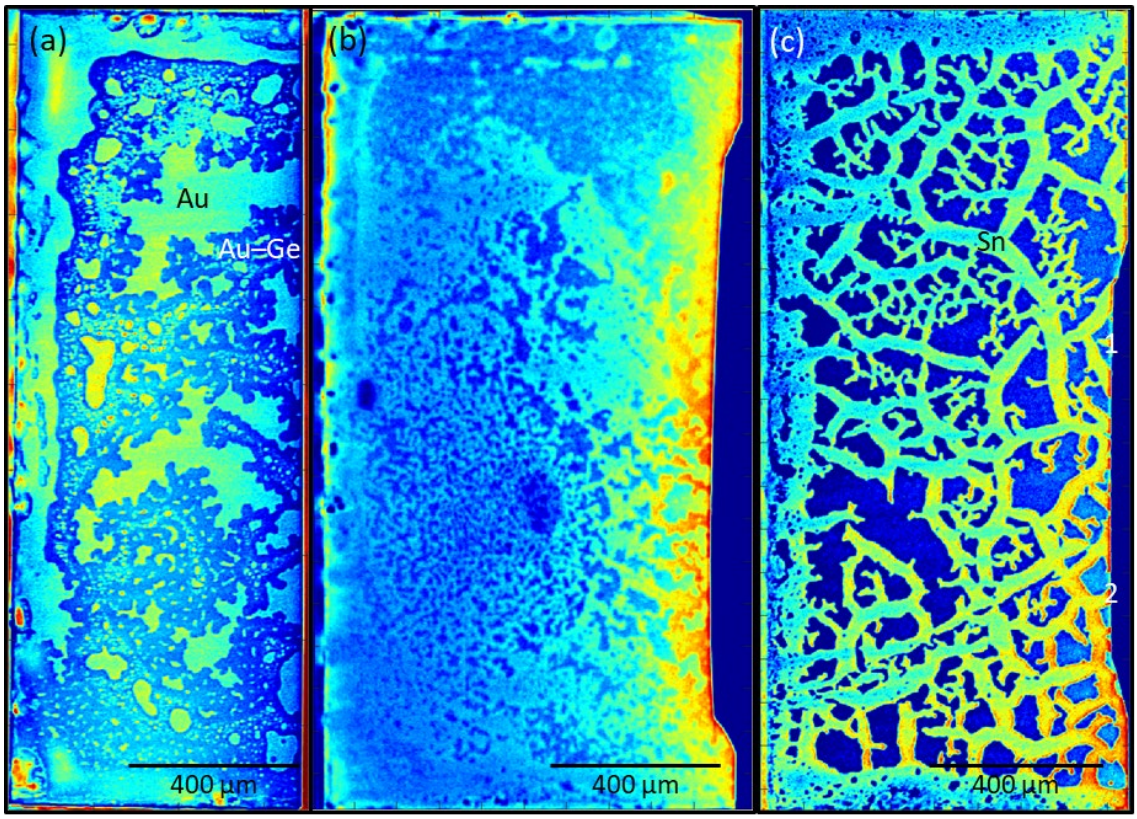

Fig. 62 ∥-plane sections from X-ray tomography of three samples (a) Au–Ge LSD sample, (b) Ni–Sn SLID sample, and (c) incomplete Ni–Sn SLID sample. The color scale is proportional to mass density. Blue is low density and red is high density. The color scale has been optimized to highlight structural features for each plot.

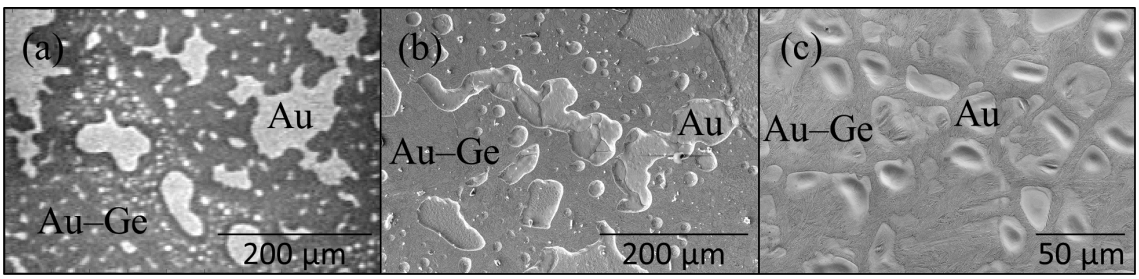

Fig. 63 Three off-eutectic Au–Ge samples showing similar features in the microstructure. (a) ∥-plane section from X-ray tomography, (b) SEM micrograph of a fracture surface, and (c) SEM micrograph of an exposed surface after a wetting test.

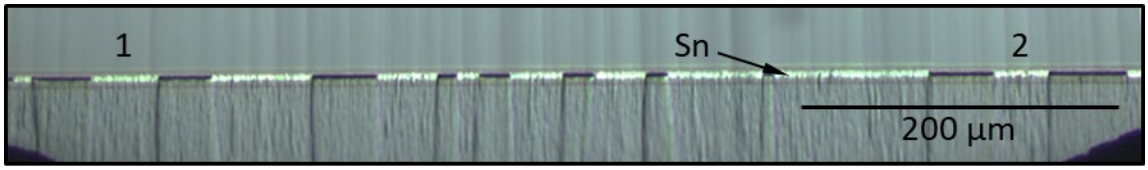

Fig. 64 Optical micrograph of the ⊥-plane cross-section from the same sample as shown in Fig. 62(c). Points 1 and 2 correspond to points 1 and 2 in Fig. 62(c).